

**University of Alberta**

Iceberg calving from a Canadian Arctic tidewater glacier

by

Hannah Maree Milne

A thesis submitted to the Faculty of Graduate Studies and Research  
in partial fulfillment of the requirements for the degree of

Master of Science

Department of Earth and Atmospheric Sciences

©Hannah Maree Milne

Fall 2011

Edmonton, Alberta

Permission is hereby granted to the University of Alberta Libraries to reproduce single copies of this thesis and to lend or sell such copies for private, scholarly or scientific research purposes only. Where the thesis is converted to, or otherwise made available in digital form, the University of Alberta will advise potential users of the thesis of these terms.

The author reserves all other publication and other rights in association with the copyright in the thesis and, except as herein before provided, neither the thesis nor any substantial portion thereof may be printed or otherwise reproduced in any material form whatsoever without the author's prior written permission.

## Abstract

Time lapse imagery, an audio recorder and geophones were used to detect iceberg calving events on the Belcher Glacier, Devon Island, in the Canadian High Arctic, in order to identify the major controls on the rate and style of calving. Eleven calving events were identified between June 4<sup>th</sup> and August 14<sup>th</sup> 2009 which accounted for 44% of the annual calving flux. Several of the events recorded in the audio data were associated with debris avalanching and disintegration of large tabular bergs. The geophones did not identify calving events but did record hydro-fracturing when terminus water-filled crevasses drained into the glacier.

None of the calving events were a direct response to an increase in ice velocity in the terminus region, break-up of the sea ice/mélange, tidal flexure of the terminus, or propagation of water-filled crevasses. The Belcher Glacier maintains a lightly grounded stable terminus position but develops a protrusion at the glacier centreline every few years. When this occurs, as it did in 2009, the meltwater plume is active in eroding the lateral stability of the protrusion by locally enhancing the calving rate. Further investigation is required to examine whether basal melt also undercuts the protrusion, eventually leading to its flotation. In 2009 the protrusion calved off as a series of tabular icebergs which strongly suggests it was floating, as do calculations of height-above-buoyancy and subglacial effective pressure. In general, calving was not driven by a single identifiable cause and its stochastic timing may reflect the progressive accumulation of damage to the ice as it is transported to the terminus. The interactions of ice flow with the ice and bed geometry, as well as ponding and hydro-fracturing of supraglacial meltwater, seemed to be the main contributors to this damage.

## Acknowledgements

Firstly, thank-you to my supervisor Dr. Martin Sharp for offering me this project and providing support throughout it, including the opportunities to attend conferences/meetings and go on several Arctic field seasons. Thanks to Dr Doug Mair for pointing me in the direction of Canada in the first place.

I gratefully acknowledge financial and logistical support from the University of Alberta for a Master's Entrance Scholarship, Alberta Ingenuity Fund, Canadian Circumpolar Institute, Institute of Geophysical Research, IPY Federal Program Office and the Polar Continental Shelf Project.

Thanks to Dr. Jeff Kavanaugh and Rob Stefaniuk for their technical expertise in helping design and create components of the geophones and audio recorder systems. E.A.R.S. Canada provided lots of advice during the implementation of the audio system, and donated a specialized microphone. Thanks also to Rescue Data Recovery Edmonton who helped to eventually retrieve audio data from a very broken hard drive after it overheated itself in the field. I'd like to thank Neil Birkbeck for setting me in the right direction during the initial stage of optical flow experiments, and Visesh Chari for making his code available. Thanks also to Dr. Javier Corripio, Dr. Daniel Bourgault and Dr. Shad O'Neel for giving me their georeferencing codes, although not all of them ended up working in our field setting. A big thank-you to Dr. Arie Croitoru for providing some georeferencing code which did work successfully and for the time and support involved in making sure it would perform well. Dr. Lev Tarasov provided data from his 2008 field season, which is gratefully acknowledged. Thanks to Dr. Jason Amundson and Anne Chapuis for useful discussions and advice about leaving complicated audio recorders in the Arctic unattended. Scott Williamson gave me some assistance with MODIS data which was very helpful. A big thank-you to all of the Arctic and Alpine Research Group for being the best work colleagues ever, and especially to Brad Danielson, Christine Dow, Faye Wyatt, Dr. Alex Gardner, Jamie Davis and Angus Duncan for useful discussions and/or data. In particular I have been very lucky to work with Brad Danielson, officemate and field partner, who gave me a lot of advice and support, particularly getting to grips with Matlab and some of the field equipment. Thank-you!

# Table of Contents

<b>ABSTRACT .....</b>	<b>2</b>
<b>ACKNOWLEDGEMENTS .....</b>	<b>3</b>
<b>LIST OF TABLES.....</b>	<b>6</b>
<b>LIST OF FIGURES.....</b>	<b>7</b>
<b>LIST OF ABBREVIATIONS.....</b>	<b>13</b>
<b>CHAPTER 1. INTRODUCTION .....</b>	<b>1</b>
1.1    MOTIVATION.....	1
1.2    REVIEW OF ICEBERG CALVING DETECTION METHODS.....	2
1.2.1 <i>Time Lapse Imagery</i> .....	3
1.2.2 <i>Audio Recordings</i> .....	5
1.2.3 <i>Geophones</i> .....	7
1.3    REVIEW OF POTENTIAL CALVING TRIGGERS.....	9
1.3.1 <i>Terminus Velocity</i> .....	10
1.3.2 <i>Water-filled Crevasses</i> .....	12
1.3.3 <i>Meltwater / Sediment Plume</i> .....	14
1.3.4 <i>Mélange / Sea ice buttressing</i> .....	15
1.3.5 <i>Tidal Flexure</i> .....	17
1.3.6 <i>Ocean Temperatures</i> .....	19
1.3.7 <i>Terminus Geometry</i> .....	22
1.4    RESEARCH OBJECTIVES.....	23
1.5    THESIS STRUCTURE.....	24
<b>CHAPTER 2. FIELD SETTING AND METHODS.....</b>	<b>25</b>
2.1    FIELD LOCATION.....	25
2.1.1 <i>Field Campaign</i> .....	30
2.2    ICEBERG CALVING DETECTION.....	32
2.2.1 <i>Time Lapse Imagery</i> .....	32
2.2.2 <i>Audio Recordings</i> .....	37
2.2.3 <i>Geophones</i> .....	39
2.3    IDENTIFYING POTENTIAL CALVING TRIGGERS.....	40
2.3.1 <i>Terminus Velocity</i> .....	40
2.3.2 <i>Water-filled Crevasses</i> .....	48
2.3.3 <i>Meltwater / Sediment plume</i> .....	50
2.3.4 <i>Mélange / Sea ice Buttressing</i> .....	53
2.3.5 <i>Tidal modelling</i> .....	54
2.3.6 <i>Ocean Temperatures</i> .....	54
2.3.7 <i>Geometry</i> .....	55
2.4    SUMMARY.....	56
<b>CHAPTER 3. RESULTS.....</b>	<b>58</b>
3.1    INTRODUCTION.....	58
3.2    ICEBERG CALVING DETECTION.....	58
3.2.1 <i>Time Lapse Imagery</i> .....	58

3.2.2	<i>Audio Recordings</i> .....	67
3.2.3	<i>Geophones</i> .....	74
3.3	POTENTIAL CALVING TRIGGERS .....	83
3.3.1	<i>Terminus Velocity Changes</i> .....	83
3.3.2	<i>Water-filled Crevasses</i> .....	88
3.3.3	<i>Meltwater / Sediment Plume</i> .....	91
3.3.4	<i>Mélange / Sea ice buttressing</i> .....	99
3.3.5	<i>Tidal Analysis</i> .....	107
3.3.6	<i>Ocean Temperatures</i> .....	109
3.3.7	<i>Geometry</i> .....	114
3.4	SUMMARY .....	119
<b>CHAPTER 4. DISCUSSION</b> .....		<b>123</b>
4.1	INTRODUCTION .....	123
4.2	BELCHER GLACIER: GROUNDED OR FLOATING? .....	123
4.3	POTENTIAL CALVING TRIGGERS .....	127
4.3.1	<i>Meltwater-driven Terminus Velocity Changes</i> .....	127
4.3.2	<i>Propagation of water-filled crevasses</i> .....	128
4.3.3	<i>Mélange / Sea ice buttressing</i> .....	129
4.3.4	<i>Tidal flexure</i> .....	130
4.3.5	<i>Ocean temperatures</i> .....	131
4.4	LIMITATIONS .....	131
4.5	IMPLICATIONS .....	133
4.6	SUMMARY .....	135
<b>CHAPTER 5. CONCLUSIONS</b> .....		<b>136</b>
<b>BIBLIOGRAPHY</b> .....		<b>138</b>

# List of Tables

TABLE 2.1. SELECTED METEOROLOGICAL INSTRUMENT SPECIFICATIONS AS STATED BY THE MANUFACTURER. ALL INSTRUMENTS WERE INSTALLED ON THE CROSS-ARM, 2M ABOVE THE SURFACE AT THE TIME OF INSTALLATION. HOURLY AVERAGES OF 15-SECOND MEASUREMENTS WERE RECORDED ON CAMPBELL SCIENTIFIC CR1000 DATA LOGGERS (TABLE FROM DUNCAN, 2011).....	37
TABLE 2.2. TESTING THE OPTIMIZATION OF OPTICAL FLOW PARAMETERS.....	47
TABLE 3.1. GLACIER CALVING-RATE COMPONENTS, RATIO OF FLUX COMPONENTS, AND SEASONAL AND ANNUAL ESTIMATES OF TOTAL VOLUME LOST FOR THE BELCHER GLACIER, 2009-2010. 65	
TABLE 3.2. A COMPARISON OF THE TIMINGS OF CALVING EVENTS TIMINGS IDENTIFIED IN TIME LAPSE IMAGERY AND AUDIO DATA FOR THE PERIOD 24 <sup>TH</sup> JUNE 2009 – 24 <sup>TH</sup> JULY 2009. IN THE IMAGE DATA FOR 15-16 JULY AND 19-20 JULY CALVING WAS OBSERVED IN THE IMAGERY BUT WAS EQUALIZED BY ICE ADVANCE AND ANOTHER PARTLY-DETACHED BERG SLIPPING FORWARD. WHEN NOTHING IS AUDIBLE IN THE AUDIO DATA, THIS WAS ALWAYS BECAUSE THE CALVING INVOLVED A SMALL EVENT LOCATED NEAR THE SOUTH MARGIN (AND THE MICROPHONE WAS POINTED TOWARDS THE NORTHERN PART OF THE MARGIN). .....	69
TABLE 3.3. GEOPHONE EVENTS AT STATION 3 (6.6KM FROM THE TERMINUS) BETWEEN JULY 16 <sup>TH</sup> AND 24 <sup>TH</sup> 2009: WHEN MOST OF THE CALVING EVENTS TOOK PLACE AT THE BELCHER GLACIER TERMINUS. COUNTS WHICH OCCURRED DURING THE KNOWN TIMEFRAME OF A CALVING EVENT (ACCORDING TO TABLE 3.2) ARE HIGHLIGHTED IN GREY. ....	80
TABLE 3.4. RESOLVABLE LAPSE INTERVAL CALCULATED BASED ON THREE DIFFERENT TIME RANGES BETWEEN OPTICAL FLOW IMAGE PAIRS. BOTH $\Delta P$ (ICE DISPLACEMENT, PIXELS AND METRES) AND $\epsilon$ (UNCERTAINTY, PIXELS) ARE NORMALIZED DAILY MEAN VALUES. THE RESOLVABLE LAPSE INTERVAL IN DAYS, $\Delta D$ , IS PRESENTED AS TWO RESULTS FOR THE OPTICAL FLOW DATA BASED ON ESTIMATES WITH A 30% AND 50% ERROR BUDGET EXPRESSED AS A PERCENTAGE ( $\epsilon_B$ ). THE AVERAGE DAILY ICE DISPLACEMENT AT THE GPS, COMPARING ONLY THE SAME TIME PERIODS EXAMINED IN THE OPTICAL FLOW ANALYSIS, IS SHOWN FOR COMPARISON WITH THE $\Delta P$ IN METRES ESTIMATED FROM OPTICAL FLOW. ....	85
TABLE 3.5. THE FIVE LARGEST CONSTITUENTS OF THE TIDE IN BELCHER FJORD, IN ORDER OF DECREASING IMPORTANCE, AS MODELED IN WEBTIDE (PAWLOWICZ ET AL., 2002). THESE RESULTS ARE AVERAGES OF 2007-2009 TIDES DURING THE RESPECTIVE FIELD SEASONS.....	107
TABLE 3.6. POINT MEASUREMENTS OF ICE CLIFF HEIGHT AND ICE THICKNESS AT THE CENTERLINE OF THE BELCHER GLACIER AND ITS CONFLUENCE WITH THE NORTHERN TRIBUTARY, AS RECORDED AT THE TERMINUS OR 500-700M AWAY, WHERE THE CREISIS ICE THICKNESS TRANSECT WAS MADE IN 2005 (SEE FIGURE 2.3). IN THE COLUMN HEADINGS, ‘T’ STANDS FOR TERMINUS. ....	115

# List of Figures

FIGURE 1.1. SEISMIC AND ACOUSTIC WAVEFORMS FROM A CALVING ON 15 <sup>TH</sup> JULY 2008 AT JAKOBSHAVN ISBRAE, SW GREENLAND, AS OBSERVED BY AMUNDSON ET AL. (2010). (A) VERTICAL COMPONENT OF THE CALVING-GENERATED SEISMOGRAM (B) CLOSE-UP OF FIGURE 1.4A SHOWING THE EMERGENT ONSET OF THE SEISMIC SIGNAL (C) ACOUSTIC WAVEFORM FROM THE CALVING EVENT (D) CLOSE UP OF FIGURE 1.1C. THE GRAY BARS IN FIGURES 1.1A AND 1.1C INDICATE THE TIME PERIODS SHOWN IN FIGURES 1.1B AND 1.1D. FIGURE AND ACCOMPANYING TEXT FROM AMUNDSON ET AL. (2010, P6). .....	6
FIGURE 2.1. GLACIERS AND ICE CAPS OF THE CANADIAN ARCTIC ARCHIPELAGO, WITH THE LOCATION OF DEVON ISLAND AND THE BELCHER GLACIER SHOWN (RED RECTANGLE). THE MAIN PANEL IS AN ENLARGEMENT OF THE RED RECTANGLE SHOWN IN THE INSET OF THE ARCTIC REGION. FIGURE ADAPTED FROM GARDNER ET AL. (2011), WHICH WAS CREATED BY G. WOLKEN. ....	26
FIGURE 2.2. THE BELCHER GLACIER (A) THE MAIN BELCHER GLACIER CATCHMENT, SHOWING VARIOUS RADAR AND BATHYMETRY TRANSECTS IN THE REGION, AS WELL AS THE LOCATION OF FOUR SUPRAGLACIAL LAKES REFERRED TO IN THE TEXT IN CONNECTION WITH DANIELSON AND SHARP (IN REVIEW), THE GENERAL REGION OF TERMINUS WATER-FILLED CREVASSES, AND THE LOCATION OF GEOPHONE AND WEATHER STATIONS DISCUSSED IN THE TEXT. (B) A CLOSE UP OF THE BELCHER GLACIER TERMINUS, THE MAIN STUDY AREA. SHOWN ARE THE LOCATIONS OF: NEARBY CTD CASTS, THE GEOPHONE STATIONS (WHICH INCLUDES THE AUDIO RECORDER AND GPS SITE AT GEOPHONE STATION 1), THE 2007/8 AND 2009 TIME LAPSE CAMERAS, THE GENERAL AREA OF WATER-FILLED CREVASSES OBSERVED FROM THE 2009 TIME LAPSE CAMERA, AND THE LOCATIONS OF CREVASSE MEASURED FOR DEPTH BY L. TARASOV AND TEAM. BASE MAP IS A LANDSAT 2000 IMAGE .....	27
FIGURE 2.3. (A) TRANSECTS ALONG THE BELCHER GLACIER CENTRELINE SHOWING ICE SURFACE AND BED TOPOGRAPHY (B) CROSS-PROFILE TRANSECT RUNNING PARALLEL TO THE BELCHER GLACIER TERMINUS, SHOWING ICE SURFACE, BED TOPOGRAPHY AND BATHYMETRY DATA FROM OFFSHORE OF THE TERMINUS; LOCATION SHOWN IN FIGURE 2.2. ICE SURFACE AND BED ELEVATIONS IN (B) AND ‘CENTRELINE TRANSECT’ IN (A) WERE OBTAINED IN 2005 FROM NASA’S AIRBORNE TOPOGRAPHIC MAPPER (ATM) LASER ALTIMETER AND THE UNIVERSITY OF KANSAS ICE PENETRATING RADAR DEPTH SOUNDER INSTRUMENTS AS PART OF THE CRESIS (CENTRE FOR REMOTE SENSING OF ICE SHEETS) PROJECT (GOGINENI ET AL., 2005; KRABILL ET AL., 2006). ‘CONFLUENCE TRANSECT’ IN (A) WAS OBTAINED IN 2000 FROM THE SURVEY OF ICE THICKNESS DESCRIBED IN DOWDESWELL ET AL. (2004). ....	28
FIGURE 2.4. DEMONSTRATION OF THE THREE CAMERA ROTATION ANGLES, WHICH HAVE VARIOUS NAMES DEPENDING ON THE PHOTOGRAMMETRY SYSTEM USED AND ARE ALL LISTED HERE FOR CLARITY AND FOR COMPARISON BETWEEN O’NEEL ET AL. (2007) AND AHN AND BOX (2010): ROLL/OMEGA ( $\Omega$ )/PSI (ROTATION CLOCKWISE AROUND X AXIS), POINTING ANGLE/PHI ( $\Phi$ )/PITCH (DIP BELOW THE HORIZONTAL ON THE Y AXIS), TILT/KAPPA ( $\kappa$ )/THETA (TILT FROM THE AZIMUTH, COUNTER-CLOCKWISE AROUND THE Z AXIS WHERE NORTH IS 90°. $\Omega/\Phi/\kappa$ IS THE MOST ACCURATE NAMING SYSTEM WHICH IS USED IN THIS THESIS.....	34
FIGURE 2.5. THE TIME LAPSE IMAGE SCENE OF THE BELCHER TERMINUS FOR 2009, WITH KEY FEATURES ANNOTATED. ....	35
FIGURE 2.6. THE ‘UBERSTATION’ SETUP WITH AUDIO RECORDER, GEOPHONES AND GPS INSTALLED NEAR THE TERMINUS (AT TNRS-6). AUDIO RECORDER IS POWERED BY THE 3 LARGE 80W SOLAR PANELS PICTURED, WHICH FEED THE BATTERY IN THE BLACK BOX. E.A.R.S. CANADA MICROPHONE PICTURED IN INSET, WITH PURPLE GORETEX WINDSHIELD COVER. SOUND	

DEVICES 702T AUDIO RECORDER PICTURED IN SECOND INSET, WITH LACIE ‘RUGGED’ HARD DRIVE WHICH WAS ALSO INSTALLED IN THE BLACK BOX ALONG WITH A CAMPBELL SCIENTIFIC DATALOGGER AND A CIRCUIT BOARD TIMING DEVICE. ....	38
FIGURE 2.7. AN EXAMPLE OF AN OPTICAL FLOW RESULT, DISPLAYED ON THE ORTHORECTIFIED TIME LAPSE IMAGE. THE IMAGES COMPARED WERE TAKEN ON 19 <sup>TH</sup> JULY 2009 AT 1AM AND 20 <sup>TH</sup> JULY 2009 AT 5AM. VECTORS ARE ENLARGED BY 5 TIMES FOR VISIBILITY. DISPLACEMENTS WHICH DID NOT EXCEED THE BEDROCK UNCERTAINTY WERE REMOVED AND A MASK IS APPLIED AROUND THE IMAGE MARGINS AS WELL AS OVER THE OCEAN AND BEDROCK. ....	42
FIGURE 2.8. A TIME LAPSE IMAGE FROM JUNE 30 <sup>TH</sup> 2009 AT 7AM WHICH SHOWS THE WATER-FILLED CREVASSES VISIBLE AT THE TERMINUS THAT WERE OUTLINED (IN RED) BY THE PIXEL-PICKING ALGORITHM DEVELOPED BY B. DANIELSON (FIGURE ADAPTED FROM DANIELSON AND SHARP, IN REVIEW). LAKES ‘A’ AND ‘B’ ARE REFERRED TO IN THE TEXT, IN SECTION 3.3.2. A SMALL WATER-FILLED CREVASSE WHICH THE ALGORITHM MISSED IS ALSO SHOWN IN THE FOREGROUND.....	49
FIGURE 2.9. COMPARISON OF THE 2007/8 TERMINUS CAMERA VIEW (A) AND THE 2009 TERMINUS CAMERA VIEW (B) WHICH DEMONSTRATES THAT MUCH MORE PLUME WATER IS VISIBLE IN THE 2007/8 IMAGERY.....	51
FIGURE 3.1. TIME-AVERAGED RATE OF AREA CHANGE OF THE CALVING FRONT, JUNE 4 <sup>TH</sup> - AUGUST 14 <sup>TH</sup> 2009. A) FULL ARRAY OF CALVING FRONT POSITIONS SUPERIMPOSED ON A TIME LAPSE IMAGE TO DEMONSTRATE SPATIAL CHANGE. B) GRAPH OF AREA CHANGE OVER THE TIME PERIOD.....	59
FIGURE 3.2. SUMMARY OF CALVING ACTIVITY, SEDIMENT PLUME ACTIVITY AND ENVIRONMENTAL CONDITIONS FOR SUMMER 2009. A) BAR CHART OF CALVING FRONT AREA CHANGE, PRESENTING ONLY SIGNIFICANT ADVANCE OR RETREAT OF THE MARGIN, AND TIMES WHEN CALVING WAS VISUALLY OBSERVED. THE TIMING OF SEA ICE INITIAL INDEPENDENT MOVEMENT AND FINAL BREAK UP ARE ALSO SHOWN. B) AIR TEMPERATURE AT LBAWS. C) SEDIMENT PLUME AREA, COMPARED TO MODELED RUNOFF VOLUME. D) AREA CHANGE OF SUPRAGLACIAL TERMINUS WATER-FILLED CREVASSES. ....	60
FIGURE 3.3. A TIME LAPSE IMAGE FROM JULY 14 <sup>TH</sup> 2009 AT 9PM WHICH SHOWS LEADS OPENING UP IN THE SEA ICE, SOME AREAS OF SEA ICE NEAR THE ICE CLIFF BEGINNING TO MOVE INDEPENDENTLY, AS WELL AS WATER-FILLED CREVASSES ON THE GLACIER SURFACE.....	61
FIGURE 3.4. COMPARISON OF ICE MARGIN POSITIONS FROM LANDSAT-7 ETM+ IMAGES AND TWO DIFFERENT METHODS OF GEOREFERENCING THE 2009 TIME LAPSE IMAGERY. ‘OBLIQUE-IMAGE’ MARGIN POSITIONS WERE DIGITIZED FOR THE AREA-CHANGE MEASUREMENTS REFERRED TO IN SECTION 3.2.1 (GEOREFERENCED USING THE METHOD OF KRIMMEL AND RASMUSSEN (1986)), WHILST ‘PLAN-IMAGE’ MARGIN POSITIONS WERE DIGITIZED FOR COMPARISON OF ACCURACY BUT WERE GEOREFERENCED FOR USE WITH THE OPTICAL FLOW DATA (SEE SECTION 2.3.1) USING THE METHOD OF CROITORU AND ETHROG (2001). ....	63
FIGURE 3.5. EXAMPLES OF FEATURES IDENTIFIED IN THE CALVING WAVEFORM: (A) HIGH WINDS (<17M/S) CAUSES CABLES TO TAP IN THE WIND ON JUNE 30 <sup>TH</sup> 2009, 3AM (B) RAINFALL AND TRICKLING MELTWATER ON JULY 7 <sup>TH</sup> 2009, 4PM.....	68
FIGURE 3.6. ACOUSTIC WAVEFORMS FROM THREE CALVING EVENTS, ON (A) JULY 18 <sup>TH</sup> (B) JULY 21 <sup>ST</sup> (C) JULY 22 <sup>ND</sup> 2009. RED ARROWS POINT TO ‘THUD’ SOUNDS, WHICH ARE INTERPRETED AS AN ICEBERG HITTING THE WATER. THE GREEN LINES IN (C) ARE THE TIMING CONFIRMATION FROM THE DATALOGGER, WHICH IS TRANSMITTED AT 12 NOON EACH DAY. IT BEEPS ALOUD THE DAY OF THE YEAR. ....	70

FIGURE 3.7. CALVING ON JULY 27 <sup>TH</sup> 2008, BETWEEN 1AM AND 2AM. A) GLACIER IS ACTIVELY CALVING AT ITS NORTHERN MARGIN, AND APPEARS TO HAVE ALREADY LOST SOME ICE, WITHIN THE PREVIOUS HOUR, WHICH HAS DISAPPEARED FROM VIEW OR DISINTEGRATED. THE BERG CAN BE SEEN ROLLING ‘BOTTOM OUT’. B) AFTER THE CALVING EVENT (4AM), THE AREA OF ICE FRONT LOST IS CLEARLY VISIBLE (THE ICE IS A DEEPER BLUE COLOUR) AND A LARGE ICEBERG WITH A LAYER OF SEDIMENT ATTACHED IS SEEN IN THE FJORD, WHICH APPEARS TO HAVE COME FROM THE PRIOR CALVING EVENT. ....	71
FIGURE 3.8 A SMALL ICEBERG NEAR THE SOUTHERN MARGIN WHICH HAS FRACTURED TO THE WATER LINE, PROBABLY FOLLOWING PREEXISTING SURFACE CREVASSES, BUT IS STILL ATTACHED ABOVE THE WATER AT THE NORTHERN END. IMAGE TAKEN BY L. TARASOV ON 30 <sup>TH</sup> JULY 2008. ....	72
FIGURE 3.9. GEOPHONE EVENTS AT STATIONS 1-3 ON THE BELCHER GLACIER ON JULY 7 <sup>TH</sup> 2009: THE DAY OF THE EARTHQUAKE IN BAFFIN BAY, DIRECTLY EAST OF DEVON ISLAND. AT ALL THREE STATIONS, THE ONLY EVENTS RECORDED WERE AT 19:12 AND 19:14 UTC (WITH 2 MIN TOTALING INTERVAL). THE NUMBER OF COUNTS RECORDED AT THE 2 GEOPHONES AT EACH STATION (A AND B) IS SHOWN; GEOPHONE A HAD A LOWER SENSITIVITY (2000) THAN GEOPHONE B (3000). ....	75
FIGURE 3.10. GEOPHONE ACTIVITY AND CALVING EVENTS AS RECORDED IN THE TIME LAPSE AND AUDIO RECORDS, BETWEEN JUNE 4 <sup>TH</sup> AND AUGUST 13 <sup>TH</sup> 2009. (A) OBSERVED AND RECORDED CALVING EVENTS, AS WELL AS SEA ICE MOVEMENT AND BREAK-UP (B) GEOPHONE COUNTS AT STATION 1 AND 2 (C) GEOPHONE COUNTS AT STATION 3. HIGH CONCENTRATIONS OF EVENT COUNTS IN A DAY ARE ANNOTATED. ....	79
FIGURE 3.11. GEOPHONE ACTIVITY AND LAKE DRAINAGE EVENTS BETWEEN JUNE 4 <sup>TH</sup> AND AUGUST 13 <sup>TH</sup> 2009. THE LAKE DRAINAGE DATASET IN (A) IS OWNERSHIP OF B. DANIELSON AND IS REPRODUCED FROM DANIELSON AND SHARP (IN REVIEW) (A) SUPRAGLACIAL AND WATER-FILLED CREVASSE LAKE AREAS (LEGEND DENOTES DISTANCE UPSTREAM OF TERMINUS) (B) GEOPHONE COUNTS AT STATION 1 AND 2 (C) GEOPHONE COUNTS AT STATION 3. HIGH CONCENTRATIONS OF EVENT COUNTS IN A DAY ARE ANNOTATED.....	81
FIGURE 3.12. STACKED TIMES OF ICEQUAKE OCCURRENCES (PER HOUR) FOR SUMMER 2009 AT STATIONS 1-3. ....	82
FIGURE 3.13. COMPARISON OF GPS AND OPTICAL FLOW DISPLACEMENTS AS MEASURED BETWEEN THE SAME IMAGE PAIR TIME INTERVALS. THE RESULT IS PRESENTED AGAINST THE START DATE OF EACH PAIR IN THE X-AXIS. DISPLACEMENTS ARE NORMALIZED (METRES/DAY). NOTE THE DIFFERENT Y-AXES BETWEEN (A) AND (B/C) IN ORDER FOR SMALL FLUCTUATIONS TO BE SEEN CLEARLY. A) IMAGES WERE PAIRED 0.5 TO 3 DAYS APART B) IMAGES WERE PAIRED 3 TO 6 DAYS APART C) IMAGES WERE PAIRED 7 TO 11 DAYS APART. GPS DATA PROPERTY OF B. DANIELSON, PRESENTED WITH PERMISSION. ....	85
FIGURE 3.14. CALVING FRONT AREA CHANGE COMPARED TO HORIZONTAL ICE SURFACE VELOCITIES MEASURED BY GPS AT TNRS-6 (GPS DATA FROM B. DANIELSON). ONLY SIGNIFICANT ADVANCE OR RETREAT OF THE MARGIN IS PRESENTED, ALONG WITH TIMES WHEN CALVING WAS VISUALLY OBSERVED. NOTE THAT MANY OF THE EVENTS REPRESENT TOTAL CHANGE IN THE PREVIOUS 24-HOURS, SO ADVANCE/RETREAT MAY APPEAR TO OCCUR THE DAY AFTER IT ACTUALLY DID. THE TIMING OF SEA ICE INITIAL INDEPENDENT MOVEMENT AND FINAL BREAK UP ARE ALSO SHOWN. B) ICE SURFACE VELOCITIES MEASURED BY GPS AT TNRS-6. ....	86
FIGURE 3.15. DETAILED COMPARISON OF CALVING EVENT TIMINGS TO GPS VELOCITY AT TNRS-6 (GPS DATA FROM B DANIELSON). THE KNOWN TIMINGS OF EACH CALVING EVENT (SEE TABLE 3.2) IN (A)-(G) IS DEFINED BY THE RED LINES, WITH THE HORIZONTAL GPS VELOCITY SHOWN IN BLUE. ....	87

FIGURE 3.16. A SMALL POTENTIALLY MELTWATER PROPAGATION-DRIVEN CALVING EVENT WHICH TOOK PLACE ON JULY 30 <sup>TH</sup> (A) JULY 27 <sup>TH</sup> , 11PM: CREVASSE, WHERE CALVING WILL LATER TAKES PLACE, WIDENS. NOTE MELT POND, AND LOCATION OF PLUME (B) JULY 29 <sup>TH</sup> , 7PM: MELT POND HAS DRAINED, AND CREVASSE HAS WIDENED AND BEGUN TO SLUMP FORWARDS (C) JULY 30 <sup>TH</sup> , 9PM: CALVING HAS TAKEN PLACE ALONG THE PRE-EXISTING CREVASSE FRACTURE AND ANOTHER MELT POND APPEARS TO HAVE FORMED AND DRAINED IN THE INTERVENING TIME. ....	90
FIGURE 3.17. SUMMARY OF CALVING ACTIVITY, SEDIMENT PLUME CALVING ACTIVITY AND ENVIRONMENTAL CONDITIONS FOR SUMMER 2007. A) BAR CHART DISPLAYING OBSERVED CALVING EVENTS AS WELL AS THE TIMING OF SEA ICE INITIAL INDEPENDENT MOVEMENT AND FINAL BREAK UP. B) AIR TEMPERATURE AT HOBO 25, A GPS STATION CLOSE TO LBAWS (WHICH WAS INSTALLED IN 2008). C) SEDIMENT PLUME AREA (MODELED RUNOFF WAS NOT AVAILABLE AS THE WEATHER STATION WAS NOT INSTALLED).....	92
FIGURE 3.18. SUMMARY OF CALVING ACTIVITY, SEDIMENT PLUME CALVING ACTIVITY AND ENVIRONMENTAL CONDITIONS FOR SUMMER 2008. A) BAR CHART DISPLAYING OBSERVED CALVING EVENTS AS WELL AS THE TIMING OF SEA ICE INITIAL INDEPENDENT MOVEMENT AND FINAL BREAK UP. B) AIR TEMPERATURE AT LBAWS. C) SEDIMENT PLUME AREA AND MODELED RUNOFF VOLUME. ....	93
FIGURE 3.19. SURFACE REFLECTANCE VALUES FROM CLOUD-FREE MYD09 AND MOD09 250M RESOLUTION BAND 1 MODIS IMAGES BETWEEN AUGUST 10 <sup>TH</sup> AND SEPTEMBER 4 <sup>TH</sup> 2009. THE RESULTS ARE PLOTTED ON THE SAME BASE IMAGE (AUGUST 11 <sup>TH</sup> 2009) WHICH IS IN COLOUR USING BANDS 1-1-2. ONLY REFLECTANCE VALUES >0.012 ARE SHOWN HIGHLIGHTED IN RED. THE RESULTS FROM AUGUST 10 <sup>TH</sup> TO 19 <sup>TH</sup> MATCH QUALITATIVELY TO THE GREENISH-GREY PLUME VISIBLE IN TRUE COLOUR (BANDS 1-4-3) JPG IMAGES (AVAILABLE AT 500M RESOLUTION) BUT THIS GREENISH-GREY IS NOT PRESENT ON AUGUST 27 <sup>TH</sup> AND SEPTEMBER 4 <sup>TH</sup> - ALTHOUGH IT IS NOT POSSIBLE TO PROVE THAT SEDIMENT IS NOT PRESENT. ....	94
FIGURE 3.20. SEQUENCE OF CHANGES IN THE MELTWATER/SEDIMENT PLUME LEADING UP TO A CALVING EVENT ON JULY 17 <sup>TH</sup> 2009 (A) FOLLOWING SEA ICE BREAK-UP, AN ICEBERG WAS LEFT PARTLY DETACHED, AND 2 SEDIMENT PLUMES WERE EMERGING ON JULY 16 <sup>TH</sup> AT 11AM (B) THE PLUMES THEN BEGAN TO EMERGE IN 3 SEPARATE PLACES, THE NEWEST ONE ON THE OTHER SIDE OF THE SOON-TO-BE-ICEBERG, SHOWN HERE ON JULY 17 <sup>TH</sup> AT 9AM (C) CALVING TOOK PLACE BETWEEN 11AM AND 1PM ON JULY 17 <sup>TH</sup> . THIS PHOTO WAS TAKEN AT 1PM. THE MELTWATER HAS REVERTED TO A SINGLE PLUME AND THE ICEBERG HAS BEEN CALVED OFF. 96	96
FIGURE 3.21. THE SEDIMENT PLUME BEGAN TO EMERGE FROM A NEW NORTHERN LOCATION BETWEEN JULY 20 <sup>TH</sup> AND 22 <sup>ND</sup> 2009, SHOWN HERE IN AN IMAGE FROM 7AM ON JULY 20 <sup>TH</sup> . THE DIGITIZED ICE MARGIN POSITIONS FROM JULY 19 <sup>TH</sup> , 20 <sup>TH</sup> AND 22 <sup>ND</sup> ARE SHOWN. NOTE ALSO THE SMALL CALVING EVENT BETWEEN JULY 19 <sup>TH</sup> (RED) AND 20 <sup>TH</sup> (YELLOW), WHICH COINCIDED WITH THE ADVANCE OF THE ICE THAT IS ABOUT TO BE CALVED ON JULY 22 <sup>ND</sup> . THE ASSUMED 'NORMAL' SUBGLACIAL ROUTE OF THE MELTWATER, AND ITS TEMPORARY ADDITIONAL REROUTING BENEATH THE ICE THAT IS ABOUT TO BE CALVED IS ALSO SHOWN..	97
FIGURE 3.22. MELTWATER PLUME DISCHARGE, LAKE DRAINAGE AND CALVING EVENTS BETWEEN JULY 11 <sup>TH</sup> AND AUGUST 13 <sup>TH</sup> 2009. THE LAKE DRAINAGE DATASET IS OWNERSHIP OF B. DANIELSON AND IS REPRODUCED FROM DANIELSON AND SHARP (IN REVIEW) (A) MELTWATER PLUME DISCHARGE AREA, AND SUPRAGLACIAL AND WATER-FILLED CREVASSE LAKE AREAS (LEGEND DENOTES DISTANCE UPSTREAM OF TERMINUS) (B) BAR CHART OF CALVING FRONT AREA CHANGE, PRESENTING ONLY SIGNIFICANT ADVANCE OR RETREAT OF THE MARGIN, AND TIMES WHEN CALVING WAS VISUALLY OBSERVED. THE TIMING OF SEA ICE INITIAL INDEPENDENT MOVEMENT AND FINAL BREAK UP ARE ALSO SHOWN. ....	98

FIGURE 3.23. LEADS OPENING IN THE SEA ICE IN THE NORTHERN BAY. PHOTO TAKEN JULY 18 <sup>TH</sup> 2008, 4.30PM, FROM THE <i>TARASOV CAMERA</i> .....	100
FIGURE 3.24. ROSE DIAGRAMS OF WIND DIRECTION, COMPARING 1 <sup>ST</sup> JUNE-12 <sup>TH</sup> AUGUST 2008 (A) TO 2009 (B) AT LBAWS.....	101
FIGURE 3.25. THE MÉLANGE OF ICEBERGS INTERMINGLED WITH SEA ICE, VIEWED FROM THE 2009 TIME LAPSE CAMERA (A), WHERE THE MÉLANGE IS OUTLINED IN RED, AND SEVERAL PERSPECTIVES FROM NEAR THE ISLAND (B-D), THE LOCATION OF WHICH IS MARKED IN (A). (B) AND (D) HIGHLIGHT THE SHARP DISTINCTION BETWEEN SEA ICE AND MÉLANGE, AND (C) SHOWS THE BUTTRESSING EFFECT OF THE SEA ICE, WHICH IS PREVENTING SEVERAL ICEBERGS AND SMALLER DISINTEGRATED CHUNKS FROM FALLING OFF THE TERMINUS. THE RED ARROWS INDICATE WHERE FEATURES IN EACH SCENE COINCIDE.....	103
FIGURE 3.26. CHANGES IN MARGIN POSITION BETWEEN FALL AND SPRING, WITH REFERENCE TO THE AREA OF ICEBERG MÉLANGE ON THE SEA ICE BY MID-SPRING FOR 2007-2009. (A) INITIAL MARGIN POSITION AND MÉLANGE, 2007 (B) LAST AVAILABLE FALL MARGIN POSITION FROM 2007 SET AGAINST SPRING 2008 MARGIN POSITION AND MÉLANGE AREA (C) LAST AVAILABLE FALL MARGIN POSITION FROM 2008 SET AGAINST SPRING 2009 MARGIN POSITION AND MÉLANGE AREA (D) FIRST SPRING POSITION AND LAST FALL POSITION FOR EACH YEAR, 2007-2009.....	104
FIGURE 3.27. STATE OF THE SEA ICE AROUND THE ISLAND JUST OFFSHORE OF THE BELCHER TERMINUS ON MAY 31 <sup>ST</sup> 2009. (A) SLABS OF SEA ICE BUILT UP AROUND THE ISLAND (B) VIEW FROM THE ISLAND OF THE DEFORMED SEA ICE AROUND ITS MARGIN.....	105
FIGURE 3.28. CROPPED JPEG DIGITAL GLOBE IMAGE FROM JUNE 24 <sup>TH</sup> 2011, SHOWING DEFORMATION OF THE SEA ICE IN FRONT OF THE BELCHER GLACIER TERMINUS (VISIBLE AMONGST LOW-LYING CLOUDS). THE AREAS OF MÉLANGE ARE ALSO VERY CLEARLY VISIBLE.....	105
FIGURE 3.29. FREQUENCY HISTOGRAMS OF PLUME AREA FOR 2007-2009 DURING INCOMING AND OUTGOING TIDES (REPRESENTED AS A BINARY VALUE).....	108
FIGURE 3.30. CTD PROFILES OF TEMPERATURE AND SALINITY COLLECTED ON 19 <sup>TH</sup> SEPTEMBER 2006 NEAR THE BELCHER GLACIER TERMINUS BY THE CCGS AMUNDSON (DENOTED BY A- CASTS) AND HERON LAUNCH VESSEL (DENOTED BY H- CASTS).....	110
FIGURE 3.31. CTD PROFILES OF TEMPERATURE AND SALINITY COLLECTED ON 22 <sup>ND</sup> AND 30 <sup>TH</sup> JULY 2008 FROM THE BELCHER GLACIER TERMINUS BY L. TARASOV. THE AVERAGE RESULTS ARE PRESENTED HERE FOR CLARITY AS 4 VERY SIMILAR CTD CASTS WERE WITHIN 50M OF EACH OTHER FROM THE GLACIER TERMINUS.....	111
FIGURE 3.32. CTD PROFILES OF TEMPERATURE AND DEPTH OFFSHORE THE BELCHER GLACIER (IN JONES SOUND, BETWEEN DEVON ISLAND AND ELLESMERE ISLAND) BETWEEN AUGUST 1978 AND AUGUST 1997. DATA FROM THE WORLD OCEAN DATABASE 2005 (BOYER ET AL., 2005).....	112
FIGURE 3.33. MONTHLY SSTA VALUES FROM THE 1KM GRID CELL CLOSEST TO THE BELCHER GLACIER TERMINUS (75.5°N, -81.5°W). NOTE THAT THE SSTA IS RELATIVE TO A 1971-2000 BASELINE.....	113
FIGURE 3.34. BATHYMETRY OFFSHORE FROM THE BELCHER GLACIER TERMINUS. DATA COLLECTED BY THE CCGS AMUNDSEN IN SEPTEMBER 2006 (BELL AND HUGHES-CLARK, 2006). NOTE THE POSITIONS OF THE GLACIER MARGIN IN JUNE AND AUGUST 2009, AS WELL AS THE	

LOCATION OF A TROUGH AND MORAINES. THE NORMAL POSITION OF EMERGENCE OF THE MELTWATER PLUME IS ALSO SHOWN..... 116

FIGURE 3.35. EXAMPLE OF SMALL WATER JETS WHICH EMERGED NEAR THE START AND END OF THE SEASON WHEN THE PLUME WAS SMALL. IMAGE (A) WAS JULY 14<sup>TH</sup> 2009 AT 3PM AND (B) WAS JULY 31<sup>ST</sup> 2009 AT 7PM (NOTE THE JET WHICH IS OFFSET FROM THE ICE CLIFF)..... 117

FIGURE 3.36. A MELTWATER PLUME EMERGES HORIZONTALLY FROM A SUBGLACIAL CHANNEL AND THE MOMENTUM OF THE WATER CAUSES IT TO FLOW AWAY FROM THE GLACIER FRONT, CREATING A CURVED TRAJECTORY. THE LARGER AND STEEPER THE GROUNDING FAN, THE CLOSER TO THE ICE FRONT THE PLUME WILL APPEAR AT THE SURFACE. ONCE AT THE SURFACE THE MELTWATER SPREADS RADIALY AS A SURFACE GRAVITY CURRENT. THE INSET SHOWS A VERTICAL CROSS SECTION OF THE PLUME IN WHICH SEDIMENT IS DROPPED AT ANGLES GREATER THAN  $\beta$  (FIGURE FROM MUGFORD AND DOWDESWELL, 2011)..... 118

## List of Abbreviations

ASTER	Advanced Spaceborne Thermal Emission and Reflection Radiometer
AVHRR	Advanced very high resolution radiometer
AWS	Automatic Weather Station
BCAWS	Belcher Camp Automatic Weather Station
BP	Before present
CAA	Canadian Arctic Archipelago
CTD	Conductivity Temperature Depth
DEM	Digital Elevation Model
ENVI	ENvironment for Visualizing Images Software
EOP	External Orientation Parameter
GCP	Ground Control Point
GEOTIFF	Georeferenced information embedded in a TIFF file
GPR	Ground Penetrating Radar
GPS	Global Positioning System
HDF	Hierarchical data format
IOP	Internal Orientation Parameter
IPCC	Intergovernmental Panel on Climate Change
IPY	International Polar Year
K1	Lunar-solar tide
LBAWS	Lower Belcher Automatic Weather Station
M2	Semi-diurnal principal lunar tide
MIMC	Multi-Image Multi-Chip
MOD09	Surface Reflectance product from the MODIS Terra satellite
MODIS	Moderate Resolution Imaging Spectroradiometer
MRT	Modis Reprojection Tool
MYD09	Surface Reflectance product from the MODIS Aqua satellite
N2	Lunar elliptic tide
NASA	National Aeronautics and Space Administration
NOW	Northern Open Water (Polynya)
O1	Diurnal principal lunar tide
PIV	Particle Image Velocimetry
RES	Radio Echo Sounding
RMSE	Root Mean Square Error
ROI	Region of Interest
S2	Principal solar tide
SLR	Sea level rise
SPOT	Système Probatoire d'Observation de la Terre satellite
SST	Sea Surface Temperature
SSTA	Sea Surface Temperature Anomaly
TIFF	Tagged Image File Format
UTM	Universal Transverse Mercator coordinate system

# Chapter 1. Introduction

## *1.1 Motivation*

The largest outlet glaciers in the world terminate in the ocean, as grounded tidewater margins, floating ice tongues or ice shelves. Glaciers connected to the ocean can lose mass by iceberg calving as well as surface melt and they may be more responsive to climate forcings because they are connected to an additional heat sink: seawater (Nick et al., 2009). Tidewater glaciers in the Northern Hemisphere, whether grounded on the bed at the calving margin or floating above it, can lose up to 50% of their total annual mass loss through iceberg calving (Rignot et al., 2008). The icebergs which calve from these margins range in size from columnar shards less than a meter wide to extremely large tabular blocks several kilometers in width. Small columnar blocks are usually lost at a frequent rate on well grounded glaciers, whilst tabular blocks are calved more infrequently from floating termini. Therefore the calving rate and style reflects whether or not a glacier is grounded to its bed. Whilst there have been several attempts to parameterize the calving process, it remains the most poorly understood component of glacier mass balance. There are many calving glaciers but recent research has focused on only a small number (e.g. Columbia Glacier, Alaska, Jakobshavn Isbrae, SW Greenland and Helheim Glacier, SE Greenland). The contribution of calving to mass loss and the processes which control it are largely unknown in some regions, such as the Canadian Arctic. The Canadian Arctic Archipelago (CAA) holds the third largest volume of land ice after the two large ice sheets on Greenland and Antarctica (Radic and Hock, 2010). The greatest Arctic contribution to sea level rise during the coming century is predicted to be from the CAA and Alaska where there are many tidewater glaciers (Meier et al., 2007; Radic and Hock, 2011). Gardner et al. (2011) recently observed that between 2007 and 2009 the CAA became the largest contributor to global sea

level rise outside the Greenland and Antarctic ice sheets ( $0.24 \pm 0.03 \text{mm a}^{-1}$  SLR). However the calving component of this mass loss is unknown and the processes governing calving in this region have not been researched in detail. The primary aim of this study is therefore to investigate the dynamics of calving mass loss on the Belcher Glacier terminus, a tidewater glacier on Devon Island in the Canadian Arctic. This will involve:

- Testing methods for detecting iceberg calving events: time lapse imagery, audio recordings, and geophones
- Identifying potential triggers for these calving events, and determining whether the timing of calving events is influenced more by:
  - Glacier dynamics (terminus velocity or proximity to buoyancy which is determined by glacier and bed geometry)
  - External variables at the ice-ocean interface (subglacial meltwater flux, the downward propagation of terminus water-filled crevasses, changes in mélange/sea ice buttressing of the glacier terminus, tidal flexure of the terminus region or changes in ocean temperature which alter basal melt rates and undercut the ice cliff)

## ***1.2 Review of Iceberg Calving Detection Methods***

Iceberg calving is the detachment of ice from the main body of a glacier which terminates in water (Benn and Evans, 2010). Calving results when new or pre-existing fractures propagate through the ice thickness, eventually isolating an ice block (Benn et al., 2007b; Cuffey and Paterson, 2010). It can occur on glaciers which end in proglacial lakes, on land-terminating glaciers with terminal ice cliffs, or on marine-terminating glaciers and ice shelves. For tidewater glaciers grounded on the fjord bed, calving takes place at the grounding line (the position where the ice starts to float because the basal water pressure exceeds the ice overburden pressure (Van der Veen, 2002)). Iceberg calving from floating tidewater glaciers can take place up to several kilometers seaward of the

grounding line. On ice shelves this may be at a distance of several hundred kilometers from the grounding line (Benn and Evans, 2010).

This section will review the field methods that have been used to detect iceberg calving events on tidewater glaciers. One of the reasons that there has been less research on iceberg calving than on surface melt is that the glacier terminus region often contains a complex crevasse field which is constantly changing and can be difficult and dangerous to access. In the last ten years digital time lapse photography, digital audio equipment, and seismometers have made it easier to monitor the terminus region from afar and detect calving events. These techniques are reviewed below.

### **1.2.1 Time Lapse Imagery**

Time lapse images are valuable sources of data for many environmental monitoring applications, including glacier change detection. One of the first studies of calving to utilize time lapse cameras was made by Krimmel and Rasmussen (1986) on the Columbia Glacier in Alaska. They used a film camera to measure the daily displacement of ice in the terminus region and changes in the position of the calving front. O'Neel et al. (2003, 2007) used Krimmel and Rasmussen's photogrammetry model to calculate the iceberg calving rate and volume of ice lost from LeConte Glacier, Alaska, with the addition of stake velocity data from O'Neel et al. (2001). These applications used mono-photogrammetry, where the two-dimensional measurements of features in a single photograph can be obtained by georeferencing their XY coordinates (Chapuis et al., 2010), an approach which is becoming more popular than traditional stereo photogrammetry. Stereo photogrammetry (where two or more images are used to rectify topography) is still necessary if the vertical coordinates of the image scene are required (Chapuis et al., 2010) but mono-photogrammetry is simple, fast and easily automated. It is ideal for change detection studies because multiple georeferenced images can easily be compared and the area of change computed. However mono-photogrammetry only produces a relative position of the terminus

based on the parameters of the camera and not a 'true' position (e.g. compared to a terminus margin mapped from georeferenced satellite images).

Images also provide information about the style of calving events that can be used to infer whether or not the glacier is grounded. For example, grounded glaciers tend to lose small amounts of mass very frequently, often as low volume columnar shards. For instance, in 2008 on Kronebreen, Svalbard, there were 41 calving events in four days, in which ice was lost mainly as columnar blocks (Chapuis et al., 2010). In contrast, floating glaciers often lose most of their mass in large, infrequent calving events which produce tabular blocks calved from up to 50% of the ice front width at once (Walter et al., 2010). Walter et al. (2010) observed the transition of Columbia Glacier from grounded to floating in time lapse imagery from 2007 and noted an associated change in the style of calving. The icebergs calved switched from frequent, low volume columns to large tabular blocks that were rifted perpendicular to flow. However, the tabular blocks calved from the Columbia Glacier tended to disintegrate during and immediately after the event, which may suggest that the highly fractured floating tongue is not stable (Walter et al., 2010). Jakobshavn Isbrae is also an unusual tidewater glacier as it is grounded in the summer and develops a floating tongue in the winter (Amundson et al., 2008). The glacier had a 10-15km long permanently floating tongue until it disintegrated in the early 2000s (Joughin et al., 2004; Motyka et al., 2010). Time lapse imagery suggests that Jakobshavn Isbrae may begin to float in the winter as the terminus advances ~5km into deeper water and calves back to a grounded position by late summer (Amundson et al., 2008).

The interval between time lapse images is also an important factor in observing calving events. A short time interval between images is ideal for capturing the full sequence of a calving event but this must be weighed against the data storage capacity restrictions of SD (Secure Digital) cards. Amundson et al. (2010) installed four cameras at the terminus of Jakobshavn Isbrae in 2008 to monitor its seasonal evolution. Image intervals ranged from 10 seconds to 6 hours. Images at

a 10 minute interval usually captured action scenes of longer duration events but an additional camera with a 10s interval gave the highest resolution results and was useful for comparison to seismic and acoustic data. However the camera operating on the 10s time interval failed to operate after one week and there was a very large data storage demand (Amundson et al., 2010). These results indicate that accurate detection of calving events, with information about the style of berg produced and its breakup pattern can only be obtained with a short interval between time lapse images; but this must be balanced against available data storage capacity and how often the data can be downloaded.

### **1.2.2 Audio Recordings**

As time lapse photography becomes more widely used, it is also being used alongside other techniques such as acoustic recording of calving events to gain further information about the timing and sequence of calving processes.

Amundson et al. (2010) were the first to use an audio recorder to obtain temporal detail about calving events from Jakobshavn Isbrae, Greenland. They installed two stereo condenser microphones located 50m apart in order to better determine the source direction. The Tascam HD-P2 stereo audio recorder made a total of 28 days of recordings between May and August 2008, although the storage medium (compact flash cards) had to be manually switched every 12 hours. A windshield was used to reduce wind noise but the recorder was installed in a relatively exposed location and some calving events were not distinguishable above background noise (J. Amundson, pers. comm., 2009). Nevertheless, the audio system detected several events, which were compared with 10s time lapse imagery and seismic data. Amundson et al. identified three types of seismic/acoustic signal:

- (1) impulsive signals, duration 1-5s, frequency 6-9Hz, sharp cracking sound ('shotgun blast')- likely to be fracturing ice
- (2) emergent signals, duration 5-300s, frequency 4-6Hz, long low rumblings- likely to be avalanching ice debris

- (3) emergent, high-amplitude signals, duration 5-60min, combination of cracks and rumbles- likely to be generated by calving icebergs, or bergs overturning in the fjord

Calving events at Jakobshavn Isbrae typically began with widespread fracturing or avalanching of debris from the terminus and were increasingly accompanied by detectable seismic activity over time. Amundson et al. (2010) were not able to detect motion at the terminus front prior to the calving being initiated. As the iceberg began to rotate and break off, the mélange of sea ice and calved debris in front of the calving margin would loosen and adjust, whilst there was an increase in the number of audible type 1 events. Amundson et al. did not observe persistent debris avalanching (type 2) during calving events at Jakobshavn. Much of the seismic energy attributed to a calving event was generated by the mélange offshore from the terminus (Amundson et al., 2010). An example of the seismic and acoustic returns from a calving event at Jakobshavn is shown in Figure 1.1.

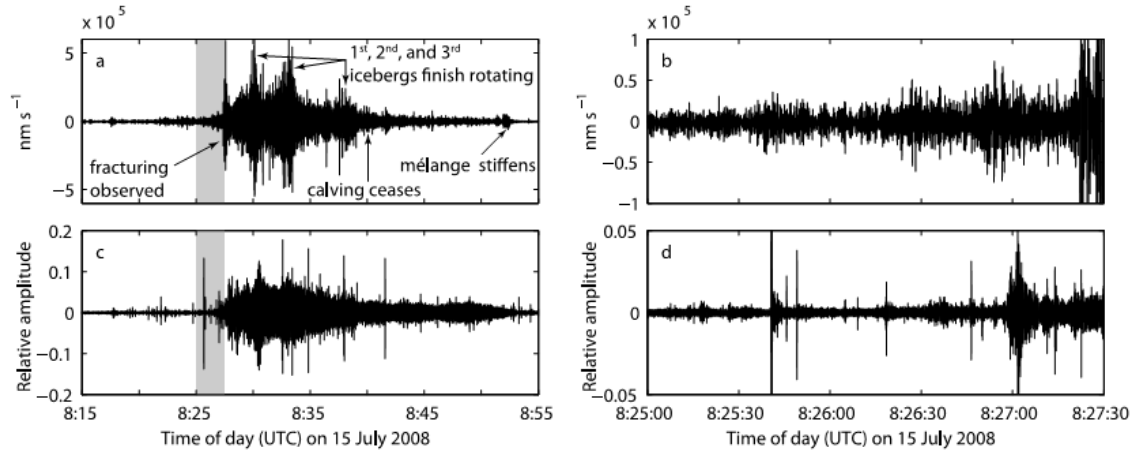


**Figure 1.1.** Seismic and acoustic waveforms from a calving on 15<sup>th</sup> July 2008 at Jakobshavn Isbrae, SW Greenland, as observed by Amundson et al. (2010). (a) Vertical component of the calving-generated seismogram (b) Close-up of Figure 1.4a showing the emergent onset of the seismic signal (c) Acoustic waveform from the calving event (d) Close up of Figure 1.1c. The gray bars in Figures 1.1a and 1.1c indicate the time periods shown in Figures 1.1b and 1.1d. Figure and accompanying text from Amundson et al. (2010, p6).

### 1.2.3 Geophones

One of the main challenges in observing and modelling iceberg calving events is the non-linear, three-dimensional character of tidewater glaciers (Pfeffer, 2007). Glaciers have fracture mechanisms comparable to those that cause an earthquake (as well as being equally hard to predict in size and timing), which led to the recent introduction of seismic monitoring to glaciology. Neave and Savage (1970) used an eight-geophone array to examine fracture events ('icequakes') at depth and on the surface of the Athabasca Glacier in the Canadian Rockies. They found that all fractures originated near the ice surface, within crevasse zones, although icequake swarms would sometimes travel in a line through a crevasse-free section of the glacier. Qamar (1988) identified several types of icequake from different source mechanisms: calving events, earthquakes, and crevassing activity. However it was not until Ekstrom et al. (2003) used a global network of 100 seismometers designed for monitoring earthquake activity to identify 'glacial earthquakes' that others were encouraged to try seismic monitoring on glaciers. The 'glacial earthquakes' produce large-amplitude, long-period teleseismic waveforms that last ~50 seconds (Tsai and Ekstrom, 2007). They had previously gone undetected as they do not generate elastic waves across a fault surface like tectonic earthquakes, which are detected in seismograms by high-frequency (1 second) *P* (primary) waves (Ekstrom et al., 2003; Nettles and Ekstrom, 2010). Teleseismic waves have long durations like large magnitude elastic waves but lack the easily detectable high frequency *P* wave (Nettles and Ekstrom, 2010). Amundson et al. (2008; 2010) demonstrated that seismograms of 'glacial earthquakes' produced at Jakobshavn Isbrae closely resemble seismic activity during known calving events, suggesting they are most likely to be a product of the same causal mechanism. Whilst it is mostly accepted that glacial earthquakes are part of the continuum of ice-generated seismic activity, the source mechanisms are still under debate and there may be several sources. The seismicity is typically located less than 1km from the terminus but could be from a number of mechanisms and is not necessarily a product of calving. Possible source mechanisms include: stick-slip sliding acceleration of the glacier terminus

(Ekstrom et al., 2003; Nettles et al., 2008), overturning icebergs which scrape the fjord bottom (Amundson et al., 2008), hydraulically-driven fracture propagation (O'Neel and Pfeffer, 2007, see below), ocean wave action (Amundson et al., 2008; MacAyeal et al., 2009) and motion of the ice mélange or sea ice (Amundson et al., 2010). The ice mélange is described as a mixture of rifted icebergs, cemented by sea ice, snow and 'bergy bits' (J. Amundson, Cryolist discussion, 01/11/2010). It is common in Antarctica and southern Greenland.

Several projects have now installed a network of passive seismometers on or near the glacier terminus to detect and monitor calving events. Calving events produce low-frequency waveforms (1-3Hz) which are emergent (long-period) and have long duration (2-1000s). Meanwhile crevassing events have impulsive onsets, short durations (0.1-1s) and a high frequency (~100Hz) (O'Neel et al., 2007). O'Neel et al. (2007) were able to reliably identify the temporal frequency, relative magnitude and hypocenter (event location) of calving events at the terminus of the Columbia Glacier, Alaska, using passive seismometers. The events were validated with time lapse images. It is only possible to infer a relative magnitude of calving events as the spectral power of the seismic records is always focused at 1-3Hz regardless of event size (O'Neel and Pfeffer, 2007). O'Neel and Pfeffer (2007) simulated these fracture events using a fluid-filled crack source model and suggest that the seismic signal is generated by fracture propagation of water-filled crevasses because both sub-aerial and submarine calving events produce waveforms with similar frequencies, indicating a common source mechanism. Walter et al. (2008) attempted to differentiate between surface and basal fracture activity, and found that basal icequakes tended to occur when basal water pressures were low, rather than following a lake drainage event which would bring temporary high basal water pressures, as they had expected. Seismic activity has also been detected upstream of the calving front, though most of the larger events tend to occur near the terminus (O'Neel and Pfeffer, 2007). This suggests that fluid-driven fracturing weakens the ice long before it reaches the terminus region. Amongst other factors such as air temperature, the role of meltwater in

crevasse fracture propagation may also explain why most calving events occur during the summer melt season (O’Neel and Pfeffer, 2007).

Monitoring seismic activity can also provide further information about the degree of buoyancy of a glacier terminus. Walter et al. (2010) observed that following the transition of Columbia Glacier to floating ice in 2007, there was a substantial reduction in the generation of seismic energy during calving events. This may partly reflect a change in source processes. They propose that calving of floating ice is not initiated by hydraulic fracture propagation of large crevasses, but by small linkages of existing damage which result in the reduction of seismic activity.

### ***1.3 Review of Potential Calving Triggers***

The termini of tidewater glaciers are in direct contact with the ocean and are therefore likely to be affected by external forcing factors that influence terminus stability and calving rate, as well as by those that control the surface mass balance of the glaciers (Dowdeswell, 2006). For example, some glaciers have been observed to be weakly or discontinuously sensitive to tidal forcings (Nettles et al., 2008; Walter et al., 2010). Other factors that can affect the short or long-term stability of tidewater termini include: buttressing of the glacier margin by ice mélange or sea ice, changes in the subglacial meltwater flux and water pressure in the subglacial drainage system, and varying basal melt rates (which are affected by ocean temperatures). However it is unlikely that any one variable is the sole controlling factor at any stage as these influences will change over time and may vary across different parts of the calving front depending on factors such as the bed geometry and the location of subglacial meltwater channels. This indicates that the terminus geometry, as well as ice flow dynamics (both categorized here as ‘internal drivers’) are significant controls on terminus dynamics and stability.

Amundson and Truffer (2010) summarized several parameterizations that have been proposed to model calving rates:

1. Relating the annual mean calving rate of 12 grounded Alaskan glaciers to water depth at the terminus (Brown et al., 1982)- which intuitively reflects glacier and basin geometry
2. Calculating the terminus position of grounded glaciers using the assumption that calving will occur if the ice thickness becomes less than the critical buoyant thickness defined by a height-above-buoyancy/flotation criterion (Sikonia, 1982; Vieli et al., 2001)
3. Equating the mean calving rate of ice shelves to the ice shelf thickness, width and longitudinal strain rate (Alley et al., 2008)
4. Calculating the terminus position based on crevasse depths, longitudinal strain rate and the amount of water ponding in crevasses, with calving being triggered once surface crevasses propagate to the glacier freeboard (sea level) (Benn et al., 2007a). This is the only model applicable to both grounded and floating termini but it still does not explain all calving variability (Amundson and Truffer, 2010). For example Jakobshavn Isbrae advances during the winter and begins to calve icebergs in early spring, before surface melt or enhanced summer velocities begin (Amundson and Truffer, 2010)

These parameterizations point to several possible internal and external forcings that might trigger calving events, which will be considered in the following section.

### **1.3.1 Terminus Velocity**

Joughin et al. (2008) observed that the terminus of Jakobshavn Isbrae exhibits a velocity increase after terminus retreat, rather than prior to it. Joughin et al., as well as Meier and Post (1987) and Howat et al. (2005), all argue that calving reduces the near terminus longitudinal stress, which translates into a velocity increase that propagates upglacier for a distance of up to 10 ice thicknesses (Vieli

and Nick, 2011). This observation is part of an ongoing debate about whether iceberg calving is a 'slave' or 'slave-driver' (Benn et al., 2007b). In the example above, calving is the 'slave-driver' but this is in direct contrast to the popular assertion by Van der Veen (2002) and many others that ice velocity is the primary control on the iceberg calving rate (calving is the 'slave'). This is based on the principle that the velocity flux determines the rate at which ice is delivered to the terminus, and then calved from its margin. Yet there is little definite evidence to suggest that iceberg calving is always a response to velocity increases, or vice versa (Benn et al., 2007b). O'Neel et al. (2003) observed that Columbia Glacier did not seem to demonstrate either 'slave' or 'master' tendencies. Meanwhile Hulbe et al. (2008) discovered that after the break-up of the Larsen B ice shelf in 2002 some of the glaciers that used to feed it accelerated and advanced in response to the loss of the shelf, whilst others demonstrated prolonged retreat and the rest maintained a stable front position. The ice shelf buttressed these glaciers but the response to calving away from the shelf was not linear despite the glaciers being in the same geographic area, and experiencing similar mass balance conditions. In this case, local geometry was the primary control on the response of the glaciers feeding Larsen B: wider glaciers retreated further as they experienced less lateral drag from their valley walls which made them more responsive to the reduced longitudinal stresses caused by the loss of shelf buttressing (Hulbe et al., 2008).

Ahn and Box (2010) used time lapse photography to examine the interactions of velocity and calving on several glaciers in West Greenland. They applied the Multi-Image/Multi-Chip (MIMC) cross correlation technique, which is often used in remote sensing (e.g. Scambos et al., 1992), to calculate the daily velocity. The images were co-registered using ground control points (GCPs, landmarks manually picked from ASTER imagery and the ASTER digital terrain model). Pixel displacements were then projected onto a flat surface based on the rotation angles of the camera position, from which velocities ( $\text{m d}^{-1}$ ) could be derived. There were large errors in the co-registration procedure as the GCPs were not

measured by GPS, giving a conservative error of  $\pm 30\text{m}$  at  $3\text{km}$  distance from the target (Ahn and Box, 2010). The *resolvable lapse interval* (the time interval over which a displacement above the uncertainty can be identified) was a function of the daily glacier velocity, the image pixel size, camera focal length, accuracy of the registration/georeferencing procedure, the image resolution and the distance from the camera to the glacier:

$$\Delta d = \left( \frac{\varepsilon}{(\Delta p / 24)} \varepsilon_b \right) \times 100\% \quad (1)$$

where  $\Delta p$  represents ice displacement in pixels per day,  $\Delta d$  is the time interval in days,  $\varepsilon$  is uncertainty (in pixels) and the error budget ( $\varepsilon_b$ ) is the proportion of error (0-1) you are willing to accept. For example selecting an error budget of 0.3 (30%) rather than 0.5 (50%) requires more confidence and makes the resolvable lapse interval longer. Rink Isbrae had a resolvable lapse interval of 4.5 hours because it moved on average  $14\text{m}$  per day (14-18 pixels). A glacier moving less than  $2\text{m}$  per day would require a time interval of  $>1$  day for displacement to exceed the uncertainty (Ahn and Box, 2010). The results suggested that major calving events on five glaciers in western Greenland drive terminus acceleration for up to 10 days after the event, after which the velocity declines as resistance to flow rebuilds. The technique only worked well for areas near the camera, for ice nearest the terminus margin, and for the fastest flowing areas. In all other regions the daily displacement was not as large as the uncertainty. Further research into the relationship between ice velocity and calving events is clearly necessary.

### 1.3.2 Water-filled Crevasses

Meltwater is thought to be a key trigger mechanism in ice shelf collapse, as water pressures in crevasses filled to the surface with water are likely to exceed the ice overburden pressure and cause the fracture to propagate through the full ice thickness (Scambos et al., 2000). For example, Larsen B Ice Shelf on the Antarctic Peninsula exhibited extensive surface melting for several years prior to its collapse in March 2002, which is likely to have weakened the ice. Final break-

up appears to have been driven by water-filled crevasse propagation (Scambos et al., 2004). However the role of water-driven crevasse propagation in triggering calving events on tidewater glaciers is less clear, and requires a detailed quantitative assessment (Vieli and Nick, 2011). It is well known that meltwater can reach the bed of temperate glaciers through hydraulic fracturing of crevasses (which often creates moulines). Water reaching the bed enhances the sliding velocity of the glacier (e.g. Iken et al., 1983), but only more recently has it been understood that this also occurs on larger ice sheets such as in Greenland (e.g. Zwally et al., 2002) and on polythermal glaciers in the High Arctic (e.g. Copland et al., 2003). Water-filled surface crevasses can propagate to the glacier bed, opening the englacial connection to the subglacial drainage system on a timescale of days (Boon and Sharp, 2003) to hours (Das et al., 2008). Benn et al. (2009) mapped englacial drainage systems within several glaciers in Svalbard, Nepal and Alaska. They observed that hydrofracturing occurred in a diverse range of glaciological regimes and that it appears to be a very widespread process, potentially occurring wherever ice is subjected to large tensile stresses, such as in icefalls and terminus crevasse zones, where there is also a high meltwater supply. Supraglacial ponds and lakes may play a particularly significant role in this process as they provide an elevated head of water at the ice surface which assists in the fracturing process (Boon and Sharp, 2003). Further information about the routing system between small water-filled crevasses in the terminus zone and the subglacial drainage system would indicate whether water is penetrating to the bed via fractures, and how quickly these connections are established. The accumulation of supraglacial meltwater on the terminus ice surface may weaken the ice and prime it for calving when the ice arrives at the margin but it is not clear whether water-driven fracture propagation actually takes place close enough to the terminus margin to actually initiate calving events. Johannessen et al. (2011) compiled a 30-year record of ice-front variations of Helheim Glacier, SE Greenland and observed a strong correlation between a retreated ice position and higher air temperatures, which explained 56% of the ice-front changes when a two-year lag was applied. They proposed that the warmer air temperatures

enhanced surface melt and led to more accumulation of water in terminus crevasses, increasing basal lubrication which presumably caused thinning, acceleration, enhanced calving and margin retreat. This suggestion also needs to be examined more closely.

### **1.3.3 Meltwater / Sediment Plume**

Glacial meltwater travels via supraglacial, englacial and subglacial routes through and over the ice, often flowing into proglacial streams and lakes, or into the ocean if the glacier is marine-terminating. Water exiting the glacier into an ocean or lake forms a meltwater plume, and is often clearly distinguishable as the water contains large quantities of sediment when it exits the base of the glacier (Powell, 1991). This sediment-laden fresh water rises quickly to the surface above the denser marine water, and it spreads laterally to form a buoyant plume (McGrath et al., 2010). This subglacial discharge can raise the basal water pressure and enhance local flotation which could trigger a calving event. The plume can also thin the surrounding ice because its turbulent fresh water enhances the basal melt rates, and this may increase the local calving rate (Motyka et al., 2003). In order to investigate these relationships, the plume extent can be mapped and used to quantify the amount of meltwater being discharged from the glacier, which can then be compared to the calving flux. Chu et al. (2009) examined MODIS satellite imagery of meltwater plumes discharged near Kangerlussuaq, W Greenland and distinguished between ‘turbid’ sediment-rich plume water found closest to the terminus which has very low salinity, and ‘brackish’ plume water found in the intermediate mixing zone between turbid and clear ocean water, where the suspended sediment concentration is lower and salinity is higher. Chu et al. (2009) focused on mapping the brackish plume and found it extended 5-65km beyond the turbid plume boundary (Chu et al., 2009). The turbid plume contains more concentrated glacier meltwater and may be a better gauge of meltwater discharge; however it has not yet been mapped in detail throughout a meltwater drainage season.

Halverson and Pawlowicz (2008) found that plume area, delimited from MODIS satellite imagery, is a robust measure of discharge which provides a high temporal resolution. Chu et al. (2009) and McGrath et al. (2010) both mapped the river plume emerging into Kangerlussuaq Fjord, West Greenland, which is fed by several outlet glaciers. Plume occurrence correlated with melt onset and conclusion but the plume appeared to disappear before meltwater runoff ended, possibly implying a late-season exhaustion of the sediment supply (Chu et al., 2009; McGrath et al., 2010). It was expected that plume area would increase directly due to supraglacial lake drainage events and melt pulses, but only 38% of lake drainages and 69% of melt pulses triggering an increase in plume area (Chu et al., 2009). Further investigation of the relationship between lake drainage events and meltwater discharge responses is needed, as well as consideration of whether large changes in subglacial discharge, which will increase basal water pressures, could instigate local flotation or ice velocity acceleration and trigger a calving event. Motyka et al. (2003) also suggest that meltwater plumes often enhance the local calving rate and create a seasonal embayment due to the mixing of the plume with seawater, which increases the basal melt rate below the waterline.

#### **1.3.4 Mélange / Sea ice buttressing**

Glaciers feeding the Larsen B Ice Shelf in Antarctica sped up following the loss of the ice shelf in 2002, as was already mentioned, and this also occurred on Jakobshavn Isbrae when the floating ice tongue broke up in the early 2000s (Joughin et al., 2008). In both situations, the ice tongue or shelf had been ‘buttressing’ the grounded ice behind it, increasing the longitudinal stress and hence impeding its flow. Large calving events can force a redistribution of resistive stresses once floating ice is lost, leading to the upglacier propagation of a velocity increase (e.g. Nettles et al., 2008). This longitudinal coupling can occur over a distance of up to 10 ice thicknesses, or 15-20km on large outlet glaciers (Vieli and Nick, 2011). However the possible buttressing effect of more

temporary features like ice mélange and sea ice has only recently been recognized and its importance has not yet been widely tested. Amundson et al. (2010) proposed that the ice mélange in front of Jakobshavn Isbrae, which is a dense mixture of calved icebergs cemented together by sea ice, becomes so rigid during winter that it may act as a floating ice tongue, buttressing the glacier's flow. During the winter it stems the production of icebergs and its buttressing effect only diminishes in the late spring when air temperatures rise. At Jakobshavn Isbrae, the onset of terminus retreat in spring coincides more strongly with the breakup of the ice mélange than with the rising air temperatures and initiation of surface melt (which begin later), indicating that the mélange may play a significant role in terminus stability. This was also the conclusion of Sohn et al. (1998), who found that the iceberg calving rate at Jakobshavn Isbrae (1950-1996) was six times higher in the summer than in winter, and that it gradually decreased as the mélange/sea ice consolidated, increasing its buttressing resistance. Vieli and Nick (2011) modeled the buttressing effect by applying a small nominal longitudinal stress of 40kPa at the terminus boundary during the winter, which was the minimum value required to recreate the seasonal variations in terminus position at Jakobshavn Isbrae. However the actual compressive strength of sea ice has not yet been measured so this value was arbitrary.

Whilst ice mélange may buttress a glacier, it is less clear whether a sea ice slab can do the same. Amundson et al. (2010) suggest that first year sea ice (<1-2m thick) may temporarily buttress tidewater glaciers and limit calving activity whilst the sea ice is present. Copland et al. (2007) found that the Ayles Ice Shelf on Ellesmere Island in the Canadian High Arctic eventually disintegrated after the warmest summer on record led to enhanced meltwater ponding on the ice surface, as well as low sea ice conditions and loss of the landfast sea ice fringe that may have been stabilizing the ice shelf. The eventual calving seems to have been driven by high winds. Reeh et al. (2001) observed that the stability of Nioghalvfjærdsfjorden glacier, a floating glacier in northeast Greenland was dependent on the presence of fast-ice cover in front of the terminus. No calving

occurred when the sea ice was present, although the glacier continued to advance, indicating the sea ice did not have enough buttressing resistance to completely halt winter glacier flow. Instead, the sea ice tended to merely prevent the partly disintegrated glacier front from calving off. It is not clear whether the same resistive capacity can be expected on grounded glaciers. Herdes et al. (in review) argued that major iceberg calving events from the Belcher and Fitzroy Glaciers on Devon Island in the Canadian High Arctic could be primarily related to the timing of the loss of sea ice, but break-up only occurs once a year and if calving takes place at other times of the year this argument does not fully explain the calving rate. Furthermore it is not clear whether sea ice break-up is associated with a major calving event every year. Williamson et al. (2008) found that some glaciers on Ellesmere Island responded to the removal of summer sea ice with a velocity increase, whilst others did not, implying that sea ice loss is not a necessary or sufficient condition for seasonal velocity changes. The buttressing resistance of sea ice and mélangé has not yet been well investigated, particularly on glaciers smaller than Jakobshavn Isbrae which produce fewer icebergs and therefore have a higher sea ice to iceberg ratio.

### **1.3.5 Tidal Flexure**

Tides have semi-diurnal (twice daily), diurnal (daily) and long-period components which may control aspects of terminus stability including ice velocity (possibly due to the influence on basal water pressure) and the proximity to flotation (which can affect the calving flux). Tides have been implicated in driving a proportion of the velocity variability of ice shelves and ice streams in Antarctica, including the Rutford Ice Stream, West Antarctica, where there is a 10-20% modulation of surface velocity in response to a fortnightly tidal periodicity (Gudmundsson, 2007; Murray et al., 2007). Walters and Dunlap (1986) identified semi-diurnal and diurnal tidal influences on the velocity of Columbia Glacier, Alaska, with a 20% modulation of velocity per meter of water height. Meanwhile O'Neel et al. (2001) observed an out-of-phase relationship between the semi-diurnal tide and

horizontal ice speed of LeConte Glacier, Alaska, due to the effect of tidal buttressing on longitudinal stress. The ice near the terminus rose and fell in phase with the tide, indicating that some of the ice nearest the terminus was close to flotation. There was also a smaller diurnal signal in ice velocities but this reflected ablation and surface meltwater input rather than the diurnal component of the tide as this was quite small (O'Neel et al., 2001). Nevertheless, there are a number of glaciers where no tidal influence on velocity can be identified, generally well grounded glaciers such as Jakobshavn Isbrae in summer (Amundson et al., 2010). De Juan et al. (2010) note that the response of tidewater termini to tidal forcing can also vary over time: for example Helheim Glacier in SE Greenland ordinarily displayed a barely-detectable response to tidal changes but following a calving event with associated glacial earthquake seismicity there was suddenly a substantial response to tidal fluctuations. They propose that a simultaneous increase in velocity and surface strain rate disrupted the subglacial drainage system, reducing the volume of subglacial channels and increasing the water pressure. This reduced friction at the ice-bed interface, allowing the glacier flow to respond more strongly to tidal changes.

Tides can also affect the meltwater plume because incoming tides push dense ocean water (beneath the plume) towards the terminus and can cause spreading of the surface plume (Dowdeswell and Cromack, 1991). Cowan and Powell (1990) found that the suspended sediment concentration (SSC) in the plume at McBride Glacier, Alaska is controlled by semi-diurnal fluctuations of the tide (mean tidal range 4.2m), with maximum settling of particles at low tide. Chu et al. (2009) assessed the meltwater plume in Kangerlussuaq Fjord, West Greenland, but found that there was no significant change in plume area in response to incoming or outgoing tidal patterns, although the tidal range in this area is negligible. The tides may also affect the stability of the terminus, particularly during spring tides (the largest in the fortnightly cycle) where the high tide creates greater flexure of the terminus ice and enhances its proximity to flotation, which is closely tied to the

subglacial effective pressure (O'Neel et al., 2003). The subglacial effective pressure ( $\rho_{eff}$ ) is defined as:

$$\rho_{eff} = \rho_i g h + \rho_{fw} g z_b - g h_w (\rho_w - \rho_{fw}) \quad (2)$$

where  $\rho_i$  is the density of ice,  $\rho_{fw}$  is the density of freshwater,  $g$  is the acceleration of gravity,  $h$  is ice thickness,  $z_b$  is bed elevation,  $h_w$  is the terminus water depth and  $\rho_w$  is the density of sea water (Meier and Post, 1987). Through their effect on subglacial water pressure, tides may also influence the iceberg calving rate. The control exerted by tidal action on the terminus stability (plume and calving flux activity) of smaller, grounded or floating tidewater glaciers has not yet been thoroughly considered.

### 1.3.6 Ocean Temperatures

Zweng and Munchow (2006) documented statistically significant warming of subsurface waters of the West Greenland Current at 400-2400m depth between 1920 and 2003, with warming of 0.2°C/decade at 600-800m depth. Holland et al. (2008) also discussed this trend, which was alluded to in Thomas et al. (2003), but implied a more rapid increase in temperatures due to a pulse of warm water originating in the Irminger Sea near Iceland which travelled up the west coast of Greenland during the late 1990s. Murray et al. (2010) note that this warm subsurface water does not normally reach the coast due to fresh waters being emitted from coastal glaciers. Nevertheless, Holland et al. reported that the warm subsurface waters flow over the sills which guard the mouths of most of the Greenland Fjords, in areas such as Disko Bay. At Jakobshavn Isbrae, the arrival of warm waters in 1997 coincided with initiation of rapid dynamic thinning of its floating tongue and the beginning of its disintegration due to increased basal melt rates (Motyka et al., 2011). Tidewater glaciers with floating termini are particularly susceptible to basal melting, which can be up to tens of metres per year (Thomas et al., 2003). For example between 1984 and 1985 Jakobshavn Isbrae experienced an average of  $0.62 \pm 0.13 \text{ m d}^{-1}$  of basal melt across the submerged floating ice tongue (Motyka et al., 2011). Rignot and Steffen (2008)

described an 80% thinning by basal melt of the floating tongue of Petermann Glacier, NW Greenland before calving took place, during the 2002-2005 observations. The warm Irminger-sourced current which has been melting Jakobshavn Isbrae is influenced by the North Atlantic Oscillation (NAO), an atmospheric phenomenon which switched to a prolonged negative phase in 1996. This produced weaker winds and allowed the North Atlantic subpolar frontal system (the boundary between cold polar waters and warm subpolar waters) to move further westward, with the warm subpolar water travelling even further west beneath the cold surface water (Holland et al., 2008). Laidre et al. (2010) were able to use temperature-salinity data gathered by tagged narwhals to investigate deep ocean temperature changes in Baffin Bay, and provided the first winter temperature data from below sea ice. The results confirmed the warming of Baffin Bay documented by Zweng and Munchow (2006), which does appear to be due to a warmer West Greenland Current. It remains unknown how long the warm water will continue to penetrate the coastline, and how far north the warm water will reach before the currents carry it south along the west coast of Baffin Bay. However new work by Andresen et al. (2011) suggests that there have been a number of episodes of enhanced iceberg calving from Jakobshavn Isbrae in the past c.5000 years due to subsurface warming of the West Greenland Current. Therefore, this most recent change in the current may be a recurrent phenomenon.

The Canadian Arctic Archipelago (CAA) is one of the major pathways for exchange of ice and water between the Arctic and Atlantic oceans, yet there is little information about water temperature changes, particularly within the channels of the archipelago. Rabe et al. (2010) provided information about the extent of the warm Atlantic-sourced water which is spreading up the coast of Greenland towards the Canadian Arctic. They examined a transect of moorings between Ellesmere Island and NW Greenland near 80°30'N. Warm saline waters existed below c.80m depth on the Greenland coast but became generally colder, fresher and thinner upon approach to Ellesmere Island, where most of the water is sourced from the Arctic Ocean via the Archipelago channels. Most of the warm

subsurface water that is following the West Greenland Current turns west in northern Baffin Bay and flows south past Baffin Island but a small proportion continues further north along Greenland and it is unknown whether any of this water actually reaches the CAA.

Murray et al. (2010) extended the evidence of ocean temperature forcing with research from the SE coast of Greenland where glaciers experienced rapid thinning, acceleration and retreat between 2003 and 2005. This also coincided with the penetration of warm Irminger subpolar water into the Eastern Greenland coastal fjords. In 2006 two of the largest glaciers in the region, Helheim and Kangerlussuaq, slowed down simultaneously and stopped thinning (Howat et al., 2007) when cold waters returned to the coast. This may have been part of a negative feedback loop, where increased meltwater discharge and calving from the glaciers increased the volume of cold, fresh water in the fjords (Murray et al., 2010). Murray et al. used moorings to monitor temperature and salinity at a range of depths, supplemented by sea surface temperature anomaly (SSTA) maps from the Reynolds SST dataset (Reynolds et al., 2002) and the MODIS SST product (Armstrong, 2002). These SST data are only representative of the ocean surface temperature but Murray et al. suggest that persistent high SSTs experienced in SE Greenland between 2003 and 2005 must also reflect the warm water at depth which was known to exist in separate measurements. Further research is clearly required to examine both this assumed association and the relationships between coastal glaciers and regional ocean temperatures more generally. Johannessen et al. (2011) examined the relationships between ocean temperatures in front of Helheim Glacier and its ice-front fluctuations from 1980 to 2010 using Argo float data and satellite imagery. They observed that warm Irminger-sourced water (up to 4°C) was reaching the glacier front below 250m depth and that 24% of the changes in terminus position over the 30-year time period could be explained by ocean temperature changes.

### 1.3.7 Terminus Geometry

Pfeffer (2007) identified a ‘dynamic instability’ in some calving glaciers in which thinning caused by rising surface air temperatures sufficiently alters the geometry of the glacier that the resistive stresses imposed by the valley walls and glacier bed can less effectively oppose the gravitational driving stress, leading to catastrophic terminus retreat. The instability is triggered when the ice thins enough to approach buoyancy, if the main resistance to flow is from basal drag. Pfeffer uses the example of the Columbia Glacier, which retreated dramatically in the 1980s. However many glaciers also experience lateral drag which introduces a stabilizing effect, generally more influential on narrower glaciers, and explains why not all glaciers exhibit this dynamic instability (Benn et al., 2007a). Pfeffer (2007) argues that once a glacier crosses the threshold into unstable geometry, the glacier is effectively decoupled from its mass balance and irreversible tidewater retreat can occur, driven by major changes in ice velocity and glacier geometry in response to seemingly insignificant climatic fluctuations. This may explain why various authors have viewed tidewater glaciers to be either sensitive (e.g. Joughin et al., 2008b) or insensitive to climate change (e.g. Meier and Post, 1987; Pfeffer, 2007). The glacier is not completely independent of mass balance, but the glacier is more indirectly affected by changing climate, compared perhaps to land-terminating or well-grounded glaciers. Nevertheless the transition into an ‘insensitive’ phase of glacier retreat is first triggered by a succession of negative mass balance years (Pfeffer, 2007).

The most recent changes in the Columbia Glacier, described by Walter et al. (2010), further demonstrate the importance of geometry in determining a glacier’s calving style and rate. Basin geometry was a key control on the development of floating ice at the Columbia Glacier in 2007: flotation only happened when the glacier retreated from an overdeepened valley constriction into a wider valley mouth which made the calving front three times longer. This also initiated fortnightly cycles of advance and retreat, with calving events affecting >50% of the glacier width at once. These changes partly reflect the water depth, as

described in the criterion by Brown et al. (1982) (which also included the Columbia Glacier in its dataset), later expanded by Pelto and Warren (1991):

$$U_C = 70 + 8.33D_W \text{ (m a}^{-1}\text{)} \quad (3)$$

Where  $U_C$  is the annual calving rate and  $D_W$  is the water depth. Nevertheless, it is primarily glacier and basin geometry that defines water depth and hence buoyancy. Each glacier system has a unique surface and basal geometry which means there may not be a physical law that can explain every aspect of a glacier's local environment.

## **1.4            *Research Objectives***

The primary aim of this study is to investigate the dynamics of calving mass loss from the Belcher Glacier in the Canadian High Arctic. There is very little information about the rate and style of calving events in this area, despite it being currently one of the largest contributing regions to global sea level rise (Gardner et al., 2011). The precise causes of individual calving events are often unclear because many factors act towards culmination in a calving event, some coincidental. Detailed analysis on an event-by-event basis may help to deconstruct the relationships between calving, glacier dynamics (ice velocity and proximity to buoyancy which is determined by glacier and bed geometry), and drivers at the ice-ocean interface (subglacial meltwater discharge, propagation of terminus water-filled crevasses, changes in mélange/sea ice buttressing, tidal fluctuations and ocean temperature changes which alter basal melt rates).

The main research questions this study will consider are:

1. Does the Belcher Glacier exhibit a calving style and rate which suggests it has a grounded or floating terminus in summer?
2. Are calving events on the Belcher Glacier triggered by:
  - a. A speed-up of the near-terminus region which may be caused by a meltwater pulse or drainage of the terminus water-filled crevasses, which enhance its proximity to flotation?

- b. Propagation of the terminus water-filled crevasses to the glacier freeboard?
- c. Removal of buttressing resistance provided by the mélange and sea ice?
- d. Tidal fluctuations, which reduce the height above buoyancy or lower the buttressing pressure of the seawater, whilst also influencing the meltwater plume discharge?
- e. A change in ocean temperatures, either at depth or at different times of the year, which could affect the sea ice concentration and/or basal melt rates?

## **1.5            *Thesis structure***

Chapter 2 introduces the field location: the Belcher Glacier on Devon Island in the Canadian Arctic, Canada. The methods used to investigate the iceberg calving and terminus dynamics of this tidewater glacier are reviewed. Field methods involved time lapse imagery, an audio recorder, geophones, GPS, meteorology stations and CTD casts.

Chapter 3 details the field data collected. The primary data source was time lapse images, supplemented with audio and geophone data to obtain an accurate calving event history. Potential triggers of calving events are identified and evaluated.

In Chapter 4 the results are further assessed to consider whether the Belcher Glacier has a grounded or floating ice terminus, and if any of the mechanisms examined can explain the calving variability on this glacier between 2007 and 2009. The implications of these results for other tidewater glaciers, particularly in the Canadian Arctic, are then summarized.

Finally, Chapter 5 reviews the conclusions drawn about the iceberg calving and terminus dynamics of the Belcher Glacier.

## Chapter 2. FIELD SETTING AND METHODS

### 2.1 *Field Location*

The Belcher Glacier is a polythermal tidewater glacier on Devon Island, Nunavut, in the Canadian High Arctic, located at 75°39'N latitude and 81°23'W longitude (Figure 2.1). It drains the northeast side of Devon Ice Cap which is a ~14,000km<sup>2</sup> domed ice mass that dominates the eastern part of Devon Island (Burgess et al., 2005). The ice cap is a remnant of the Innuitian Ice Sheet which formed during the Last Glacial Maximum and retreated ~10.3 ka BP (Dyke, 1999). The Belcher Glacier is approximately 35km long and has a drainage area of 718km<sup>2</sup> (Duncan, 2011). The main glacier trunk flows north through a mountainous fjord landscape and terminates in Jones Sound alongside a slower moving unnamed northern tributary glacier (catchment 6 in Figure 2.2, tributary 2 in Burgess and Sharp, 2008), which does not contribute to the flow of the main glacier trunk (Figure 2.2) (Burgess and Sharp, 2008). The Belcher Glacier trunk is 2.4km wide at the terminus. The final 5km length of the Belcher Glacier is heavily crevassed and has an average surface slope of 0.3°. Its terminal ice cliff has an average height of 50.45m.a.s.l. and the ice thickness at the terminus ranges from 36m - 320m. Average water depth near the terminus is 217m.

Historical aerial photographs indicate that terminus position has been essentially stable since 1960 (Burgess and Sharp, 2004; F. Wyatt (pers. comm.)). However ice volume loss from the basin between 1960 and 1999 was  $11.19 \pm 1.44 \text{ km}^3$  w.e. and its surface has been thinning by  $0.35 \pm 0.04 \text{ m a}^{-1}$  along the entire glacier length (Burgess and Sharp, 2008). Over this period, iceberg calving from the Belcher Glacier accounted for around 30% of the net mass loss from the whole ice cap (Burgess et al., 2005). Belcher Glacier may lose approximately 36% of its annual mean net mass loss by calving (calculated following Burgess et al., 2005; Burgess and Sharp, 2008; Boon et al., 2010; A. Gardner (unpublished data)). Consequently the Belcher Glacier is of

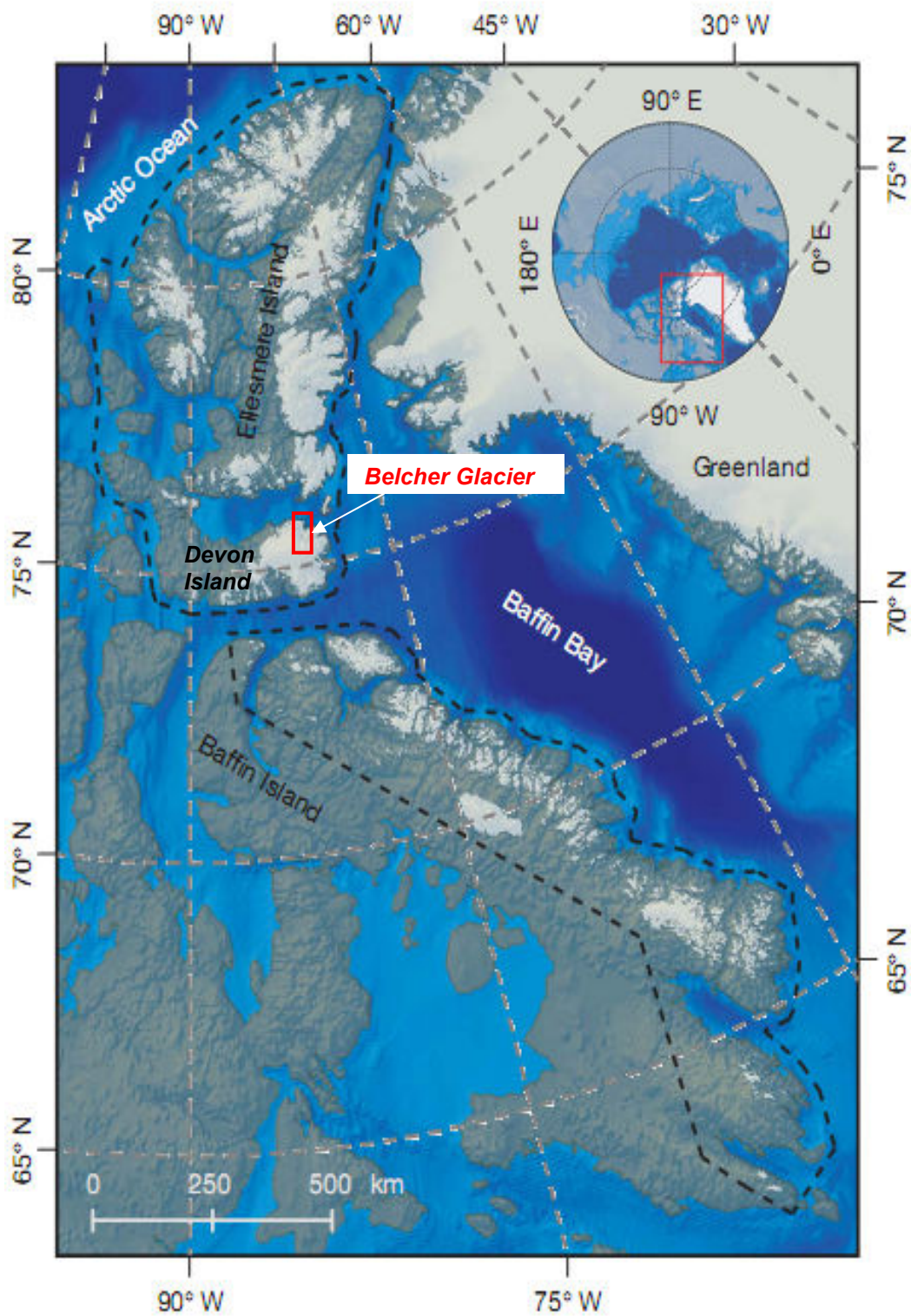
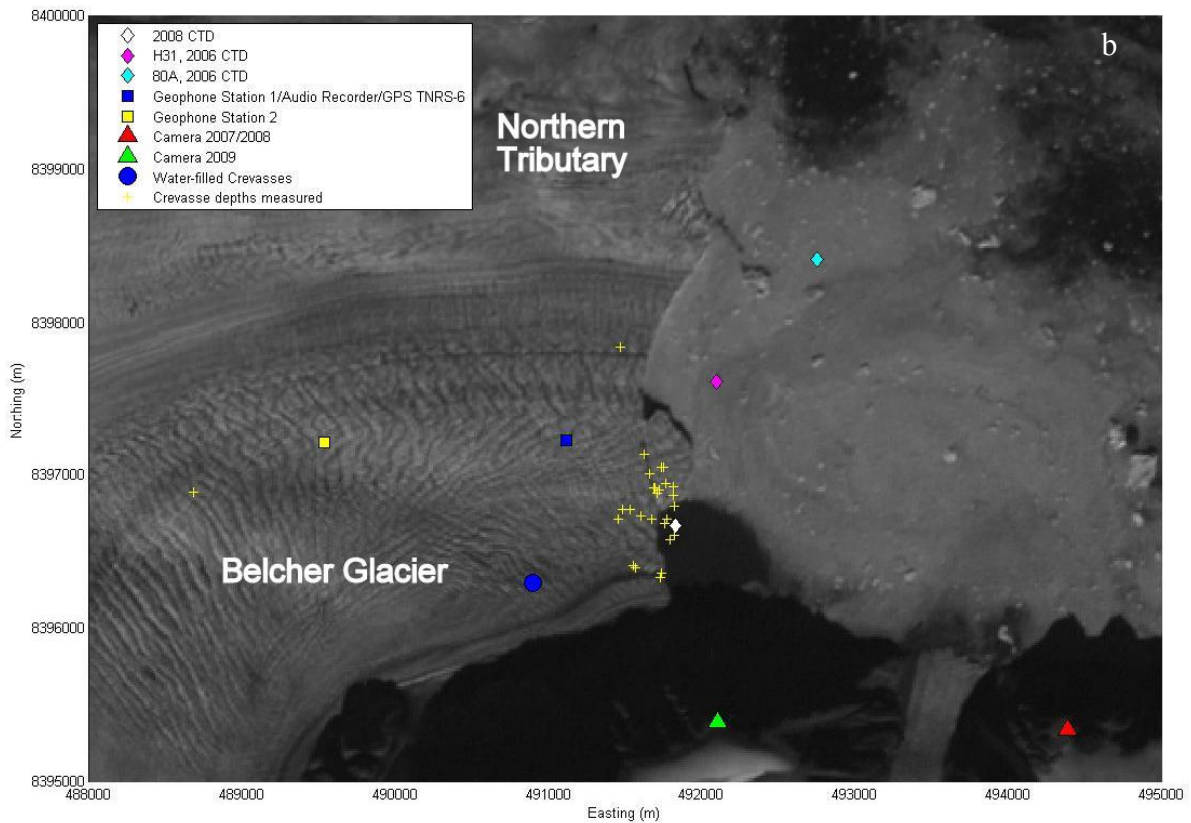
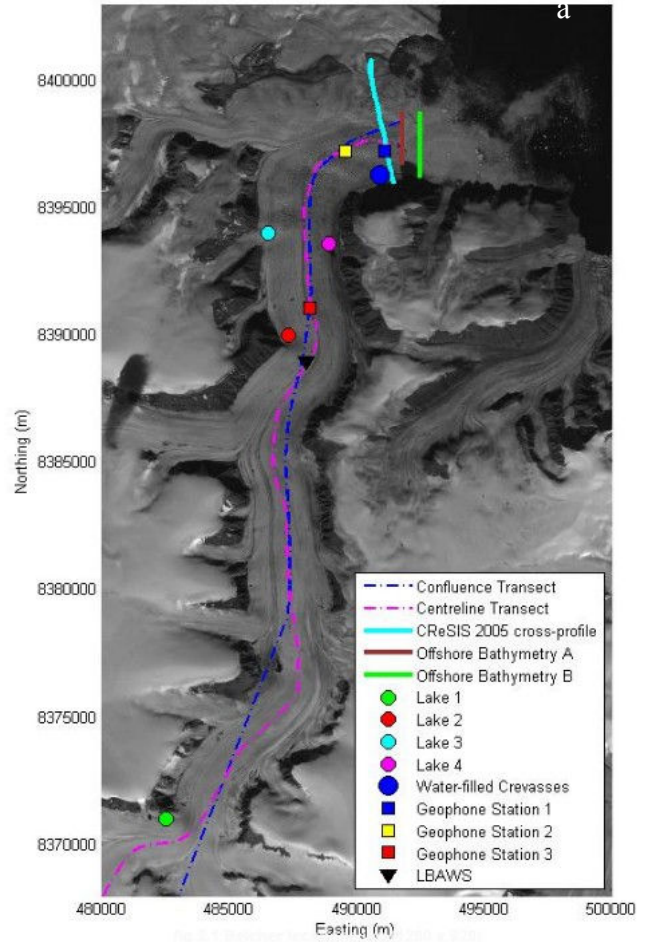
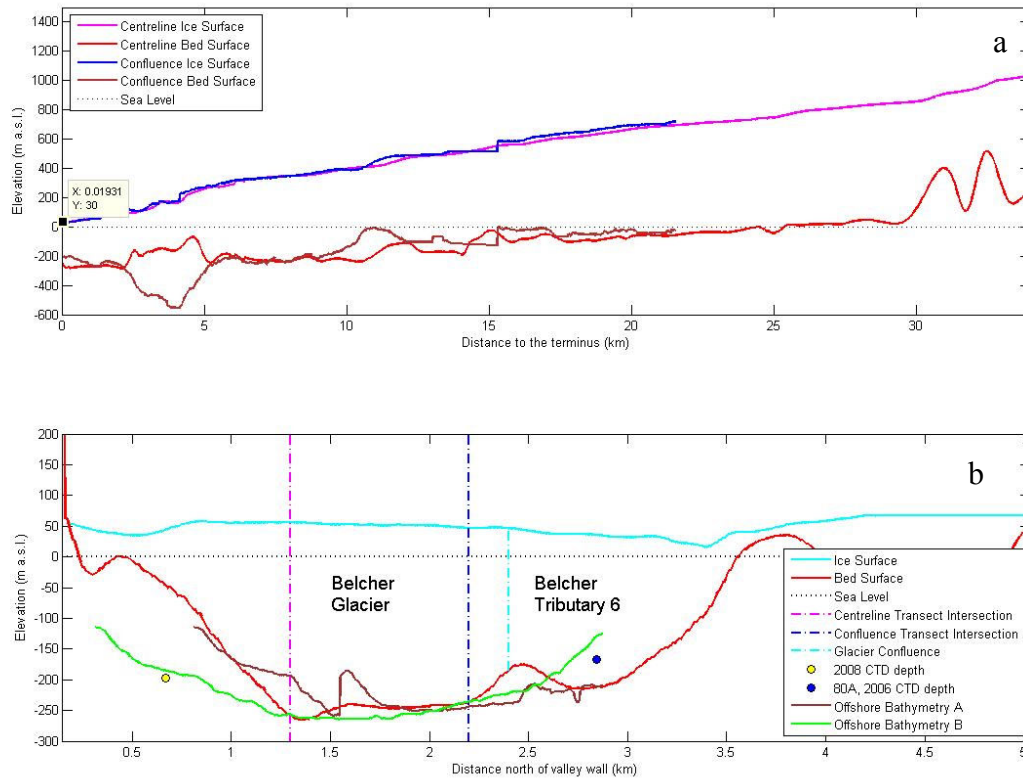


Figure 2.1. Glaciers and ice caps of the Canadian Arctic Archipelago, with the location of Devon Island and the Belcher Glacier shown (red rectangle). The main panel is an enlargement of the red rectangle shown in the inset of the Arctic region. Figure adapted from Gardner et al. (2011), which was created by G. Wolken.

**Figure 2.2. The Belcher Glacier (a) The main Belcher Glacier catchment, showing various radar and bathymetry transects in the region, as well as the location of four supraglacial lakes referred to in the text in connection with Danielson and Sharp (in review), the general region of terminus water-filled crevasses, and the location of geophone and weather stations discussed in the text. (b) A close up of the Belcher Glacier terminus, the main study area. Shown are the locations of: nearby CTD casts, the geophone stations (which includes the audio recorder and GPS site at Geophone Station 1), the 2007/8 and 2009 time lapse cameras, the general area of water-filled crevasses observed from the 2009 time lapse camera, and the locations of crevasse measured for depth by L. Tarasov and team. Base map is a Landsat 2000 image**





**Figure 2.3. (a) Transects along the Belcher Glacier centreline showing ice surface and bed topography (b) Cross-profile transect running parallel to the Belcher Glacier terminus, showing ice surface, bed topography and bathymetry data from offshore of the terminus; location shown in Figure 2.2. Ice surface and bed elevations in (b) and ‘centreline transect’ in (a) were obtained in 2005 from NASA’s Airborne Topographic Mapper (ATM) Laser Altimeter and the University of Kansas ice penetrating Radar Depth Sounder instruments as part of the CRISIS (Centre for Remote Sensing of Ice Sheets) project (Gogineni et al., 2005; Krabill et al., 2006). ‘Confluence transect’ in (a) was obtained in 2000 from the survey of ice thickness described in Dowdeswell et al. (2004).**

significant interest for the contribution of calving to both its own mass balance and that of the Devon Ice Cap.

Belcher Glacier is grounded below sea level for a distance of around 25km upstream from its terminus and has a minimum bed elevation of 300m below sea level in the centre of the fjord, within 2km of the ice margin (Figure 2.3) (Burgess et al., 2005). Along the centreline of the glacier, the bed elevation increases upglacier but there is a steep reverse slope around 5km from the margin which is manifest as an ice fall at the surface. A high resolution DEM of bed topography is not available, but the abrupt changes in bed surface apparent in the contrast between the airborne ice penetrating radar transects surveyed along the Belcher Centreline (Gogineni et al., 2005; Krabill et al., 2006) and across the confluence between the Belcher glacier and its tributary (J. Dowdeswell, 2000, unpublished data) are an insight into the substantial roughness of the glacier bed, which is likely to affect the glacier flow dynamics. There is a significant c. 250m overdeepening evident in the ‘confluence’ transect (Figure 2.3) which is not present at the centreline, only 2km away. Along the confluence the ice surface has a distinct wave-like topography which may be due to the overdeepening as well as the joining of two ice masses (B. Danielson, pers. comm.).

The eastern half of Devon Island is composed of Precambrian Shield gneisses (Frisch, 1988), while the region offshore from the Belcher Glacier (Jones Sound) has a floor of Cretaceous-Tertiary clastic sediments filling in grabens in the Precambrian gneisses (Dyke, 1999). The Canadian High Arctic climate is generally cold and dry although there is a strong east-west precipitation gradient over Devon Island and the east-facing Belcher Glacier receives precipitation of  $\sim 500\text{kg m}^{-2} \text{a}^{-1}$ , mostly as snow (Duncan, 2011). The North Open Water (NOW) polynya, an area of northern Baffin Bay where there is usually open water throughout the winter, is a primary moisture source for the Devon Ice Cap (Koerner, 1977). The mean surface air temperature in winter (December-March) for 2008-09 at 500m.a.s.l. on the Belcher Glacier was  $-27.8^{\circ}\text{C}$ , whilst in summer

(June-August) it was 1.2°C (B. Danielson, unpublished data). Koerner (2005) noted that in the Canadian High Arctic there is typically low interannual variability in precipitation but high variability in melt production due to annual differences in summer solar insolation. Gardner et al. (2011) found that between 2007 and 2009 the Canadian Arctic Archipelago was the largest regional contributor to eustatic sea level rise outside Greenland and Antarctica ('overtaking' Alaska during that period, but in 2010 Alaska was almost certainly the bigger contributor again). Sharp et al. (2011) have suggested that the significant increase in summer air temperatures since 2005 is a response to a summer atmospheric circulation configuration that favoured heat transport from a region of anomalously high sea surface temperatures (SSTs) in the North Atlantic. Summer melt rates in the Canadian Arctic and NW Greenland appear to be most responsive to variations in solar insolation (Koerner, 2005; Duncan, 2011), whilst in other parts of Greenland high melt may occur under cloudy skies, as in Norway (Giesen et al., 2008).

### **2.1.1 Field Campaign**

The Belcher Glacier project was a major collaborative study developed for the 2007-2009 International Polar Year (IPY). The aim of the project was to research the dynamic response of Arctic tidewater glaciers to climate change under an international project called GLACIODYN. GLACIODYN was proposed by the International Arctic Science Committee Network on Glaciology (IASC-NAG) and involved collaborators from 18 countries. In situ and remote sensing fieldwork on Devon ice cap took place alongside research on ten other glaciers in the Circumpolar Arctic including several in Svalbard and Alaska. Collaborators on Devon Ice Cap included the Geological Survey of Canada, the Universities of Ottawa and Lethbridge, Simon Fraser University, Memorial University of Newfoundland, and University of Alaska Fairbanks. Previous collaborations with NASA and the University of Cambridge generated airborne geophysical

measurements of ice surface topography and ice thickness for the whole Devon Ice Cap, and Belcher Glacier in particular.

The ultimate goal of the Belcher Glacier project is to develop and validate a high resolution coupled model of the hydrology and dynamics of the Belcher Glacier (G. Flowers, S. Pimentel) that can be nested within a lower resolution model of the whole ice cap (L. Tarasov). It will be used to investigate the dynamic response of tidewater glacier flow to changes in climate, sea level, and ocean temperatures, as well as investigating the role of meltwater input variations and iceberg calving in this process. A DEM (Digital Elevation Model) of the ice thickness and subglacial topography is being developed by W. Clavano and J. Kavanaugh using GPR (Ground Penetrating Radar) and RES (Radio-echo sounding) data. Snow accumulation patterns in the catchment have been mapped by T. Sylvestre (Sylvestre, 2009). A surface melt/mass balance model developed by R. Hock and C. Tilm-Reimer has been applied to Belcher Glacier by A. Duncan (Duncan, 2011). Mapping of the seasonal development of the ice cap supraglacial drainage system was conducted by J. Padolsky and F. Wyatt. The influence of meltwater supply on ice velocity using GPS measurements and time lapse imagery is being investigated by B. Danielson (Danielson and Sharp, in review). Synoptic scale multi-temporal velocity mapping of the Belcher Glacier using RadarSat-2 speckle tracking was completed by W. Van Wychen and L. Gray (Van Wychen, 2010). Reconstruction of annual velocity fields 1999-2009 using gradient correlation methods has been applied by J. Davis to Landsat-7 imagery to look at long-term variability in ice flow and calving fluxes. Finally, mapping of the fjord seafloor bathymetry was completed in 2006 (Bell and Hughes-Clark, 2006). The relationship between iceberg calving rate and glacier flow dynamics is the focus of this M.Sc. project.

## **2.2            *Iceberg Calving Detection***

The next section outlines the methods used to collect the data for this study. The primary field season was May-August 2009. The datasets collected primarily by the author to identify calving events were as follows: time lapse imagery, audio recordings, and geophone logs. However some time lapse imagery was collected in 2007 and 2008 which was primarily installed by B. Danielson, and L. Tarasov and team.

### **2.2.1 Time Lapse Imagery**

In this study of the Belcher Glacier terminus, time lapse images were used to identify iceberg calving events, to calculate the area of ice lost, and to provide qualitative information about the style of the calving events which may indicate whether the glacier is floating or grounded. Time lapse images of the calving front were gathered at 2 hour intervals between June 4<sup>th</sup> and August 14<sup>th</sup> 2009. The camera system consisted of a Pentax K110D 6 Megapixel digital SLR with an adjustable lens set to 18mm focal length, timed by a Harbotronics Digisnap and powered with a 7Ah lithium gel cell battery and 10W solar panel. The largest calving events were identified by visual inspection of imagery supplemented by audio data information, as described in section 2.2.2. Smaller events and their precise locations were identified via manual digitization of the glacier margin position. Repeat digitizing of the margin allowed quantification of the magnitude of each calving event in terms of the area of ice lost. The UTM coordinates of the margin and the area of ice lost (in square metres) were calculated using a simple photogrammetry model based on Krimmel and Rasmussen (1986), which was developed as Matlab® code by M. Truffer and utilized in O’Neel et al.. (2007).

The position of the terminus margin is calculated using the static-surveyed locations of two GCPs on bedrock summits within the camera view, as well as the focal length of the lens, and an initial estimation of the Exterior Orientation parameters (EOPs, the X, Y, Z position coordinates of the camera and the three

rotation angles: roll ( $\omega$ ), pointing angle ( $\phi$ ) and tilt ( $\kappa$ )) (see Figure 2.4) (Ahn and Box, 2010). The focal length and EOPs were checked using Photomodeler camera calibration software. The position of the margin is then projected to a horizontal plane (the intersection of the ice cliff with the sea surface) on which UTM Zone 17 map coordinates can be calculated. Tidal amplitude data from the Fisheries and Oceans Canada Webtide Model (Hannah et al., 2008) were incorporated into the code to solve for the varying height of the sea level plane ( $\pm 1.5\text{m}$  near the Belcher Glacier). The code was further developed in this project to include a different digitizing routine (using a Matlab function rather than red pencil) and automatic image control point (ICP) identification. This was done by assuming a stable camera frame (assuming the camera does not wobble substantially in the wind) rather than accounting for any shifts through ICP identification (which has its own error associated with manual pixel picking). The camera box had been newly secured strongly to the rock, was not exposed to high winds and any observable wobble was less than the error associated with manual digitizing of the terminus position.

Prior to georeferencing, the calving margin position was digitized in daily time lapse images covering the study period (June 4<sup>th</sup> to August 14<sup>th</sup> 2009). The margin position was defined as the intersection of the ice front with sea level. It was digitized in Matlab and the pixel coordinates were then imported into the photogrammetry code described above. This produced UTM coordinates for the calving front position. Histogram thresholding, image enhancement and edge detection were tested to aid automatic detection of the margin but the terminus environment was too complex for this to be done reliably. Sea ice, crevasses, and a large range in lighting conditions posed the main challenges in this regard. Daily images were used as a shorter time interval would not generate terminus position changes that are large enough to be detectable above the manual digitizing error. The 2009 image set was digitized twice to compare the manual digitizing variability. Over stable ground in the near scene, the manual digitizing RMSE is approximately 0.36m, extending to 5.19m at the island in the background

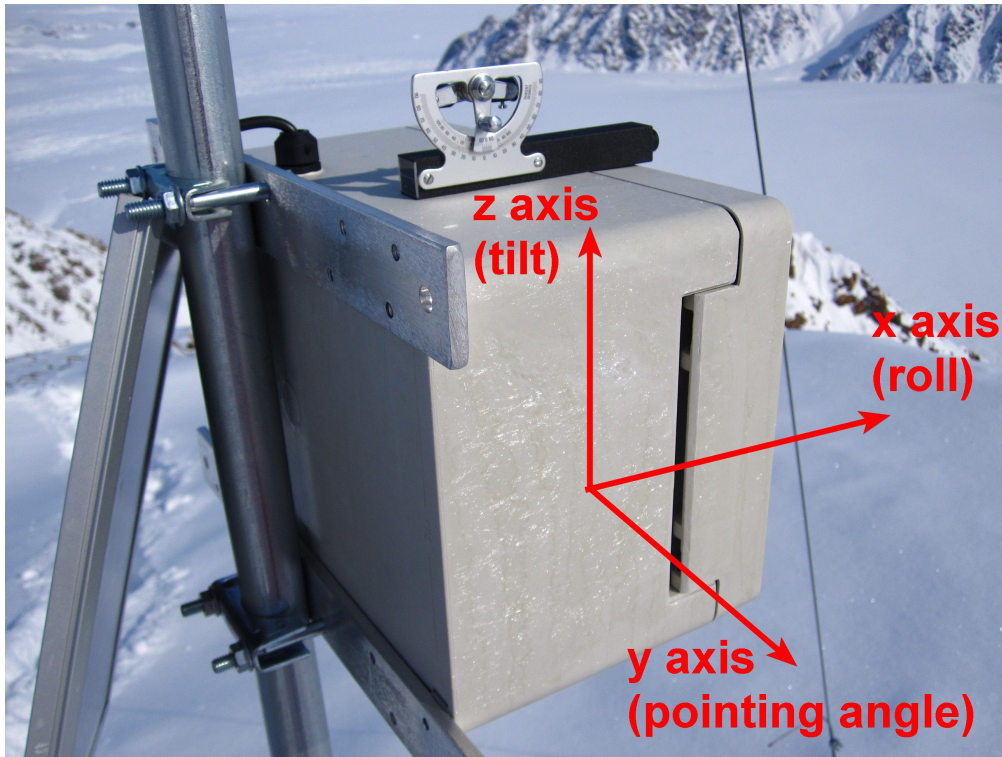


**Figure 2.4. Demonstration of the three camera rotation angles, which have various names depending on the photogrammetry system used and are all listed here for clarity and for comparison between O’Neel et al. (2007) and Ahn and Box (2010): ROLL/omega ( $\omega$ )/psi (rotation clockwise around X axis), POINTING ANGLE/phi ( $\phi$ )/pitch (dip below the horizontal on the Y axis), TILT/kappa ( $\kappa$ )/theta (tilt from the azimuth, counter-clockwise around the Z axis where North is  $90^\circ$ ).  $\omega/\phi/\kappa$  is the most accurate naming system which is used in this thesis.**

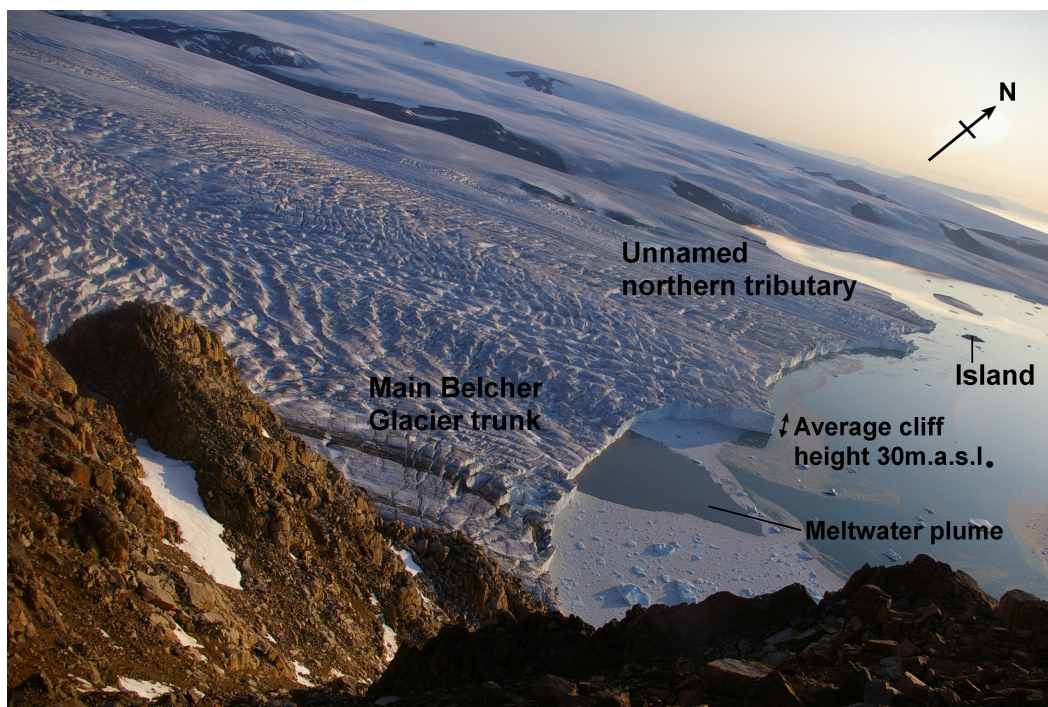


**Figure 2.5.** The time lapse image scene of the Belcher terminus for 2009, with key features annotated.

(Figure 2.5). Change in the terminus position was computed using a box area measurement method, as opposed to a single along-flow reference line, because it is often the case that some regions of the terminus advance while others simultaneously retreat (Moon and Joughin, 2008). The box used was bounded by the digitized margin at the downstream end, by parallel lines along its lateral margins and by an arbitrary reference line upstream (Moon and Joughin, 2008). The difference in the area of each polygon between successive images is the area change of the front ( $dA/dt$ ) whilst the average displacement distance ( $L$ ) is calculated by dividing the area of retreat by the polygon width (Howat et al., 2010). In order to somewhat account for manual digitizing errors and the influence of tides, area gains or losses of less than  $0.005\text{km}^2$  were not included in the area change results. This value was less than the area of calved ice in the smallest observed calving event but larger than the digitizing RMSE of each of the two separate digitized datasets: both sets would include errors, neither being a ‘true’ estimate. The reliability of the margin position estimate, and the

photogrammetry model, was assessed through comparison with digitized margins in quasi-monthly Landsat-7 ETM+ images from the same time period (resolution  $\pm 30\text{m}$ ). MODIS (Moderate-Resolution Imaging Spectroradiometer) images could not be used for additional mapping as they were usually too cloudy to allow mapping of the full terminus, and the 250m resolution was not accurate enough to allowing mapping of changes in the terminus position of a glacier that flows at  $<300\text{m/yr}$ . Landsat-7 images were downloaded from the USGS Global Visualization Viewer (GLOVIS).

Throughout this study, the results are compared to results from several other time lapse cameras as well as to meteorological conditions measured at several Automatic Weather Stations (AWS) established on the glacier. Reference is made to the Lower Belcher Automatic Weather Station (LBAWS) installed by A. Duncan in 2008 and the Belcher Camp Automatic Weather Station (BCAWS) installed by B. Danielson in August 2006 (Figure 2.2). Hourly measurements of air temperature, wind speed and direction, and snowfall are used to quantify changes in weather conditions (see Table 2.1). Time lapse cameras were also installed at the terminus in 2007 and 2008, but in a different location (Figure 2.2). This viewing angle was more ‘face-on’ to the terminus and did not allow for accurate delimitation of the daily margin position using the method described above. However, they were useful for monitoring the meltwater/sediment plume, and major calving events were still visible. The cameras had the same equipment and setup as described for the 2009 camera above, but the time lapse interval was 3 hours in 2007, and 1 hour in 2008. Another time lapse camera was also installed by L. Tarasov on a moraine at the glacier’s southern margin between July 7<sup>th</sup> and August 1<sup>st</sup> 2008. For differentiation, this camera is hereafter referred to as the ‘*Tarasov camera*’. In this study it is used to provide more detailed information about the calving and sea ice dynamics near the southern margin during this time period, supplementing the wider perspective of the 2008 time lapse camera position. However the camera is not used to calculate the area of ice lost or changes in the meltwater plume as the camera is very close to the glacier and does

not capture any GCPs in its field of view. Its position was also adjusted several times during its field installation.

**Table 2.1. Selected meteorological instrument specifications as stated by the manufacturer.**

**All instruments were installed on the cross-arm, 2m above the surface at the time of installation. Hourly averages of 15-second measurements were recorded on Campbell Scientific CR1000 data loggers (table from Duncan, 2011)**

VARIABLE	SENSOR	RANGE	ACCURACY
Air Temperature	Campbell Scientific HMP45C212	-50 to +50°C	±0.1°C
Relative Humidity (RH)	Campbell Scientific HMP45C212	0 to 100% non-condensing	±2% RH (0 to 90% RH) ±3% RH (90 to 100% RH)
Wind speed	RM Young 05103AP-10 wind monitor	0 to 60m s <sup>-1</sup>	0.3m s <sup>-1</sup>
Wind direction	RM Young 05103AP-10 wind monitor	360° (mechanical)	3°

## 2.2.2 Audio Recordings

A Sound Devices 702T audio recorder was installed on the glacier ~400m from the calving front (Figure 2.2). It collected acoustic signals continuously from June 24<sup>th</sup> – July 24<sup>th</sup> 2009. These were used to supplement the calving event history detailed by the time-lapse imagery. The recorder was stored in a sturdy, water-tight box which also contained the batteries. The microphone was attached to a steel pipe drilled into the ice, on which three solar panels were also mounted. Data were recorded in stereo using an Environmental Audio Recording Systems (E.A.R.S. Canada) 48V phantom-powered omni-directional condenser microphone, protected by a custom Gore-Tex windshield (Figure 2.6). The frequency response of the microphone ranges from 10Hz to 40Hz. The microphone preamplifier used a high pass filter to reduce sensitivity to wind noise (low frequency signals <240Hz). Wind noise was also reduced by use of the

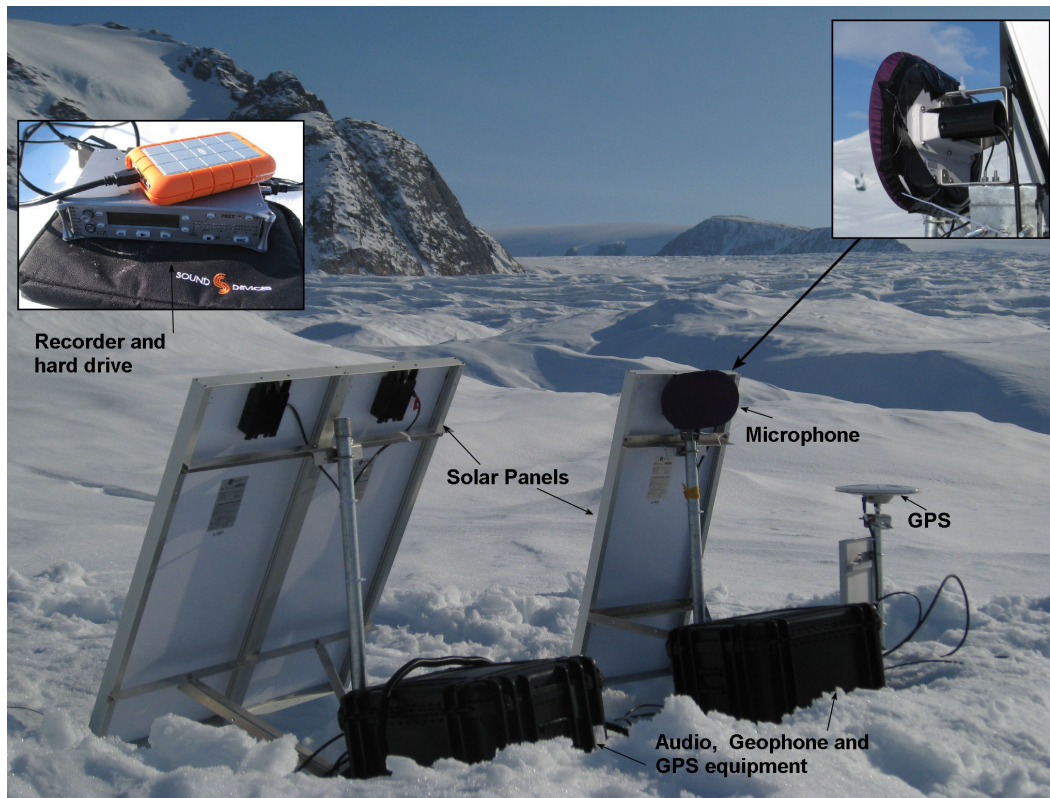


**Figure 2.6. The ‘Uberstation’ setup with audio recorder, geophones and GPS installed near the terminus (at TNRS-6). Audio recorder is powered by the 3 large 80W solar panels pictured, which feed the battery in the black box. E.A.R.S. Canada Microphone pictured in inset, with purple Goretex windshield cover. Sound Devices 702T audio recorder pictured in second inset, with LaCie ‘rugged’ hard drive which was also installed in the black box along with a Campbell Scientific datalogger and a circuit board timing device.**

windshield and by locating the equipment on a serac in a depression on the ice surface. This is important as wind noise can potentially mask other sounds, but strict elimination of this noise may hide calving events, which also produce low frequency signals (1-2 Hz) (Qamar, 1988). The recorder gain range was 25 to 70dB; it logged with a sampling rate of 44.1 kHz and recorded 500Mb MP3 files to a LaCie bus powered FireWire drive. The recorder was set for a delayed start using a custom relay device designed by R. Stefaniuk and J. Kavanaugh that interfaced with the clock from a Campbell Scientific CR10X datalogger. The relay device was also used to monitor the audio recorder time code using a buzzer which beeped aloud the day of year at a specified time each day. The clock drift was only +60 seconds after one month of continuous recording (consistent with

the stated accuracy of the datalogger clock) but tracking this was necessary in case power inputs dropped below a threshold and the relay device cut recording until enough power was available to restart it. This did not prove necessary as the system was powered by three 80W solar panels and two 100Ah batteries, as well as by a 4600mAh lithium-ion battery in the recorder. The Sound Devices recorder is hardy and well-designed but can consume up to 20W/hr depending on the number of active functions such as phantom microphone powering. On July 24<sup>th</sup> the FireWire drive crashed due to overheating in its insulated black box whilst on continuous recording for a month, but the data were eventually recovered.

### **2.2.3 Geophones**

A set of simply-constructed geophones were installed on the Belcher Glacier to test whether different source mechanisms of ice fracture events could be detected and differentiated (for example identifying calving events and surface crevassing activity). Three seismic stations were placed along the glacier centreline, 0.4km, 1.5km and 6.6km upstream of the terminus (Figure 2.2). Each station consisted of a pair of two-component, 4.5Hz geophones at a depth of 5m, approximately 1m apart. The geophones were interfaced with a Campbell Scientific CR10X data logger through a simple circuit board. They counted the number of seismic events above a defined ‘gain’ and output the total number of counts to the datalogger every 2 minutes. The logger and circuit board were stored in a small sturdy box attached to a steel pole drilled into the glacier ice, which also supported a 10W solar panel. The geophones were set to different gain sensitivities (2000 and 3000) to obtain additional detail about the relative size and location of events. During each 2 minute measuring interval the circuit board counts the number of events that have local amplitudes greater than the threshold gain value but neither the magnitude nor timing of the events within this interval are recorded (Kavanaugh and Clarke, 2001). A gain of 2000 was found to provide a good compromise between sensitivity and noise rejection in studies at Trapridge Glacier, Canada (Kavanaugh and Clarke, 1997). This value was also used by Copland et al. (2003)

in work on John Evans Glacier, Canada. However as this gain only picked up the largest seismic events, in our study the second geophone was set to a higher sensitivity of 3000. These geophones differ from other bedrock or ice geophones as they are not three-component and hence do not detect vertical movement. Two-component geophones are only able to provide relative timing, location and magnitude of seismic events because without a large network of seismometers it is impossible to distinguish between small, local and large, distant activity. Nevertheless as the geophones were spaced some distance apart it may be possible to identify the general location of events by noting which geophones recorded counts and the propagation of responses along the glacier (Copland et al., 2003).

## **2.3            *Identifying Potential Calving Triggers***

The three potential triggers for iceberg calving listed here were primarily identified from time lapse imagery: changes in the terminus velocity, changes in the subglacial meltwater flux (determined by the extent of the meltwater/sediment plume, as well as the timing of drainage of water-filled crevasses) and changes in sea ice buttressing of the glacier terminus. The methods of identifying these features are presented, followed by a review of the methods used to identify tidal interactions, ocean temperature methods and calculations of the glacier's proximity to flotation (a reflection of terminus ice and bed geometry). These results are supplemented by tidal data, CTD casts and bathymetry maps, weather station and GPS data, which were collected by other collaborators who are cited at appropriate points in the text. All analyses of these processed datasets are my own.

### **2.3.1    *Terminus Velocity***

*Optical flow* is potentially a new technique for measuring the flow of a glacier. In the computer vision literature, it is currently used to compute change between two sequential oblique camera images. The motion of pixels between two images is

tracked, relative to the static position of the observer, on the assumption that pixel brightness is similar in both images (Atcheson et al., 2009). In this sense, the method is not dissimilar to *feature tracking*, which follows groups of pixels (rather than individual pixels) between image pairs. Optical flow is also similar to the *MIMC cross correlation* technique recently tested on oblique time-lapse imagery by Ahn and Box (2010). This method can be used to derive a full spatial velocity field for the whole oblique image, providing much higher spatial resolution of displacements than point-based GPS measurements. This is particularly useful at the hazardous, rapidly changing calving front (Ahn and Box, 2010). It would also have a much better temporal resolution than most satellite imagery, with the potential for at least daily velocity maps on relatively fast-flowing glaciers. An example of the spatial resolution of the results, superimposed on an orthorectified image, is shown in Figure 2.7. The method has the potential to be more fully automated than cross correlation methods, which require manual picking of registration points. Optical flow is being tested because the spatially dense velocity grid may reveal connections between the terminus flow and iceberg calving events: for example localized speed up may occur in response to changes in longitudinal stresses following a calving event (Benn, 2007b). However the accuracy of optical flow results is highly dependent on the images having closely comparable lighting conditions and not being obscured by clouds, and this requirement results in sparse data availability.

Optical flow algorithms have improved substantially since their first use in the computer vision literature by Lucas and Kanade (1981) and Horn and Schunk (1983). For example, discontinuities in the flow field are minimized by applying smoothness constraints, large displacements are resolved using a coarse-to-fine iterative strategy ('warping'), and slight changes in brightness between images

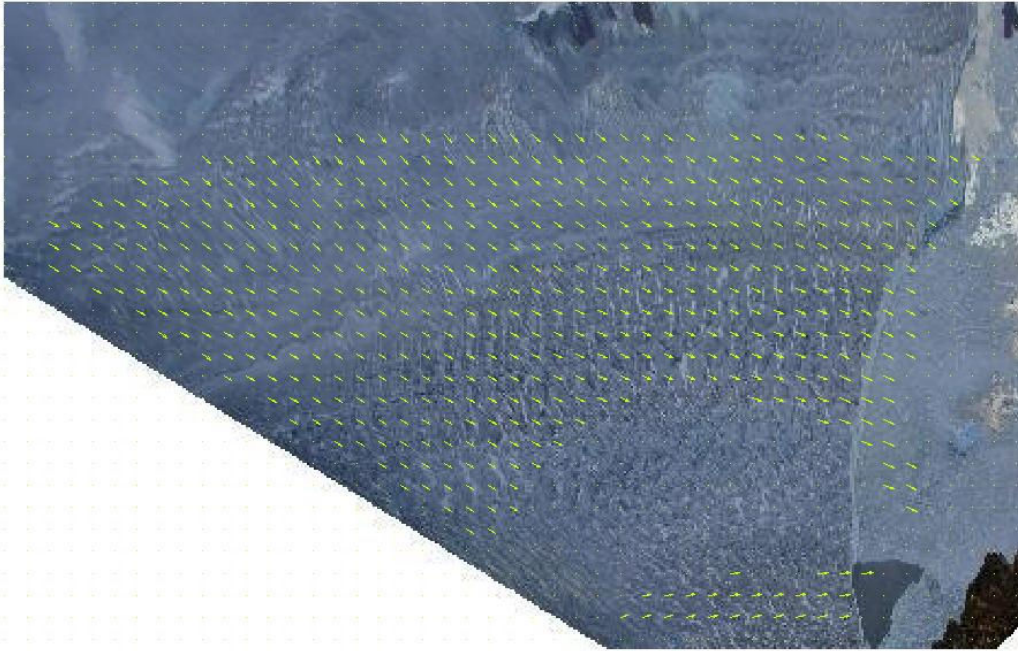


**Figure 2.7. An example of an optical flow result, displayed on the orthorectified time lapse image. The images compared were taken on 19<sup>th</sup> July 2009 at 1am and 20<sup>th</sup> July 2009 at 5am. Vectors are enlarged by 5 times for visibility. Displacements which did not exceed the bedrock uncertainty were removed and a mask is applied around the image margins as well as over the ocean and bedrock.**

(due to natural lighting conditions) are acceptable with a gradient constancy assumption (Brox et al., 2004). These improvements may make it possible to take optical flow algorithms out of the computer lab and test them on natural scenes. Yang et al. (2000) used the Horn and Schunk (1983) algorithm to locate ‘singular features’ such as ocean vortices in sea surface temperature (SST) data from satellite images. Optical flow has not yet been applied in glaciology but the closest example is a project on the Nisqually Glacier in Mt Rainier National Park, where a sparse velocity grid was mapped from double-exposed oblique time-lapse photographs using an early version of Particle Image Velocimetry (PIV) (Conley and Cloud, 1986). PIV tracks velocity by pattern matching the displacement of

laser speckle or a tracer fluid and applying cross correlation in a similar fashion to the speckle tracking technique used for satellite radar imagery (e.g. Short and Gray, 2005). This method is most commonly applied to turbulent flow fields (Adrian, 2004). It was tested on river ice in the St Lawrence River, Canada, but the complex cloud and lighting conditions influenced the results too much for the method to be successful (Bourgault, 2008).

There are a large number of different optical flow algorithms in the computer vision literature, along with several alternative methods for computing displacement such as normalized cross-correlation, feature tracking, and PIV. On the Belcher Glacier, we used optical flow because it can produce a dense velocity field on oblique or orthorectified photographs, is automated and lacks a requirement for manual GCP picking, and can be computationally inexpensive. The algorithm chosen was ‘High Accuracy Optical Flow’ by V. Chari which is freely available in the Matlab File Exchange. Chari adapted the essential numerics from Brox et al. (2004) and Brox (2005), with the addition of different colour channel analysis and a local smoothing function from Sand and Teller (2006) and Sand (2006). The Sand algorithm addition was used as it was point-based, making it computationally faster than the basic Brox function. Optical flow measurement was initially performed on the original time lapse image (2000x3008) but each pair took up to 3 hours to be processed. When optical flow was run on orthorectified images (295x465), processing times were around two minutes and additional errors associated with the aperture problem were reduced. The aperture problem is an error in the interpretation of movement in oblique images that occurs when the camera is not positioned directly perpendicular to the main flow vectors. The Brox-Sand algorithm attempts to mitigate this problem and others using a variational approach which combines brightness constancy, global smoothness and gradient constancy constraints. It was chosen because the Brox et al. (2004) results remain the most accurate reconstruction of flow in the Yosemite image test sequence, a natural mountain scene that includes clouds (Chen and Barron, 2010) and which compares best to the Belcher Glacier scene.

The code was integrated into a multi-image loop which involves semi-automated image selection and a graphical display of results. Whilst the optical flow code is robust to some natural lighting changes, it operates on grayscale intensity values and assumes brightness constancy so these variations must be kept to a minimum (Brox et al., 2004). A pre-processing selection step removes cloudy, foggy, shadowed and highly illuminated images based on file size and histogram thresholds of intensity and saturation. This is one of the most crucial steps in achieving reliable results. Ahn and Box (2010) reported a 15-20% image loss rate due to factors such as cloud cover. Falling precipitation, strong winds, and lens reflections were not problematic in the Belcher Glacier image sequence but 16.4% of images were discarded due to cloud and fog, whilst only 9% had lighting conditions suitable for optical flow analysis. Late evening and early morning imagery was best as lighting was generally diffuse; uniform high cloud cover also achieved similar conditions but fog, low cloud, light reflectance off water and cliff shadow covering parts of the glacier produced distinctive flow anomalies. Significant snowfall or snowmelt can produce misleading results, as with speckle tracking of radar imagery (Van Wychen, 2010), but there were only two significant changes in ice conditions in the May-August 2009 period, and these were easily avoided in the image selection stage.

In order for the optical flow measurements to be converted from pixel displacement to velocity, the time-lapse images first had to be orthorectified. Orthorectification is the transformation of an oblique or otherwise distorted photograph to one which has a uniform scale on which you can measure distances. It essentially translates the position of each pixel from oblique to plan view with the help of a DEM and the internal and external camera orientation parameters. It was not possible to use the Krimmel and Rasmussen (1986) method in this application because it only accounts for elevations which intersect with sea level or some other flat plane. DEM elevations (which range from 10-240m.a.s.l. in the terminus region) are required to create an accurate projection, otherwise the

coordinates on a flat plane are stretched several kilometers beyond their true position. The 2009 image scene also has a large roll angle ( $13^\circ$ ) so a fully parameterized solution was required to produce a realistic result. For this reason code used in Corripio (2004) and Bourgault (2008) did not make an accurate translation of the Belcher imagery because not all of the camera parameters were included. Instead a fully parameterized solution was created by A. Croitoru, which was based on Croitoru and Ethrog (2001). The inputs to this procedure were the 2007 SPOT SPIRIT DEM, the EOPs (camera position, elevation and  $\omega$ ,  $\phi$ ,  $\kappa$ ), and the interior orientation parameters (IOPs: focal length, X and Y image coordinates of the central pixel). The procedure uses affine transformation to convert pixel image coordinates to image coordinates, which are then restructured to create the final orthoimage. The initial estimates of the EOPs (measured in the field) were optimized alongside estimates of the IOPs from the Photomodeler calibration software and the locations of GCPs, described in section 2.2.1. As a result, the solution is accurate within its own reference system but may not be directly comparable with on-the-ground measurements or georeferenced satellite images. This is acceptable because the result required is an absolute displacement distance, rather than the true position of known features.

Uncertainties due to the difference between actual and assumed brightness conditions as well as camera motion were assessed by the root mean square error (RMSE) of pixel movements over a 15 x 20 pixel area of stable ground in the image foreground that was unaffected by snowmelt (Haug et al., 2010; Ahn and Box, 2010). Any images with an RMSE above 0.5 pixels displacement in any direction were removed from the dataset; whilst in the rest of the images any displacements that were less than the apparent movement over bedrock were masked from the results. Displacements within 10 pixels of the image margin were also masked to minimize edge effects, along with areas outside the region of interest (the main glacier trunk). Once images with excessive bedrock movement were removed, the average displacement RMSE was  $0.18 \pm 0.27$  pixels. The image registration uncertainty described by Ahn and Box (2010) in this case is the

orthorectification error, which cannot easily be determined but is conservatively estimated to be no more than 0.3 pixels.

Several experiments were performed to test the effect on the displacement results of changing the optical flow parameters. In the optical flow literature this is done with a hidden ground-truth field (visible only with a fluorescent camera) (Baker et al., 2007), but in the Belcher Glacier imagery the optimizations were done qualitatively, judging a balance between computation time and the elimination of outlying vectors which were clearly orientated in the wrong direction. Edge effects were apparent within 10 pixels of the image margin but within this boundary most displacements were uniform in magnitude and direction. The results of the parameter testing are presented in Table 2.2. The *alpha global* and *local* terms are regularization parameters which assume neighbouring pixels move in a similar direction but will allow discontinuities to occur at edges, for example near a crevasse. They are a response to the aperture problem and the assumption that each pixel goes somewhere (instead of perhaps vanishing into a crevasse). The global term has the strongest smoothing effect on the whole image and should be set higher when textureless regions are involved, whilst the local variable only affects immediately neighbouring pixels in a gradient dependent manner which helps preserve flow discontinuities (Brox et al., 2004). The optimized values are minimum numbers needed to smooth major outliers but which do not undermine the importance of the main data term (the difference in image intensities). The *downsampling value* is the factor by which each layer in the Laplacian pyramid is resampled and warped. The *Laplacian pyramid* is a coarse-to-fine method of solving for flow and accounting for large displacements (Brox et al., 2004). The first image is a coarse, small pixel-sized version of the original image for which basic optical flow is calculated and then used as the initialization for the next image which has more pixels and is less smoothed (Brox et al., 2004). A large downsampling factor has more warping stages and produces a more accurate result with less outliers at the edges, but too many iterations requires significantly more computation time (Sun et al., 2010).

**Table 2.2. Testing the optimization of optical flow parameters**

PARAMETER	TYPICAL RANGE	RANGE IN ELAPSED TIME (SEC)	OPTIMIZED VALUE SELECTED
Alpha global	15-30	22-34	15
Alpha local	20-100	26-31	20
Downsampling factor	0.5-0.95	5-125	0.8

Velocities determined by optical flow analysis of time lapse imagery were compared to velocity measurements from a network of continuous logging Trimble NetRS dual-frequency GPS systems established by B. Danielson in 2007. TNRS-206 was at the site of the audio recorder and first geophone, ~400m from the ice front in May 2009. The GPS logged data with a 15 second measurement and 5 minute position schedule and referred to a base station near BCAWS to provide a stable local reference frame (Figure 2.2). The GPS data were processed, filtered and analyzed by B. Danielson, as described in Danielson and Sharp (in review). The raw data were converted into Rinex files and differentially post-processed in kinematic mode using Track kinematic software produced by the Massachusetts Institute of Technology. Positions with a horizontal uncertainty  $\sigma > 0.05\text{m}$  and vertical position  $\sigma > 0.1\text{m}$  were removed from the dataset. A 4-hour wide sliding window across the velocity measurements removed the effects of high-frequency noise. The time series which will be presented here is the horizontal displacement uniformly-sampled at 1-hour intervals from May – August 2009 (Danielson and Sharp, in review). The horizontal ice displacement is the difference between the GPS position at the time of the first and second time lapse images being compared in optical flow. This dataset is preferable to the horizontal ice velocity, which is normalized over a daily time step, because the optical flow data also compare positions between the first and second image.

### 2.3.2 Water-filled Crevasses

The time-lapse imagery was also used to map water-filled crevasses visible on the terminus ice surface during the summer. These ‘water-filled crevasses’ are a collection of small ponds which accumulate between crevasse walls and may overflow onto the glacier surface. Water-filled crevasses are distinguished from supraglacial lakes by their size, as they tend to be small and numerous (Figure 2.8), rather than a single large water body. The aerial extent of water-filled crevasses could provide valuable information about the terminus stability as water-filled crevasses have been known to weaken and propagate through the ice, leading to the break-up of ice shelves e.g. Hulbe et al. (2004) and Rignot and Steffen (2008). The timing of crevasse water drainage is also important because the meltwater released may enter the subglacial drainage system and its release at the margin could trigger a calving event. Danielson and Sharp (in review) developed a method to calculate the area of these ponds, using a similar approach to that used for digitization of the calving margin (as described in section 2.2.1). A semi-automated detection procedure is very useful in this situation because there are at least 30-50 small lakes visible on the ice surface (Figure 2.8), which would be tedious to identify and map manually. The results will be compared with measurements of the size of the meltwater plume to determine if the crevasses are directly connected to subglacial drainage system during drainage events. If they are, then initiation of drainage of the crevasses should lead to a larger meltwater plume discharge. The main results of the camera lake-mapping project are presented in Danielson and Sharp (in review) but the water-filled crevasse data are presented here for comparison with the calving and meltwater plume results. The 2009 terminus time lapse imagery is of group ownership; the data analysis was performed by B. Danielson; the data presentation and interpretation were made by H. Milne.

The accumulation of water on the glacier surface can be semi-automatically identified using image pattern recognition, where a function is ‘trained’ to

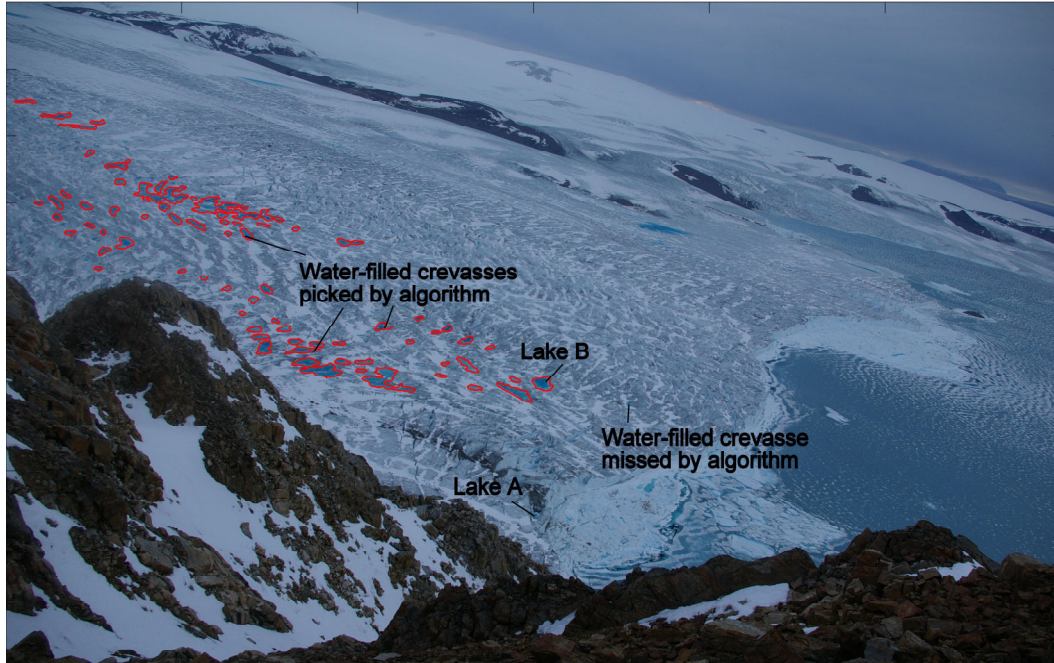


**Figure 2.8.** A time lapse image from June 30<sup>th</sup> 2009 at 7am which shows the water-filled crevasses visible at the terminus that were outlined (in red) by the pixel-picking algorithm developed by B. Danielson (figure adapted from Danielson and Sharp, in review). Lakes ‘A’ and ‘B’ are referred to in the text, in section 3.3.2. A small water-filled crevasse which the algorithm missed is also shown in the foreground.

compare each pixel in an image against a set of criteria to determine whether the pixel fits in the Target Class (water) or another category (ice, snow, rock or shadow) (Danielson and Sharp, in review). The classification is made using different categories of HSV (hue, saturation, value/intensity) and  $L^*a^*b$  (luminance, red-green chromaticity, blue-yellow chromaticity) color space which allowed the varying water colors of the crevasse lakes to be detected. The function can then be ‘trained’ using a K-means algorithm in Matlab, which allowed the user to cluster certain pixels into categories (such as water or ice) and then apply this ‘remembered’ clustering to a series of images. The user then verifies the pixel classification before the lake outline is drawn and the position converted to UTM coordinates using the georeferencing technique described in section 2.2.1 (Danielson and Sharp, in review). This pixel-picking algorithm, developed by B. Danielson, was then used to monitor the changing area of water-filled crevasses

visible at the surface of the Belcher Glacier terminus. An ice/ocean mask was applied to exclude the ocean and sea ice from the detection process.

### **2.3.3 Meltwater / Sediment plume**

The limits of the meltwater/sediment plume can also be digitized from the time-lapse imagery in a similar manner to the calving front position and the water-filled crevasse area. Measurements of changes in plume area can then be used to determine whether the water in the crevasses drains quickly and directly to the subglacial drainage system and thus to the meltwater/sediment plume, whether changes in subglacial meltwater flux (observed from differences in extent of the plume) can trigger a calving event, or if the plume responds to supraglacial lake drainage events, also indicating a surface connection to the subglacial drainage system. A supraglacial lake drainage dataset for 2009 is now available (Danielson and Sharp, in review), to which the meltwater plume flux will be compared. A number of studies have found a significant correlation between river discharge from land-terminating glaciers and plume area (e.g. Lihan et al., 2008; Chu et al., 2009; McGrath et al., 2010) but this relationship has yet to be tested for marine-terminating glaciers. The evolution of the Belcher Glacier meltwater/sediment plume was observed by time-lapse camera. The 2007 and 2008 terminus time lapse camera position offered an excellent view of the plume so they are included here (Figure 2.9), whilst the 2009 camera position did not produce such useful data for this application. In the region where the plume emerges near the ice front, the manual digitizing RMSE is c.7.3m, which would improve as the plume flows closer to the camera at its 2007/8 position. Every cloud-free image of the visible plume was digitized manually and plume edge positions were translated to UTM coordinates to allow calculation of plume area. Automatic detection of plumes posed an additional challenge because the plume water changed colour with different lighting conditions and, as with the calving front position, made application of a ‘trained’ detection algorithm too difficult. Nevertheless, for the purpose of manual digitization, the plume boundary is usually quite distinct

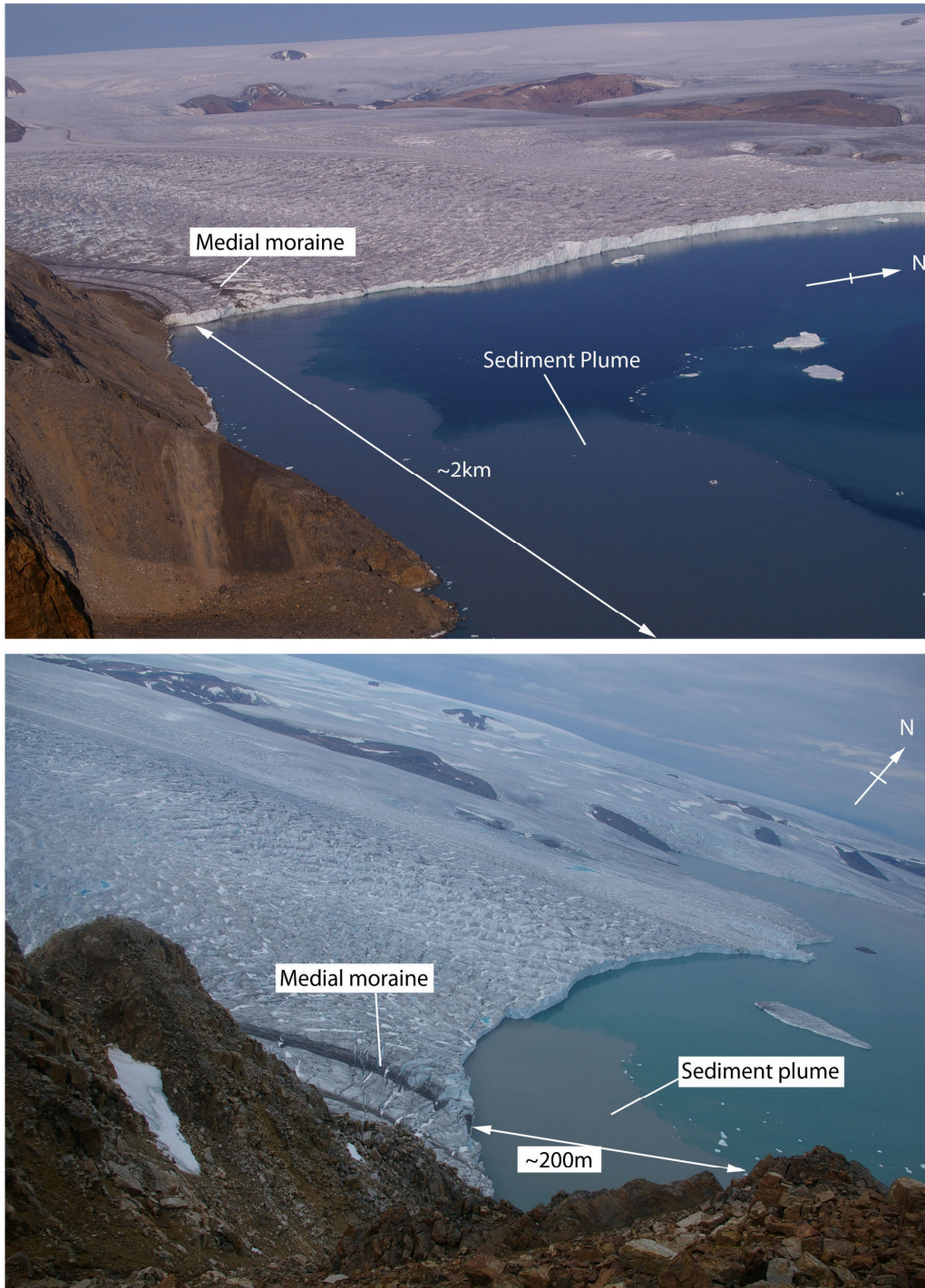


**Figure 2.9. Comparison of the 2007/8 terminus camera view (a) and the 2009 terminus camera view (b) which demonstrates that much more plume water is visible in the 2007/8 imagery.**

because the glacial meltwater is rich in suspended sediment (Chu et al., 2009; McGrath et al., 2010). In this paper the focus is on the ‘turbid plume’, formed from the most sediment-rich water and found closest to the terminus, which is the easiest part of the plume to identify in time-lapse imagery.

MYD09 and MOD09 250m resolution band 1 MODIS imagery (available daily) was evaluated to determine its suitability for validating the time-lapse plume extent maps, as well as to confirm how much further the turbid plume extends beyond the camera. Chu et al. (2009) and McGrath et al. (2010) used MODIS imagery to map the area of the ‘brackish’ sediment plume, which extended 5-65km from the Kangerlussuaq shoreline in West Greenland. In the time-lapse imagery suspended sediment is most clearly visible in the ‘turbid’ plume which occurs closest to the ice front. However whilst most of this plume was captured from the 2007/8 camera position, it sometimes extended beyond the camera’s field of view. Available MODIS images from 2008 and 2009 were compared with time lapse images from the same dates to determine whether a distinction could be made between the turbid and brackish plumes based on the SSC (see section 1.3.3), and how much area was being missed due to the camera position. The MODIS instrument on the NASA Terra and Aqua satellites was used as it offers daily coverage of the study area. MOD09 (Terra) and MYD09 (Aqua) 250m resolution surface reflectance products were downloaded from the NASA Warehouse Inventory Search Tool (<https://wist.echo.nasa.gov/api/>). Only high quality ‘clear-sky’ images were extracted, following the definition by Chu et al. (2009). The hierarchical data format (hdf) files were converted to geotiff using the freeware MODIS Reprojection Tool (MRT) and delineated to a local region of interest (ROI) using ENVI. A land mask was created in MATLAB using Band 2 (820-870nm) to focus the analysis on the Belcher Fjord, following McGrath (2009).

Surface reflectance values are dimensionless and range from -100 to 16000. This range was used to convert values to percent surface reflectance. Chu et al. (2009),

McGrath et al. (2010) and Miller and McKee (2004) analyzed the red portion of the visible spectrum seen in band 1 (620-670nm) for a threshold reflectance value that depicts suspended sediment near the water surface. Lahet and Stramski (2010) compared the reliability of band 1 to band 4, and found that band 1 offers higher spatial resolution and better highlights the distribution of runoff near a coastline, making it ideal for this application. Chu et al. (2009) observed that a surface reflectance percentage of  $>0.12$  matched the spatial distribution of the sediment plume in Kangerlussuaq Fjord, based on an empirical model calibrated with ground-truth measurements. McGrath et al. (2010) also found similar values for this region. However Lahet and Stramski (2010) caution against applying these thresholds to other regions because they depend on environmental conditions such as the catchment size, as well as the solar zenith angle (Miller and McKee, 2004) and factors such as the melt and sediment contributions to the plume. The solar zenith angle is a function of time, day and latitude, which differs significantly between the Kangerlussuaq ( $66^{\circ}57'N$ ) and Belcher catchments ( $75^{\circ}39'N$ ).

#### **2.3.4 Mélange / Sea ice Buttressing**

The buttressing strength of the sea ice in front of the Belcher terminus will be assessed qualitatively using the time-lapse imagery and other photographic evidence acquired in July 2008 and May 2009. The evolution of the sea ice from its solid winter form to summer breakup will be described, and the timing of the breakup will be examined in relation to the timing of calving events between 2007 and 2009 and any glacier velocity changes seen in the optical flow and GPS data which might be a response to the loss of resistance at the terminus. The amount of 'mélange' left on the surface/incorporated into the sea ice close to the ice front will also be discussed, particularly with respect to winter calving events.

### **2.3.5 Tidal modelling**

Dunphy et al.. (2005) and Hannah et al.. (2008) created the Fisheries and Oceans Canada Webtide model, which can be used to compute coastal tidal predictions within the Canadian Arctic Archipelago. In this study the modeled tidal height dataset will be compared statistically to the timing of calving events to determine whether tidal fluctuations played a role in triggering an event, which is more likely if the glacier is floating as they can then exert flexure on the floating tongue and increase the bending stress (O’Neel et al., 2003). Tidal fluctuations could also affect the flow of the meltwater plume in ways that might lead to a calving event (e.g. by reducing meltwater outflow at high tide, and increasing basal water pressure and proximity to flotation).

Webtide is a finite element model with a static ice field to partially account for sea ice coverage. It models the five major tidal constituents in this region: the semi-diurnal principal lunar (M2), principal solar (S2) and lunar elliptic (N2), and the diurnal principal lunar (O1) and lunar-solar (K1) constituents (Gudmundsson, 2007). The model is validated by a month-long data set from ‘Belcher Point’ (Figure 2.2), which improves its reliability in our area of study as it is located only 13km north of the Belcher Glacier terminus, and within the same fjord (Greisman et al., 1986; Hannah et al., 2008). The model predictions also compared well to measurements from a tide gauge installed in the fjord beyond the glacier terminus in July 2008 (L. Tarasov, unpublished data). The maximum tidal range recorded over the 10-day measurement period was  $\pm 1.46\text{m}$ , whilst the modeled tidal range for that time period was  $\pm 1.40\text{m}$ . The root mean square error (RMSE) of the difference between the 10-day measured tide and model predictions was  $0.196\text{m}$  and the correlation coefficient was  $r=0.96$ .

### **2.3.6 Ocean Temperatures**

Murray et al. (2010) analyzed the interaction of glacier flow and changing ocean temperatures in southeast Greenland using measurements of glacier flow speed,

terminus position, surface mass balance, and ocean temperature and salinity. Following Murray et al., ocean temperatures offshore from the Belcher Glacier were measured with CTD casts and spatial changes in SSTs were analyzed using mean sea surface temperature anomaly (SSTA) maps available as a product from Advanced Very High Resolution Radiometer (AVHRR) data ([http://iridl.ldeo.columbia.edu/SOURCES/.NOAA/.NCEP/.EMC/.CMB/.GLOBAL/.Reyn\\_SmithOlv2/.monthly/.ssta/](http://iridl.ldeo.columbia.edu/SOURCES/.NOAA/.NCEP/.EMC/.CMB/.GLOBAL/.Reyn_SmithOlv2/.monthly/.ssta/)) (Reynolds et al., 2002). This SSTA series uses the time period 1971-2000 as the baseline from which the anomalies are calculated. Murray et al. (2010) also compared their results to a MODIS weekly product and a Landsat radiance product, but as the Reynolds SSTA product were found to be reliable, and are easily available, only this dataset was used here. Whilst the SST dataset only represents the temperature of the topmost surface of the ocean, Murray et al. (2010) argue that it was hard to explain the consistently high SSTs observed in their study area without warm water occurring at depth as well. This hypothesis will also be considered more closely.

Series of CTD casts was made in the Belcher Fjord in September 2006 and July 2008, in order to examine the ocean temperature profile. Seven casts were taken from the CCGS Amundsen Icebreaker and the Heron launch vessel on 19<sup>th</sup> September 2006, and L. Tarasov made 5 casts on 22<sup>nd</sup> and 30<sup>th</sup> July 2008. Practical Salinity,  $S_p$  (PSS-78), was converted to the new standard, Absolute Salinity ( $S_A$ ), using the Gibbs Seawater (GSW) Matlab Oceanographic Toolbox of TEOS-10 (Thermodynamics and Equation of State of Seawater). The casts taken in 2008 had pressure converted to depth following UNESCO (1983), whilst conductivity was converted first to Practical Salinity and then to Absolute Salinity using the method described above.

### **2.3.7 Geometry**

The stability of a glacier is strongly influenced by the ice and bedrock geometry at the terminus. Instabilities often arise when the terminus ice approaches buoyancy, caused by thinning due to a change in surface mass balance, enhanced basal or

terminal ice cliff melt (especially below the waterline), or increased velocity or calving rate. Wide bays or large basal over-deepenings are examples of bedrock features which are more likely to promote catastrophic retreat from unstable glacier termini. Calculation of the height-above-buoyancy (Sikonia, 1982) indicates how well grounded the glacier is and provides information about the stability of the terminus region. The height-above-buoyancy,  $H_b$ , is:

$$H_b = H - \frac{\rho_w}{\rho_i} D_w \quad (4)$$

where  $H$  is the effective cross-sectional ice thickness,  $D_w$  is the water depth,  $\rho_w$  is the density of sea water and  $\rho_i$  is the density of ice. Water depth is interpreted from the CTD data (described above) and the bathymetry map produced by the CCGS Amundsen in September 2006. The bathymetry was mapped by imaging deeper parts of the fjord using the EM300 30kHz multi-beam on the Amundsen ship, along with detailed mapping closer to the tidewater front using the 300kHz multi-beam on the Heron launch vessel (Bell and Hughes-Clark, 2006). CTD casts made from the Heron Launch Vessel only went to 150m depth, but CTD casts by L. Tarasov and those from the CCGS Amundsen reached the fjord floor, and can be used as additional measurements of water depth.

## 2.4 *Summary*

The Belcher Glacier is a tidewater glacier located on Devon Island in the Canadian High Arctic. The main aim of this project is to investigate those aspects of the dynamics of the glacier's terminus region that influence the timing and rate of iceberg calving in the summer period. In particular, the research is aimed at determining whether the glacier is grounded or floating in summer, and whether individual calving events are related to the timing of changes at the ice-ocean interface (subglacial meltwater flux variations, the downward propagation of terminus water-filled crevasses, changes in mélange/sea ice buttressing of the glacier terminus, tidal flexure of the terminus region, or changes in ocean temperature which alter basal melt rates) or in glacier dynamics (terminus velocity

or proximity to buoyancy, which is controlled by glacier and bed geometry). In order to consider these questions, several datasets were collected. The audio and geophone data were gathered to supplement information about the history of calving events that was derived from time-lapse photography. The time-lapse and MODIS imagery, tidal height, CTD and AWS data were used to investigate the linkages between weather conditions, meltwater/sediment plume extent, sea ice conditions, tidal variability and the occurrence and magnitude of calving events. The time lapse imagery, analysed using optical flow, and compared with GPS data may inform us about the spatial and temporal patterns of ice flow variability in the terminus region. Finally the CTD and bathymetry data are used to assess the ocean temperatures, and the long-term stability of the glacier terminus region.

## Chapter 3. RESULTS

### 3.1 *Introduction*

This section describes data collected at the Belcher Glacier between 2006 and 2010. The primary field data are from 2009 though they are supplemented by evidence from previous years that was gathered by other field researchers. Further details are supplied in the text. The first section presents the iceberg calving results, detected using time lapse imagery, audio recordings and geophones. The following section then summarizes the results of optical flow analysis, water-filled crevasse area mapping, meltwater/sediment plume mapping, sea ice buttressing, ocean temperature and tidal analysis, and the glacier and basin geometry.

### 3.2 *Iceberg Calving Detection*

#### 3.2.1 Time Lapse Imagery

The primary method of identifying calving events was from daily digitized positions of the glacier margin, which made it possible to locate small advances and retreats not immediately visible to the eye. The time-averaged rate of change in the position of the calving front ( $dL/dt$ ) and the change in area of the glacier terminus region ( $dA/dt$ ) between June 4<sup>th</sup> and August 14<sup>th</sup> 2009 are shown in Figure 3.1b. From June 4<sup>th</sup> to July 15<sup>th</sup> the terminus advanced in a stepwise fashion at a mean net rate of  $0.0014\text{km}^2 \text{d}^{-1}$ . The maximum rate of margin advance ( $0.0092\text{km}^2 \text{d}^{-1}$ ) occurred on July 1<sup>st</sup>-2<sup>nd</sup>. Figure 3.2a clearly shows significant advance of the ice cliff over a period of five days prior to sea ice breakup on July 16<sup>th</sup>, the first day on which major calving was observed. This advance increased the terminus area by  $0.0275\text{km}^2$ . It also followed a rise in air temperature at LBAWS where air temperature remained continuously positive between July 10<sup>th</sup>

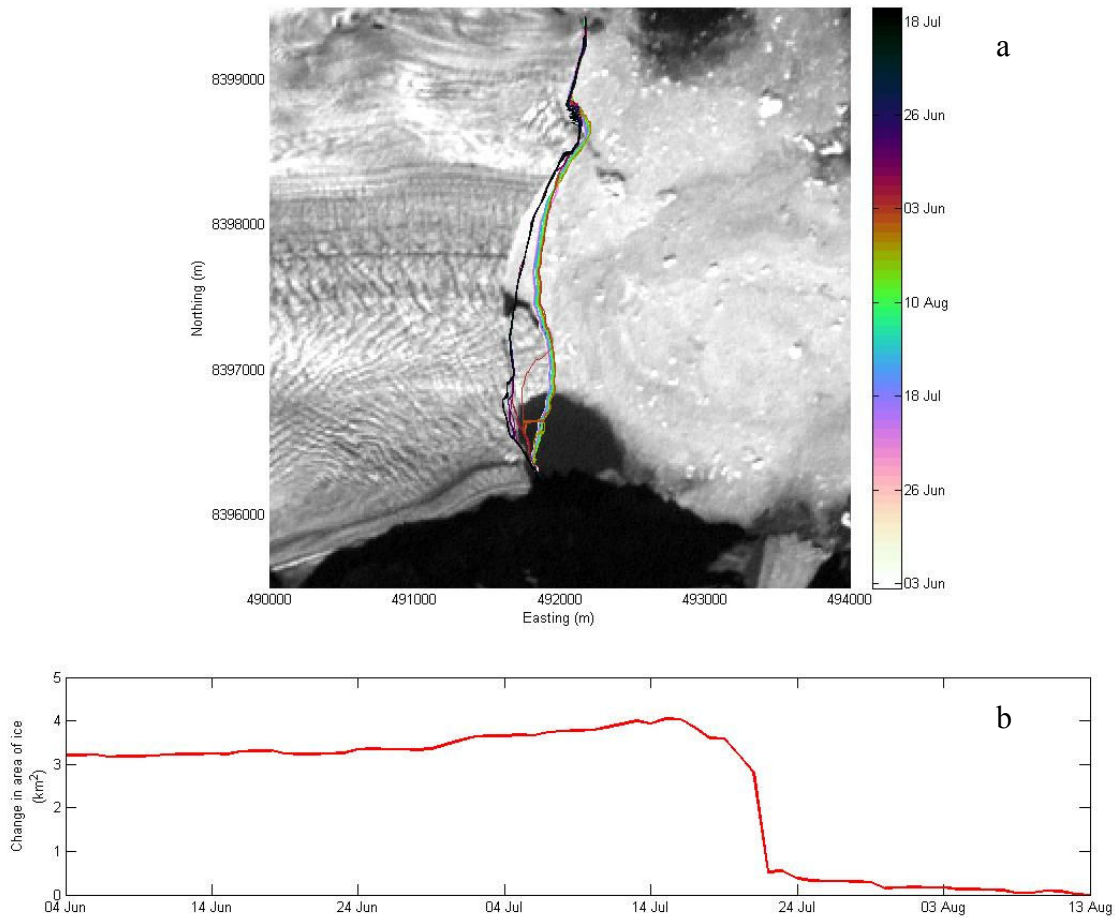


**Figure 3.1. Time-averaged rate of area change of the calving front, June 4<sup>th</sup>- August 14<sup>th</sup> 2009. a) Full array of calving front positions superimposed on a time lapse image to demonstrate spatial change. b) Graph of area change over the time period**

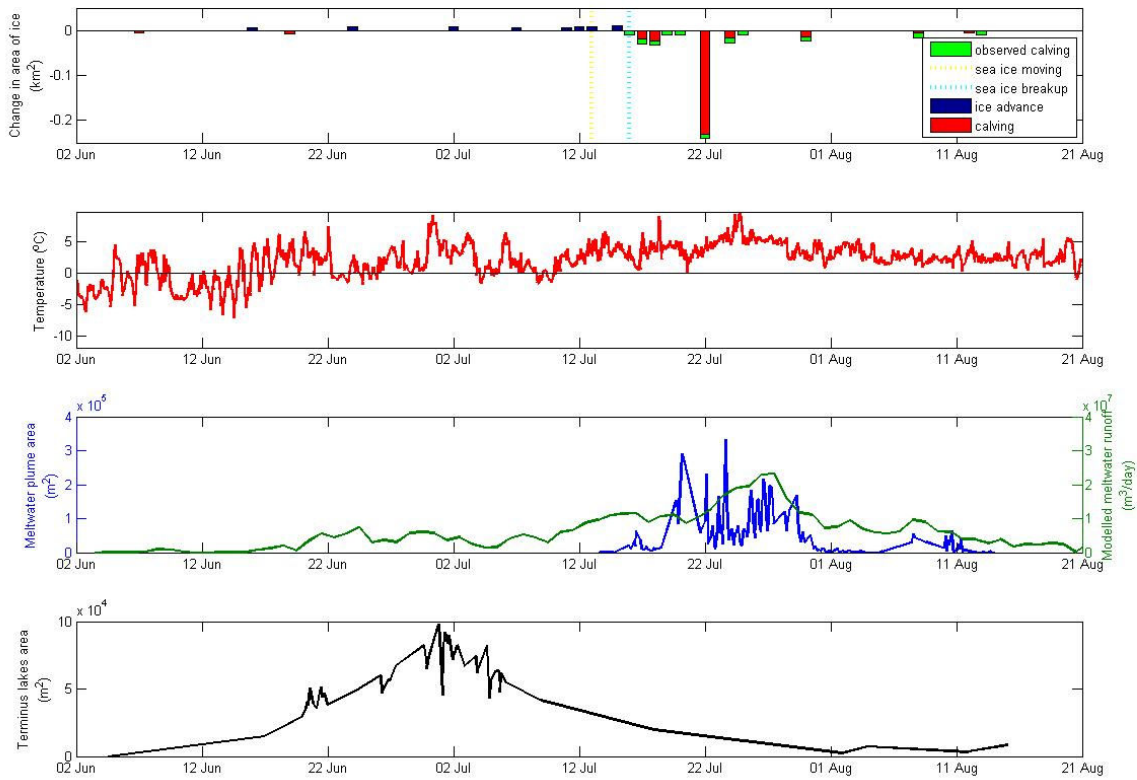


**Figure 3.2. Summary of calving activity, sediment plume activity and environmental conditions for summer 2009. a) Bar chart of calving front area change, presenting only significant advance or retreat of the margin, and times when calving was visually observed. The timing of sea ice initial independent movement and final break up are also shown. b) Air temperature at LBAWS. c) Sediment plume area, compared to modeled runoff volume. d) Area change of supraglacial terminus water-filled crevasses.**

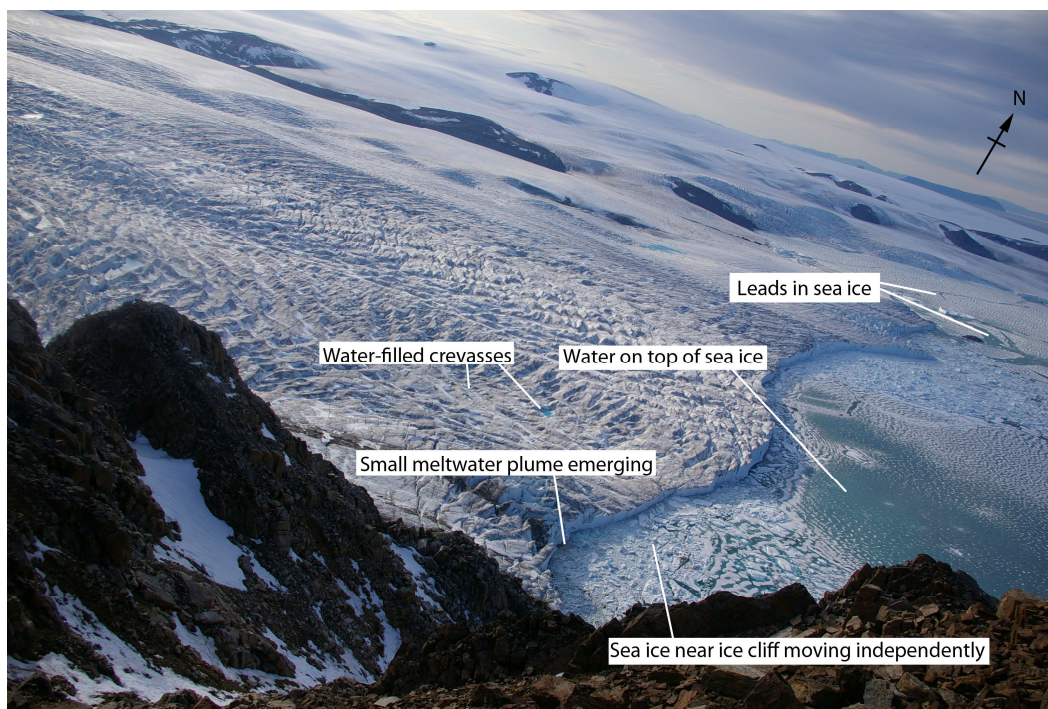


**Figure 3.3.** A time lapse image from July 14<sup>th</sup> 2009 at 9pm which shows leads opening up in the sea ice, some areas of sea ice near the ice cliff beginning to move independently, as well as water-filled crevasses on the glacier surface.

and 20<sup>th</sup> (Figure 3.2b). In addition, the sea ice close to the cliff began to move independently on July 14<sup>th</sup> whilst the meltwater/sediment plume became visible for the first time (Figure 3.3). Furthermore, the sea ice in the bay north of the Belcher Glacier terminus changed significantly on July 14<sup>th</sup>, with large leads opening up and some pockets of open water becoming visible (Figure 3.3). In front of the Belcher terminus, it was the sea ice up to 200m from the ice front (which also contained iceberg remnants) that disintegrated first (Figure 3.3). Sea ice chunks began to rotate with the wind and tides but were encased in a large expanse of sea ice that was still intact even though its surface was flooded. Prior to this, the sea ice slab had begun to rise and fall noticeably with the tides on July 3<sup>rd</sup>, and more obviously by July 10<sup>th</sup> when the frontal sea ice slab started to partially disintegrate. No calving event was recorded in the terminus area change record on July 16<sup>th</sup> (Figure 3.2a) even though a small event did occur on that day, because another berg had slumped forward but did not completely detach, giving

the impression of a small ice advance (which was not above the error bounds). On June 7<sup>th</sup> and 19<sup>th</sup> the digitized results imply a calving retreat but these losses were not visible in the imagery. The audio recorder did not begin recording until June 24<sup>th</sup> so it is not possible to confirm these events with those data. However, the computed total loss is as substantial as that observed on July 25<sup>th</sup>, and may therefore have been due to a series of minor losses none of which is clearly visible to the eye. The most significant ice loss (a total of 0.23km<sup>2</sup>) occurred on July 22<sup>nd</sup>. The overall margin position varied little between July 24<sup>th</sup> and August 14<sup>th</sup>, and no significant advance was recorded due to a few small calving events. The area difference between the start and end of the measurement period was -0.33km<sup>2</sup>, though the difference between the maximum ice area on July 9<sup>th</sup> and the minimum on August 13<sup>th</sup> was -0.4 km<sup>2</sup>. The total gain in ice area between June 4<sup>th</sup> and August 14<sup>th</sup> was 0.06km<sup>2</sup>, which, when subtracted from the total ice losses of 0.33km<sup>2</sup>, gives a net calving loss for the period June 4<sup>th</sup> to August 14<sup>th</sup> of 0.27km<sup>2</sup>.

The time-lapse derived calving positions were compared with front positions digitized from quasi-monthly Landsat-7 imagery over the same time period in order to evaluate the accuracy of the georeferencing of the time lapse imagery (Figure 3.4). Two images from the start and end of the time-lapse monitoring period were orthorectified using the alternative georeferencing method described in section 2.3.1 (Croitoru and Ethrog, 2001), and are shown for their comparable accuracy. Each method has its own inaccuracies, but the Landsat imagery is likely to be most reliable. There appears to be a systematic error in the area-change margin positions (digitized from oblique time lapse imagery, using the method of Krimmel and Rasmussen (1986)), in which the easting position is approximately 100m west of the Landsat position and the margins digitized in plan view imagery (orthorectified using the method of Croitoru and Ethrog (2001)). The Croitoru and Ethrog method appears to be a better match to the Landsat imagery, indicating it

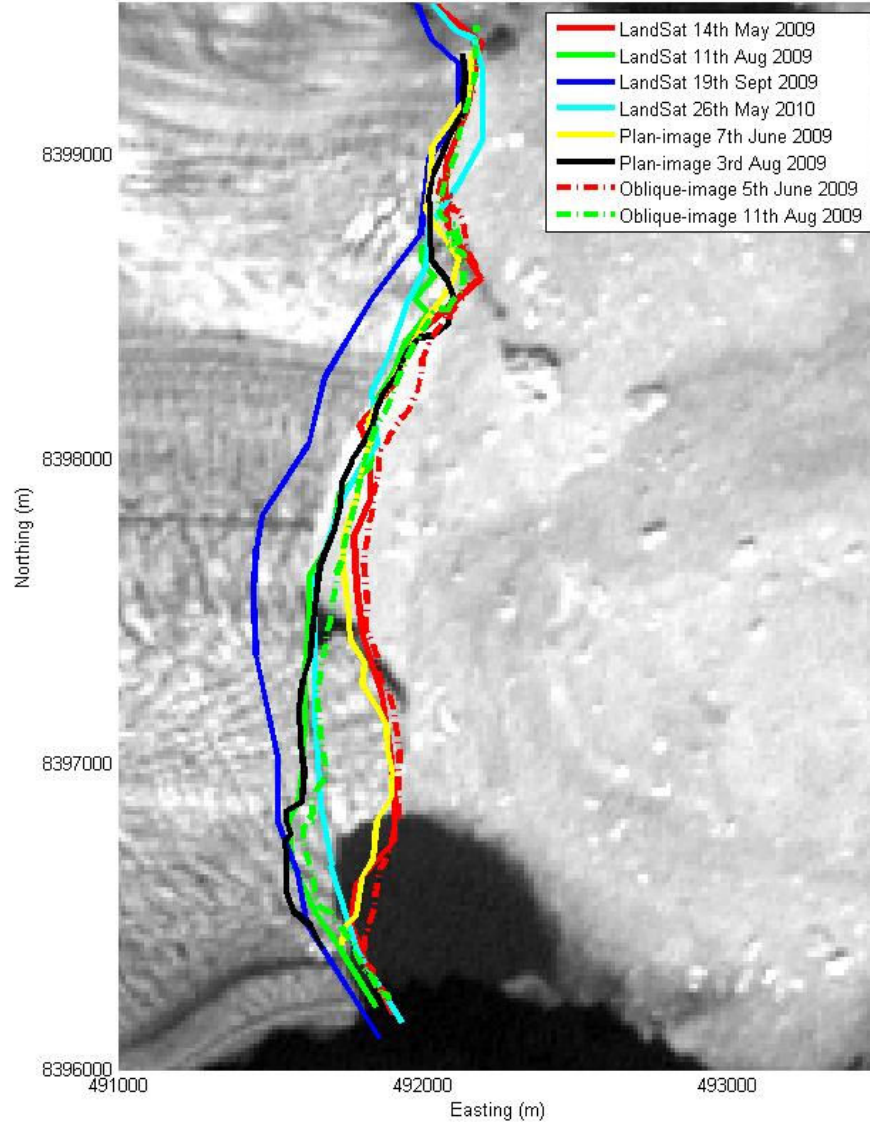


**Figure 3.4. Comparison of ice margin positions from Landsat-7 ETM+ images and two different methods of georeferencing the 2009 time lapse imagery. ‘Oblique-image’ margin positions were digitized for the area-change measurements referred to in section 3.2.1 (georeferenced using the method of Krimmel and Rasmussen (1986)), whilst ‘Plan-image’ margin positions were digitized for comparison of accuracy but were georeferenced for use with the optical flow data (see section 2.3.1) using the method of Croitoru and Ethrog (2001).**

is more accurate than the Krimmel and Rasmussen method, which is expected as it uses the full array of camera rotation angles to solve the photogrammetry problem. Figure 3.4 also shows that the glacier retreated substantially further in the period after removal of the time-lapse camera on August 14<sup>th</sup> 2009, as indicated by the margin position in Landsat imagery on September 19<sup>th</sup> 2009. The loss of area between the Landsat positions of August 11<sup>th</sup> and September 19<sup>th</sup> was 0.297km<sup>2</sup>.

The net calving rate for the summer period can be calculated from the volume of ice lost due to advance or retreat of the terminus and the flux of ice through the terminus region (Williamson et al., 2008). The volume of ice lost due to glacier length change is calculated from the surface area of ice lost and the glacier ice thickness. The average ice thickness across the main Belcher Glacier trunk width (2.4km) is 217m, which does not include the tributary alongside its northern margin (Figure 2.3). Danielson and Sharp (in review) integrated the ice thickness across the glacier width and found the cross-sectional area to be almost exactly the same as that calculated using the average glacier thickness. Therefore:

$$Q_{\text{loss}} = A_{\text{loss}} \times H \quad (5)$$

Where  $Q_{\text{loss}}$  is the net volume of ice lost,  $A_{\text{loss}}$  is the area of ice lost and  $H$  is the average ice thickness. Meanwhile, the flux of ice through the terminus region (the calving volume) is determined from the mean annual ice displacement and the cross-sectional area of the flux gate at which the displacement is measured (Williamson et al., 2008). The annual surface flow rate near the centreline at the terminus in 2009 was  $267 \pm 0.1 \text{ m a}^{-1}$ , as measured with repeat differential static GPS surveys (Danielson and Sharp, in review). This value is assumed to reflect the depth-averaged displacement, as the terminus flow is almost entirely due to basal motion (Burgess et al., 2005) and therefore the surface and depth-averaged displacements are the same (Williamson et al., 2008). This means there is an annual flux due to ice displacement through the terminus region of  $0.139 \text{ km}^3 \text{ a}^{-1}$ .

**Table 3.1. Glacier calving-rate components, ratio of flux components, and seasonal and annual estimates of total volume lost for the Belcher Glacier, 2009-2010.**

DATES	IMAGE SOURCE	TERMINUS AREA CHANGE (KM <sup>2</sup> )	TERMINUS VOLUME CHANGE FLUX (KM <sup>3</sup> )	ICE FLUX THROUGH TERMINUS GATE (KM <sup>3</sup> )	TOTAL VOLUME LOST (KM <sup>3</sup> )	RATIO OF ICE FLUX TO TOTAL VOLUME LOST
4 June 2009 to 14 August 2009	Time Lapse	-0.27	0.061	0.027	0.088	0.31
8 June 2009 to 11 August 2009	Landsat	-0.586	0.127	0.024	0.151	0.16
11 August 2009 to 19 Sept 2009	Landsat	-0.297	0.064	0.013	0.077	0.17
14 May 2009 to 26 May 2010	Landsat	-0.261	0.057	0.139	0.196	0.71

The results of the calculation of volume change, ice flux and total volume lost for several different time periods are shown in Table 3.1. Between June 4<sup>th</sup> and August 14<sup>th</sup> 2009, the time lapse observation period, the total volume lost by calving was 0.088km<sup>3</sup>; but only 31% of this seasonal calving rate can be explained by ice flux through the terminus. The area of change between several Landsat images on which the margin had been digitized was also calculated. In the Landsat imagery, the volume change during the time lapse observation period (8<sup>th</sup> June to 11<sup>th</sup> August 2009) was -0.151 km<sup>3</sup>, with only 16% of this calving explained by ice flux through the terminus. Both estimates are likely to contain errors, and it is expected that the time lapse data would underestimate the calving mass loss as a large margin of error was included which probably also removed evidence of real calving. Equally, the Landsat imagery has a resolution of ±30m which could have overestimated the changes through errors in the digitizing the margin. From August 11<sup>th</sup> to September 19<sup>th</sup> 2009, after the time lapse camera had

been removed, the Belcher Glacier lost a further  $0.077\text{km}^3$ . Yet the annual calving rate, between May 14<sup>th</sup> 2009 and May 26<sup>th</sup> 2010, was  $0.196\text{km}^3 \text{ a}^{-1}$  and in comparison 71% of the annual calving rate was explained by ice flux through the terminus. The total volume lost between June and September was 84% of the annual calving rate, confirming that most of the annual calving takes place in the summer but that calving definitely takes place in the winter (or between mid-September and mid-May). Throughout the year, the glacier is losing mass faster than it can be replenished at the terminus, but this loss is fastest during the summer and partly replenished in the winter. The 2009-2010 annual calving rate was 27% less than the estimate of  $0.268\text{km}^3 \text{ a}^{-1}$  by Burgess et al. (2005) for the period 1960-1999, assuming that 47% of the total ice volume calved from Devon Ice Cap was lost from the Belcher Glacier. This is likely to reflect differences in method rather than real change, particularly as Burgess et al. extrapolated the calving flux estimates over a long time period and assumed velocities and ice thicknesses remained the same, based only on less than a year of surface velocity measurements on InSAR (Satellite Interferometry) data and the same ice thickness dataset (Dowdeswell et al., 2004).

These estimates of calving volume loss actually reflect total mass loss by iceberg calving and basal and terminus ice cliff melt, although the proportion of basal/ice cliff melt is currently unknown. The 2009 time lapse imagery did not capture calving as it was taking place, so it is not known whether the calving events affected the full ice thickness, or whether subaqueous calving, or significant basal melt also took place. Calving of full thickness icebergs is often observed on floating glaciers, so this information could be used to provide anecdotal evidence about whether the glacier is grounded or floating (Amundson et al., 2010). On July 30<sup>th</sup> 2008 at 12.30am iceberg debris appeared in front of the terminus, visible in the Tarasov Camera, which may have been due to subaqueous calving as it was not lost from the ice cliff, but no other evidence exists.

Figure 3.2a shows 11 observed calving events between June 4<sup>th</sup> and August 14<sup>th</sup> 2009 and five major events where the area of ice lost could be identified from the change in margin position. The largest calving events took place on July 22<sup>nd</sup>, in two separate events in which large tabular blocks were lost from the ice front, affecting ~1.5km of the glacier's 2.4km width (Figure 3.1). However the time lapse imagery was not of high enough temporal resolution to observe whether a single tabular berg was discharged or if the block disintegrated into several icebergs. Further evidence of disintegration is presented in the audio data (section 3.2.2), but this was not recorded in the 2-hour time-lapse imagery because the icebergs were immediately washed or blown out of view, restricting post-event analysis. Following the calving of two large tabular bergs on July 22<sup>nd</sup>, all other calving events were much smaller in area, though still larger than the 'columnar blocks' which are often calved from grounded glaciers (Chapuis et al., 2010).

### **3.2.2 Audio Recordings**

The audio data provide a useful event history and supplement the calving dataset described in section 3.2.2. The 2009 time lapse images were collected only every 2 hours and were often obscured by cloud, so the continuously recorded audio data potentially provide more detailed event timings and insight into the calving style. Detailed analysis or filtering of the waveforms collected was difficult as the large .wav files could not be opened in Matlab. Comparison with audio clips from the data presented in Amundson et al. (2010) was useful for identifying a calving waveform, which has a distinctive amplitude in comparison to the short-duration, rapidly decaying signals produced by rainfall or cables tapping in the wind (see Figure 1.1 and Figure 3.5). In addition to recording calving events, the audio data also provide a qualitative record of active melt (running surface meltwater), rainfall, wind conditions, and small avalanches of local ice debris. The audio data that were available during known lake drainage events, ice speed-ups, and major seismic events (see the geophone data, section 3.2.3) were examined especially carefully but there was no evidence of local fracturing or unusual surface

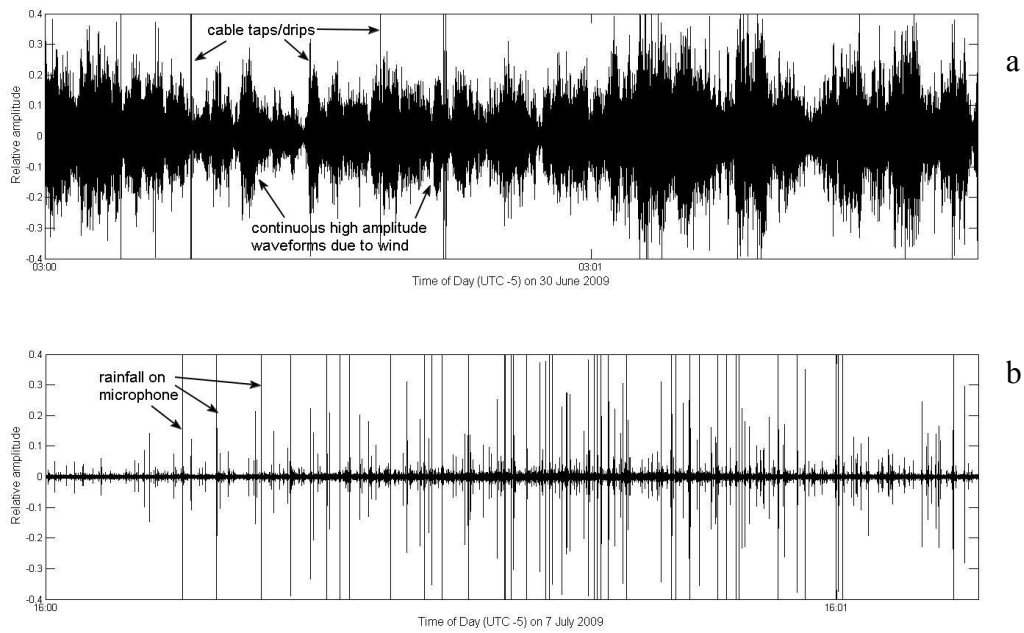


**Figure 3.5. Examples of features identified in the calving waveform: (a) high winds (<17m/s) causes cables to tap in the wind on June 30<sup>th</sup> 2009, 3am (b) rainfall and trickling meltwater on July 7<sup>th</sup> 2009, 4pm**

meltwater drainage at any of these times. In Table 3.2, the timing of calving events identified in the audio data is compared with that of events detected in the time-lapse imagery during the period when the recorder was operating (24<sup>th</sup> June – 24<sup>th</sup> July 2009). It was not possible to improve the estimated timing of the sea ice break up on 15<sup>th</sup>-16<sup>th</sup> July as any evidence for this was muffled by the sound of running meltwater and gusts of wind. The microphone was orientated towards the northern part of the terminus, so any calving events occurring near the southern ice margin would be harder to detect. Probably for this reason, small calving events observed near the southern glacier margin in the imagery from July 17<sup>th</sup> and 19<sup>th</sup> were not identifiable in the audio data.

**Table 3.2. A comparison of the timings of calving events identified in time lapse imagery and audio data for the period 24<sup>th</sup> June 2009 – 24<sup>th</sup> July 2009. In the image data for 15-16 July and 19-20 July calving was observed in the imagery but was equalized by ice advance and another partly-detached berg slipping forward. When nothing is audible in the audio data, this was always because the calving involved a small event located near the south margin (and the microphone was pointed towards the northern part of the margin).**

EVENT	TIMING FROM IMAGERY DATA	TIMING FROM AUDIO DATA
Calving observed (small)	15/7/09, 0900 – 16/7/09, 1100	-
Calving (0.0191km <sup>2</sup> )	17/7/09, 0900 – 1100	-
Calving (0.0233km <sup>2</sup> )	18/7/09, 1700 – 1900	18/7/09, 1823 – 1828
Calving observed	19/7/09, 0100 – 20/7/09, 0500	-
Calving (0.0767km <sup>2</sup> )	20/7/09, 1700 – 22/7/09, 0300	21/7/09, 2230 – 2231
Calving (0.2305km <sup>2</sup> )	22/7/09, 1100 – 1300	22/7/09, 1147 – 1158
Calving (0.0168km <sup>2</sup> )	24/7/09, 0100 – 0300	Recorder malfunctioned at 0116

The audio recorder detected three distinct calving episodes which provide further evidence of the style and precise duration of calving. All of the events can be categorized as Type 2/3 acoustic signals (see section 1.2.2). At Jakobshavn Isbrae, calving events generally began with widespread fracturing (type 1) or avalanching debris from the terminus (type 2) (Amundson et al., 2010). On the Belcher, all of the recorded events began with the rushing/rumbling sounds of avalanching debris, and loud fractures were notably absent. In each event, the relative baseline amplitude was ~0.01 as there was lots of trickling meltwater in nearby streams and crevasses (Figure 3.6). The energy then built as a series of rushing/rumbling sounds, and culminated in a thud, which is interpreted as the face of a newly formed iceberg hitting the water. The rushing and rumbling noises appear to be debris avalanching from the ice front into the water but it is not known whether the bergs were released as a tabular piece or as smaller chunks, or whether the sounds reflect a large berg disintegrating when it contacted the water. This is important to determine as it may have some bearing on the stability of the glacier. For example, Walter et al. (2010) observed that the tabular blocks produced by the

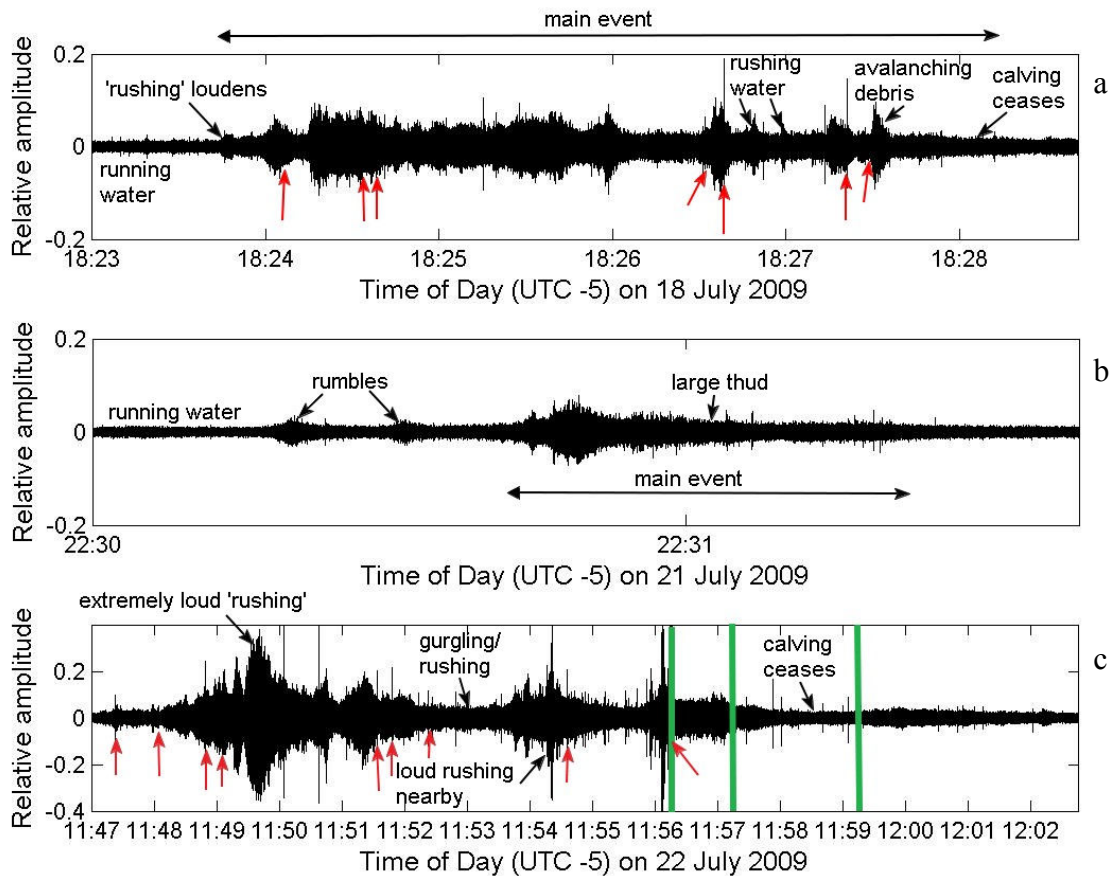


**Figure 3.6. Acoustic waveforms from three calving events, on (a) July 18th (b) July 21st (c) July 22nd 2009. Red arrows point to ‘thud’ sounds, which are interpreted as an iceberg hitting the water. The green lines in (c) are the timing confirmation from the datalogger, which is transmitted at 12 noon each day. It beeps aloud the day of the year.**

Columbia Glacier in 2007 disintegrated immediately and suggested that this might mean that the glacier’s floating tongue was not stable. However iceberg disintegration is best identified with high resolution time lapse imagery (~10s interval), which was not available for this project. Similarly with this imagery and acoustic evidence it is not possible to determine whether the bergs ‘topped out’ or ‘bottomed out’. Which of these situations occurs is dependent on the size of the berg, the amount of basal melting which has taken place before calving, and the resistive forces acting on the iceberg (such as the mélangé) (Amundson et al.,

2010). The 2007-2009 time-lapse cameras only captured one calving event when it was actually taking place, on July 27<sup>th</sup> 2008 (Figure 3.7). This event affected at least 50% of the ice front, although the area of ice lost is unknown. One of the icebergs is captured rolling ‘bottom out’, which Amundson et al. (2010) suggests sometimes happens when subglacial meltwater is being discharged in the area but this event was much further north than the Belcher Glacier plume. In Figure 3.7b an iceberg with basal sediment is visible in the fjord, suggesting calving affected the full ice thickness (sometimes more common on floating glaciers, Amundson et al., 2010), although it is not clear whether iceberg disintegration occurred during or after the calving event.



**Figure 3.7. Calving on July 27<sup>th</sup> 2008, between 1am and 2am. a) Glacier is actively calving at its northern margin, and appears to have already lost some ice, within the previous hour, which has disappeared from view or disintegrated. The berg can be seen rolling ‘bottom out’. b) After the calving event (4am), the area of ice front lost is clearly visible (the ice is a deeper blue colour) and a large iceberg with a layer of sediment attached is seen in the fjord, which appears to have come from the prior calving event.**

There were several differences in the sound of calving events from the Belcher Glacier which diverged from those recorded at Jakobshavn Isbrae, presented in Amundson et al. (2010). The absence of fracturing sounds implies that the events in Table 3.2 are type 2 signals rather than calving generated; however, the duration of the event and the presence of ‘thudding’ sounds suggest that these events represent a different style of type 3 calving event. Amundson et al. (2010)



**Figure 3.8** A small iceberg near the southern margin which has fractured to the water line, probably following preexisting surface crevasses, but is still attached above the water at the northern end. Image taken by L. Tarasov on 30<sup>th</sup> July 2008.

defined calving-generated type 3 events as those with a duration of five minutes or longer.

The event on the 21<sup>st</sup> July lasted only 1.5 minutes, so it may only be a type 2 signal. Despite this there was a large thud one minute into the event (Figure 3.6), a phenomenon not discussed by Amundson et al., which may represent an iceberg hitting the water as it rotated away from the ice cliff. There were also a number of thuds in the other events (seven in the five-minute long signal from July 18<sup>th</sup> and eight in the eleven-minute long signal from July 22<sup>nd</sup>) (Figure 3.6). From their duration alone, these are likely to be calving-generated signals. Amundson et al. were able to use 10-second resolution time-lapse imagery and seismic data to identify when three calved icebergs had finished rotating. This termination was

characterized by a peak in seismic energy but was less marked in the audible frequencies. Peaks in audible frequency at the Belcher Glacier generally coincided with the culmination of the rumbling sounds (which were not persistent during calving events at Jakobshavn, Amundson et al., 2010) and were generally followed by the thudding sound. The thud may reflect icebergs hitting the water and suggests that calving events took place in several stages, but higher-frequency images are required to verify this.

The lack of type 1 fracture events at Belcher Glacier during the 2009 summer may reflect the particular style of calving on this glacier, as well as the location of events. For example, the location of a calving event may have been predetermined by the location of crevasses and micro fractures (Pralong and Funk, 2005). Thus in order to detach an iceberg, fracturing need only occur below the waterline (where it is inaudible at the surface from some distance away). The time lapse imagery suggests that the extent of about 50% of the 2009 summer calving events could be delimited afterwards from the locations of pre-existing crevasses. Equally, however, there are many surface crevasses and it is impossible to know before an event which fracture(s) will propagate to define the iceberg. Figure 3.8 shows an example of an iceberg formed in 2008 that was well-defined by pre-existing surface crevasses but which was presumably still attached to the glacier below the water surface. Nevertheless the 2009 time lapse data show that calving did not always occur from pre-defined fractures, and also did not involve the largest, most-established crevasses. For example, the large berg that calved on July 22<sup>nd</sup> was not defined by crevasses along the edge where the iceberg calved off, but the equally large berg calved on July 24<sup>th</sup> was quite clearly delimited by pre-existing surface crevasses. Unfortunately the audio recorder malfunctioned at 1:16am on July 24<sup>th</sup>, shortly before this large calving event, so the acoustic energy differences between these events could not be compared.

### 3.2.3 Geophones

A network of three geophones was deployed near the glacier terminus in 2009 to identify fracturing events and differentiate between several potential source mechanisms: iceberg calving, surface and basal crevasse fracturing, as well as so-called 'glacial earthquakes' and land earthquakes. The data loggers all recorded data from 30<sup>th</sup> May to 14<sup>th</sup> August 2009.

It was expected that the geophones would only detect seismic energy associated with icequakes as they were installed on the glacier centreline <2km from the valley sides and on ice that is <800m deep. Nevertheless the geophones were still connected enough to the bedrock to detect a large fault earthquake 260km away in Baffin Bay. Devon Island is near the passive margin of North America. This region was previously assumed to be geologically stable, but following a large  $M_S=7.3$  earthquake in Baffin Bay in 1933 and several subsequent events, the region is now known to be quite seismically active (Bent, 2002). Large earthquakes can travel over long distances and it is important to check that events assumed to be related to glacial activity did not originate on earthquake faults. Several events detected with a geophone on Kronebreen, Svalbard, have been correlated with large seismic events ( $M_S=5$ ) in other parts of the world (A. Chapuis, pers. comm., 2010). Belcher Glacier geophone count timings were compared to world earthquake events from the USGS/NEIC 1973-present catalogue

([http://earthquake.usgs.gov/earthquakes/eqarchives/epic/epic\\_global.php](http://earthquake.usgs.gov/earthquakes/eqarchives/epic/epic_global.php)) and the earthquake wave arrival timings at the Belcher Glacier terminus were calculated using [http://neic.usgs.gov/neis/travel\\_times/compute\\_tt.html](http://neic.usgs.gov/neis/travel_times/compute_tt.html) (Kennett and Engdahl, 1991). There was one significant earthquake in the vicinity of Devon Island at 75.2753°N, -72.2013°W during the summer 2009 data collection period. The earthquake was a magnitude 6.1 on the Richter scale and occurred at 19km depth. It was detected by GLISN (Greenland Ice Sheet Monitoring Network) stations at Resolute Bay (74.68923°N, -94.896164°W), Eureka (80.05322°N, -

86.41575°W) and Alert (82.5033°N, -62.35°W). Seismograms were downloaded using JWEED from the IRIS Data Center ([www.iris.edu/data](http://www.iris.edu/data)).

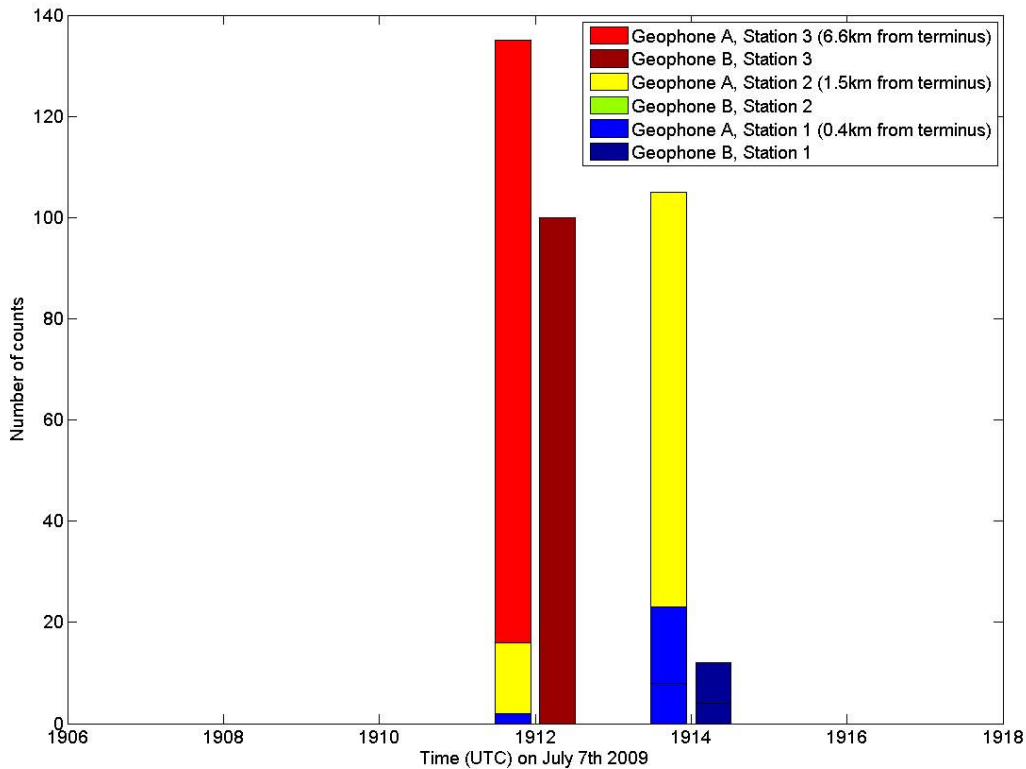


**Figure 3.9. Geophone events at Stations 1-3 on the Belcher Glacier on July 7<sup>th</sup> 2009: the day of the earthquake in Baffin Bay, directly east of Devon Island. At all three stations, the only events recorded were at 19:12 and 19:14 UTC (with 2 min totaling interval). The number of counts recorded at the 2 geophones at each station (A and B) is shown; geophone A had a lower sensitivity (2000) than geophone B (3000).**

The earthquake at 19:11 UTC on 7<sup>th</sup> July 2009 coincided with the largest seasonal peak in geophone counts, which was recorded simultaneously at all three stations on the glacier at 19:12 UTC (Figure 3.9). The earthquake, which occurred directly east of Devon Island, would have produced waves that travelled from its hypocenter to the Belcher Glacier in 37 seconds. It is recorded as counts at 19:12 and 19:14 because the logger only recorded the number of counts every 2 minutes, and travel times would have been different for the faster primary and slower

secondary body waves, which would have taken an extra 29 seconds to arrive. Geophones at stations 1 and 2 identified more events at 19:14 than 19:12, whilst station 3 picked up more at 19:12 (Figure 3.9). Yet, station 3 is the furthest from the earthquake source. This indicates that station 3 may be better connected to the bedrock (station 1 and 2 are in the highly fractured terminus crevasse zone so ice near the glacier centreline may not be well connected to the valley walls and bed). Alternatively, the number of counts may reflect ice fracture events in response to the initial earthquake, rather than a passive record of the seismic waves. Nothing unusual was recorded in the audio data at 19:12 UTC on July 7<sup>th</sup> 2009, though the sound of rain may have masked the sound of ice fracture responses to the earthquake.

Once the major earthquake was eliminated from the dataset, the geophone results were then compared with the time lapse imagery and acoustic record of calving events at the Belcher terminus in 2009. Figure 3.10 displays the geophone counts for Stations 1-3 over the 2009 summer period, compared with the known calving events. Geophone activity recorded at Station 3 during the main calving time period (July 16<sup>th</sup> to 24<sup>th</sup> 2009) is shown in

Table 3.3. No events were recorded at Stations 1 and 2 (closer to the terminus) during this time period, except 2 counts at 17:46 on July 18<sup>th</sup> at Station 2. This came just before a known calving event at 18:23 on the same day. According to

Table 3.3, the only geophone counts which may have been associated with a calving event on the 19<sup>th</sup> and 20<sup>th</sup> July, which was poorly constrained in the time lapse imagery (occurring sometime between 1am on July 19<sup>th</sup> and 5am on July 20<sup>th</sup>). As Station 3 was ~6.6km from the terminus, this station is unlikely to have detected the calving event, particularly as none of the stations closer to the terminus detected any calving events during the summer, even the largest ones. These results suggest that no major geophone activity occurred during the major calving events. The geophones were simply too far from the calving front and only responsive to local fracturing. Stations 1 and 2 were installed on seracs (ice blocks isolated by large crevasses) at the terminus and were only drilled in to a depth of 5m. This might explain why the upper geophone (Station 3) recorded 1879 counts between June 2<sup>nd</sup> and August 14<sup>th</sup> 2009 whilst station 2 recorded 497 and station 1 counted only 132, despite being closest to the terminus. Station 3 was not installed in close proximity to major crevasses and therefore was better connected to the glacier, whilst Station 1, only ~400m from the terminus, was likely the poorest connected to other parts of the glacier. This meant it identified only very local events and did not respond to calving events. The lack of detected seismic activity released during calving events could also mean that the glacier is floating. In this case, calving often occurs along pre-existing crevasse fractures and releases very little seismic energy (Walter et al., 2010). However a geophone would have to be installed much closer to the terminus for this to be confirmed.

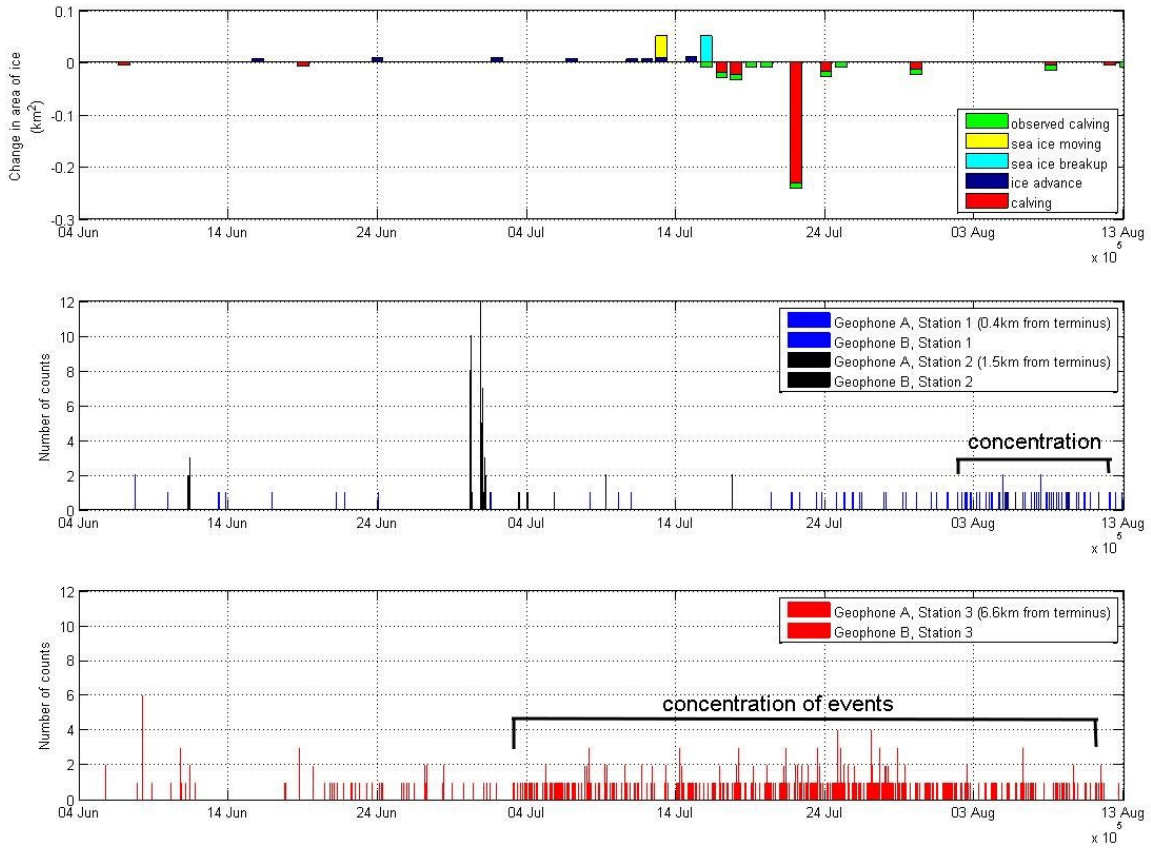


**Figure 3.10. Geophone activity and calving events as recorded in the time lapse and audio records, between June 4<sup>th</sup> and August 13<sup>th</sup> 2009. (a) Observed and recorded calving events, as well as sea ice movement and break-up (b) Geophone counts at Station 1 and 2 (c) Geophone counts at Station 3. High concentrations of event counts in a day are annotated. a**

b

c

**Table 3.3. Geophone events at Station 3 (6.6km from the terminus) between July 16<sup>th</sup> and 24<sup>th</sup> 2009: when most of the calving events took place at the Belcher Glacier terminus. Counts which occurred during the known timeframe of a calving event (according to Table 3.2) are highlighted in grey.**

DATE	TIME	COUNTS AT GEOPHONE A	COUNTS AT GEOPHONE B
16 <sup>th</sup> July 2009	21:50	2	2
	21:54	2	1
18 <sup>th</sup> July 2009	00:36	2	1
	03:04	3	3
19 <sup>th</sup> July 2009	03:14	2	2
20 <sup>th</sup> July 2009	01:52	2	1
21 <sup>st</sup> July 2009	02:38	2	2
	07:04	2	1
	07:36	3	3
	23:38	2	2
22 <sup>nd</sup> July 2009	02:22	2	1
	08:42	2	1
	18:58	2	0
23 <sup>rd</sup> July 2009	08:20	2	2
	08:26	3	3
	08:30	3	1
	12:56	2	1
24 <sup>th</sup> July 2009	17:38	4	2
	17:40	2	2
	23:38	2	1
	23:42	3	1
	23:52	2	1

There was a significant period of icequake activity at Station 2 on June 30<sup>th</sup> and July 1<sup>st</sup> which was not associated with calving events (Figure 3.10). The fractures detected at Station 2 occurred in clusters around 6am on June 30<sup>th</sup>, 11pm on June 30<sup>th</sup> to 4am July 1<sup>st</sup>, and ~2pm on July 1<sup>st</sup> (Figure 3.11). A few events were detected at Station 1, close to the terminus. The water-filled crevasses at the terminus also began to drain at 7pm on June 30<sup>th</sup> (see section 3.3.2 for more details). This icequake activity coincides well with the initiation of crevasse water draining which took place over several days. The fractures appear to have occurred as the connection from the ice surface to the subglacial drainage system

was established. The water-filled crevasses were also closest to Station 2, so it is logical that the largest number of events were detected there, and that none were recorded at Station 3, several kilometers away. The geophones do not appear to strongly detect other icequakes associated with the lake drainage events reported in Danielson and Sharp (in review) (Figure 3.11), presumably again as the geophones only pick up very local fractures so basal fracturing in response to increased subglacial discharge was not detected through the thick ice.

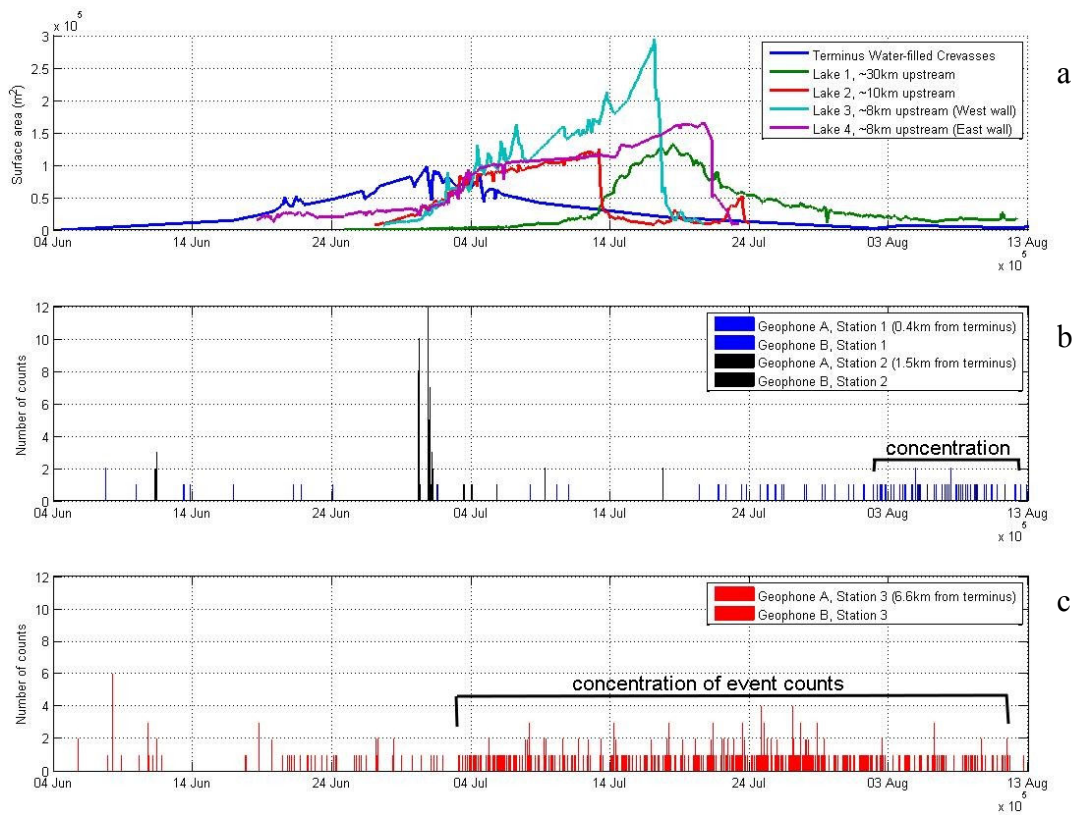


**Figure 3.11. Geophone activity and lake drainage events between June 4<sup>th</sup> and August 13<sup>th</sup> 2009. The lake drainage dataset in (a) is ownership of B. Danielson and is reproduced from Danielson and Sharp (in review) (a) Supraglacial and water-filled crevasse lake areas (legend denotes distance upstream of terminus) (b) Geophone counts at Station 1 and 2 (c) Geophone counts at Station 3. High concentrations of event counts in a day are annotated.**

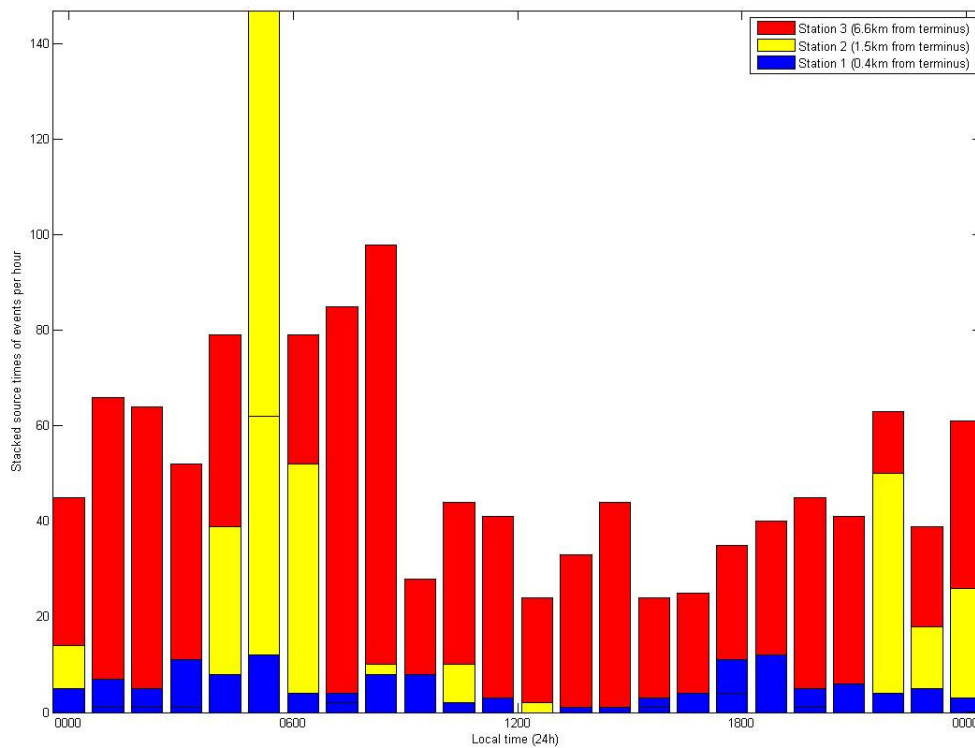


**Figure 3.12. Stacked times of icequake occurrences (per hour) for summer 2009 at Stations 1-3.**

There were no other periods of major icequake activity in the summer 2009 geophone data, but the concentrations of small numbers of counts may also be significant. Stations 1 and 3 demonstrated contrasting patterns of ‘concentrated counts’ (see Figure 3.11) whilst Station 2 did not have any concentration of counts at all. A high concentration of events (at least 1 count every 2 minutes, several times a day) occurred at Station 3 between June 4<sup>th</sup> and August 9<sup>th</sup> 2009, whilst Station 1 has a shorter ‘concentrated’ period, from August 2<sup>nd</sup> to 9<sup>th</sup>. At Station 3, this concentration appears to be when the glacier was most active: with calving events, ablation, meltwater drainage and runoff. At Station 1, the concentration appears after the major calving events had occurred, but when the meltwater plume and drainage network were still active. If these concentrated periods of counts reflect hydro-fracturing activity, the largest number of events would be expected during the warm afternoon hours of the day when melt and drainage are at their peak (Walter et al., 2008). However most of the events occurred in the late evening and early morning hours (Figure 3.12). Walter et al. (2008) found that

seismic energy sourced at the glacier bed, which was often recorded in the late evening and early morning, may be from tensile fracturing due to diurnal basal and englacial water-pressure fluctuations. Without further information about the source of icequake events on the Belcher Glacier, it is assumed that late evening and early morning fracture activity is a response to diurnal water pressure fluctuations, and events in the afternoon (during the warmest part of the day) are caused by surface fracturing.

In summary, the geophone stations on the Belcher Glacier did not detect any calving events but did identify one major land earthquake on July 7<sup>th</sup> 2009. One of the stations recorded lots of fracturing activity on June 30<sup>th</sup> and July 1<sup>st</sup>, which primed the terminus region for the draining of the water-filled crevasses. Other local fracture events may be connected to meltwater drainage, as the counts were more concentrated in July and early August when the meltwater plume was particularly active.

### **3.3 *Potential Calving Triggers***

#### **3.3.1 Terminus Velocity Changes**

It is expected that ice near the terminus may respond to a calving event: either advancing prior to calving or accelerating after the ice is lost. These changes may not happen uniformly across the whole glacier, so optical flow analysis of time lapse imagery is used to assess the spatial variations in terminus flow (Figure 2.7). In order to produce a reliable result, the resolvable lapse interval was calculated, following Ahn and Box (2010) (equation 1, section 1.3.1). This helped ensure that displacements between image pairs exceeded the combined image registration/orthorectification and optical flow uncertainty of  $0.48 \pm 0.27$  pixels (see section 2.3.1). A range of image pair intervals were tested, from 12 hours to 11 days, and the resolvable lapse intervals are shown in Table 3.4. Given that the average daily displacement at the terminus GPS (TNRS-6) was an average

0.9m/day between June 4<sup>th</sup> and August 14<sup>th</sup> 2009, and given that each pixel in the orthorectified image equates to 10m on the ground, the approximate expected pixel displacement per day would be 0.09 pixels. However in Table 3.4 the displacements in pixels/day and metres/day actually decrease with the increasing time intervals between image pairs, even though the normalized daily displacements would be expected to be similar. Furthermore, when images were selected at 0.5-3 day spacings and the resolvable lapse interval was calculated from this, the ideal resolvable lapse interval was estimated to be 3-5 days. Yet when images were paired at this ideal lapse interval, the suggested resolvable lapse period became 22-37 days, which suggests the data may be erroneous. To examine this conflicting relationship between the image pair interval and the observed displacement further, the displacements were compared with the terminus GPS data. A 21x27 pixel window (210x270m) was centered over the GPS location, which accounted for its position change between June 4<sup>th</sup> and August 14<sup>th</sup> 2009. The normalized velocity in metres/day was extracted to match the start and end of the optical flow image pairs, and they are compared in Figure 3.13. The wildly fluctuating optical flow results in Figure 3.13a, and the large overestimation above the GPS velocity, indicates that a resolvable lapse interval of 0.5-3 days was too short to produce reliable results. In Figure 3.13b, the GPS and optical flow data align more similarly but the optical flow data still shows unexpected fluctuations (such as the erroneous peak on June 28<sup>th</sup>) and this time the optical flow velocity is c.0.5m underestimated. A resolvable lapse interval of 7-11 days provides the best relative match of the GPS data (Figure 3.13c), as they have a 95% significant correlation ( $r=0.62$ ), though the optical flow is 0.5-1m below the normalized GPS results. It suggests that the optical flow algorithm can provide a relative measurement of displacement, over fairly long time intervals (7-11 days) but cannot detect absolute velocities. A lapse interval of 7-11 days also means the method is not very valuable for identifying motion prior to or following a calving event, as a lot can happen in the intermediate time. Finally, when the optical flow vector maps were examined (as in Figure 2.7), many of the vectors did not make physical glaciological sense, with vectors on successive days

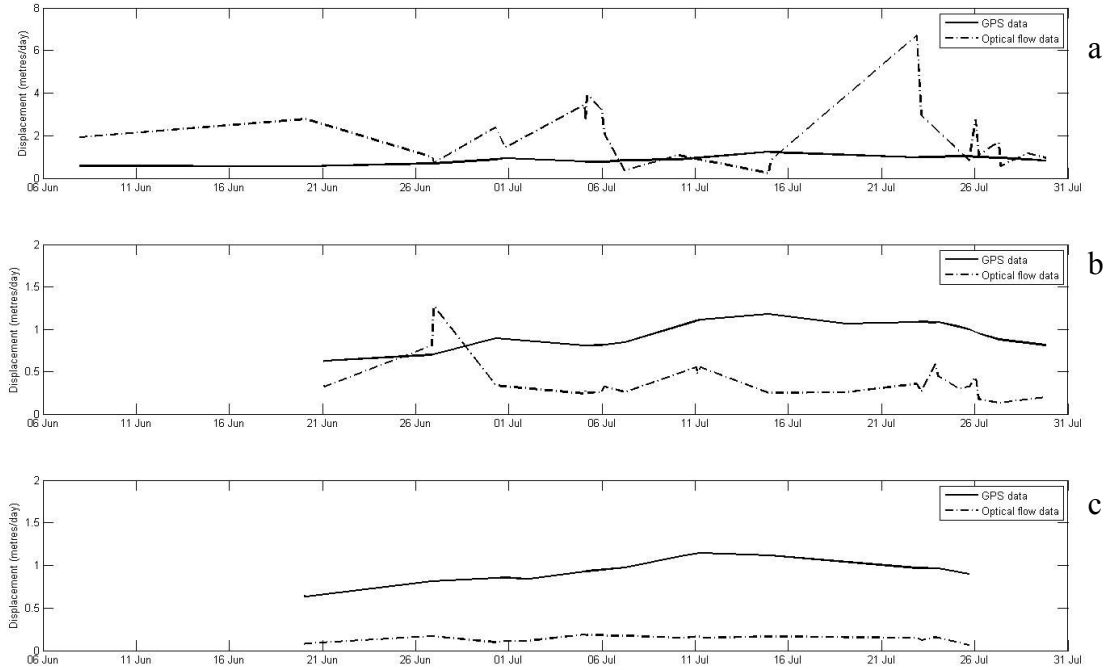


**Figure 3.13. Comparison of GPS and optical flow displacements as measured between the same image pair time intervals. The result is presented against the start date of each pair in the x-axis. Displacements are normalized (metres/day). Note the different y-axes between (a) and (b/c) in order for small fluctuations to be seen clearly. a) Images were paired 0.5 to 3 days apart b) Images were paired 3 to 6 days apart c) Images were paired 7 to 11 days apart. GPS data property of B. Danielson, presented with permission.**

**Table 3.4. Resolvable Lapse Interval calculated based on three different time ranges between optical flow image pairs. Both  $\Delta p$  (ice displacement, pixels and metres) and  $\epsilon$  (uncertainty, pixels) are normalized daily mean values. The resolvable lapse interval in days,  $\Delta d$ , is presented as two results for the optical flow data based on estimates with a 30% and 50% error budget expressed as a percentage ( $\epsilon_b$ ). The average daily ice displacement at the GPS, comparing only the same time periods examined in the optical flow analysis, is shown for comparison with the  $\Delta p$  in metres estimated from optical flow.**

IMAGE PAIR INTERVALS (DAYS)	$\epsilon$ (PIXELS)	$\Delta P$ (PIXELS)	$\Delta P$ (METRES)	GPS $\Delta P$ (METRES)	$\Delta D$ (WITH 50% $\epsilon_B$ )	$\Delta D$ (WITH 30% $\epsilon_B$ )
0.5 – 3	0.14	0.29	2.9	0.89	3.08	5.14
3 – 6	0.05	0.038	0.38	0.93	22.5	37.47
7 – 11	0.018	0.012	0.12	0.92	7.08	11.8

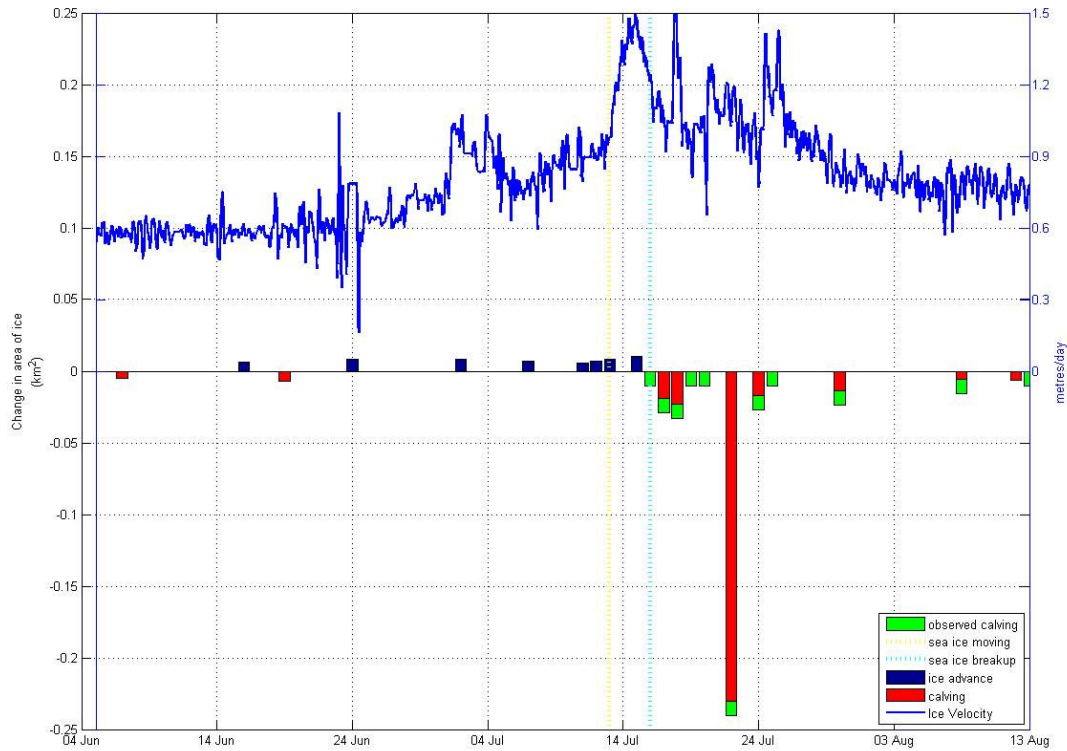


**Figure 3.14. Calving front area change compared to horizontal ice surface velocities measured by GPS at TNRS-6 (GPS data from B. Danielson). Only significant advance or retreat of the margin is presented, along with times when calving was visually observed. Note that many of the events represent total change in the previous 24-hours, so advance/retreat may appear to occur the day after it actually did. The timing of sea ice initial independent movement and final break up are also shown. b) Ice surface velocities measured by GPS at TNRS-6.**

flowing in completely different directions and some of them travelling upglacier. Therefore, it is surmised that when carefully applied, the algorithm may be able to identify relative velocity changes, although further testing is required on a faster moving glacier where the resolvable lapse interval would be shorter. Great care also needs to be taken with camera setup particularly that the camera is orientated perpendicular to the main flow velocity vectors (in this study there was a roll angle of  $13^\circ$ ) (Krimmel and Rasmussen, 1986). Nevertheless one useful result from this aspect of the study was that the georeferencing method utilized from

Croitoru and Ethrog (2001) proved to be accurate and is thus potentially useful in future oblique photogrammetry projects.

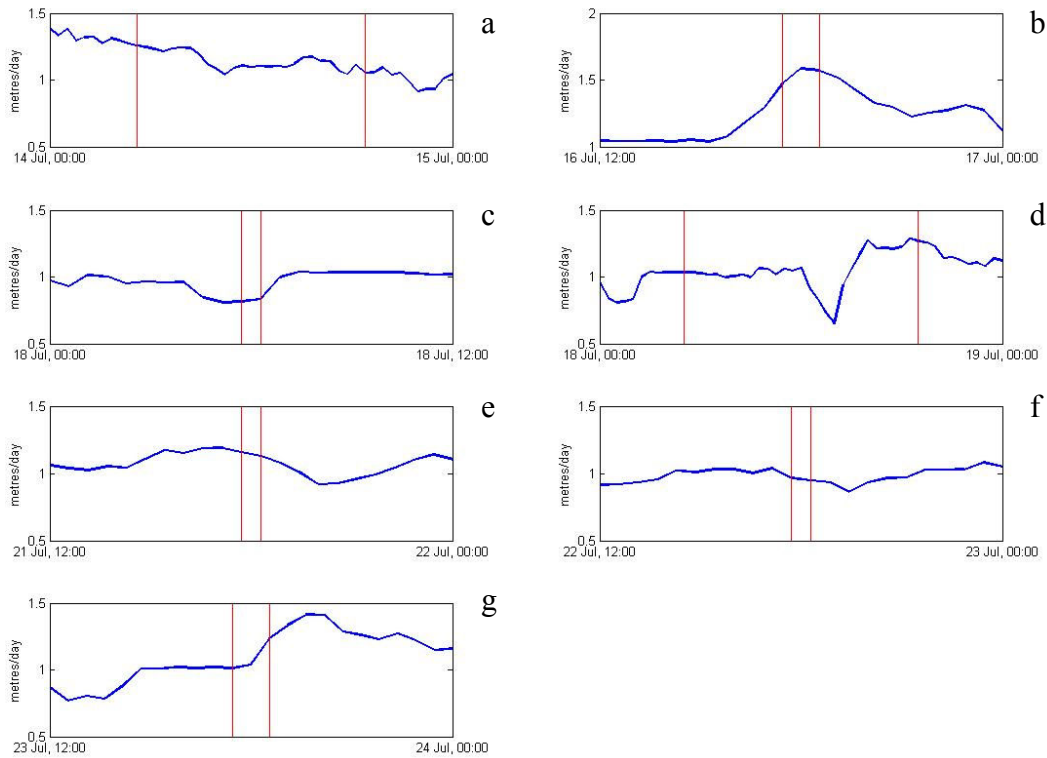


**Figure 3.15. Detailed comparison of calving event timings to GPS velocity at TNRS-6 (GPS data from B Danielson). The known timings of each calving event (see Table 3.2) in (a)-(g) is defined by the red lines, with the horizontal GPS velocity shown in blue.**

As optical flow did not produce reliable velocity records, the GPS ice surface velocity on the glacier centreline at the terminus was compared to the timing of calving events to determine whether there is any relationship between velocity changes and calving events. Horizontal ice velocity measured by GPS at TNRS-6 (Figure 2.2) is shown alongside the calving event dataset from summer 2009 in Figure 3.14. The timings of major calving events are presented alongside the velocity record from the specific event periods in Figure 3.15, for more detailed comparison. There is no clear unidirectional relationship between calving and velocity during these events: in some instances there is a slow increase in velocity during a calving event, but in others there is a slow velocity decrease. In the hours

prior to and following an event there is usually no apparent linear connection. This could be because the GPS is too far from the terminus (~300m away) to detect coupling between velocity and calving events. However Vieli and Nick (2011) expect instantaneous redistribution of stresses in the terminus region in response to calving events, within a longitudinal coupling distance of around 10 ice thicknesses (which equates to ~2.17km on the Belcher Glacier). There was no obvious velocity response to such redistribution- if it occurred- even during the largest calving events on July 22<sup>nd</sup> 2009.

### **3.3.2 Water-filled Crevasses**

In this section, the growth and drainage of the area of water-filled crevasses at the terminus, shown in Figure 3.2d, will be compared with the timing of calving events and fluctuations in meltwater plume area. The data are unevenly spread due to the inherent problems with time lapse imagery: cloud cover and severe lighting conditions (e.g. extremely bright or low light). The highest temporal resolution data were collected between June 29<sup>th</sup> and July 7<sup>th</sup> 2009, when some diurnal fluctuations in water area may be discernible. In 2009, the crevasse ponds began to form on June 4<sup>th</sup> and were visible on the terminus throughout the summer until the camera was removed on August 14<sup>th</sup>, though they were most prolific in June and early July. The total lake area peaked at 0.098km<sup>2</sup>, at 7pm on June 30<sup>th</sup>. This was followed by a steady loss of water area until July 6<sup>th</sup> (area change of -0.043 km<sup>2</sup>) after which the dataset became much sparser but the water area continued to decline. The lake area peak coincided with one of the warmest days in 2009, when air temperatures reached 8°C. The crevasses all appeared to drain downwards into the glacier rather than across the surface, the implications of which will be discussed in section 3.3.3. These water-filled crevasses grew to a total lake area of 0.083km<sup>2</sup> over a 27 day period from their initial emergence, and then decreased in area by almost the same amount over 44 days during the latter part of the season. Qualitative comparison of the time-lapse imagery with Digital Globe® imagery (<http://browse.digitalglobe.com/imagefinder/main.jsp>) indicates

that the camera only captures around 70% of the total area of water-filled crevasses at the terminus. Therefore the results only relate to a sample of the area of water-filled crevasses but it is assumed that the timing of meltwater accumulation and release these ponds is representative of the population as a whole. In terms of accuracy, to allow for errors in the image georeferencing and the lake picking algorithm, these results will be primarily examined for changes in trend between water filling and draining, rather than precise changes in area which may not be temporally correct due to the sparsely sampled dataset.

The change in trend of the area of water-filled crevasses will now be compared to the timing of calving events, ice fracturing events, margin advances and GPS velocity data. It has already been shown that the timing of the drainage of water-filled crevasses seems to coincide with a series of major fracturing events recorded by the terminus geophones that are likely to have been caused by hydrofracturing when the crevasse water establishes a drainage connection to the bed (see section 3.2.3). However the drainage of the water-filled crevasses does not seem to relate directly to the timing of calving events, the largest of which occurred between July 16<sup>th</sup> and 24<sup>th</sup> 2009. In Figure 3.2 it can be seen that crevasse water drainage, which was initiated temporarily on June 20<sup>th</sup>-21<sup>st</sup> and again on June 30<sup>th</sup>, had been going on for some time before calving took place. The water-filled crevasses area data are also sparse during the period of major calving, so it is difficult to make a more thorough interpretation of this relationship. Instead, the initiation of drainage appears to be more closely linked to advances of the terminus margin which first occurred on June 22<sup>nd</sup> and then again on July 2<sup>nd</sup>. As discussed in section 3.3.1, these margin advances also coincided with velocity increases measured in the GPS record (Figure 3.14) (Danielson and Sharp, in review). The advance of the terminus margin in response to water-filled crevasse drainage indicates that these water-filled crevasses play at least a small indirect role in driving calving by increasing the ice flux through the terminus region. Danielson and Sharp (in review) estimated that the seasonal ice

acceleration due to the total water-filled crevasses and supraglacial lake drainages throughout the 2009 summer explained 4.8% of the summer calving flux.

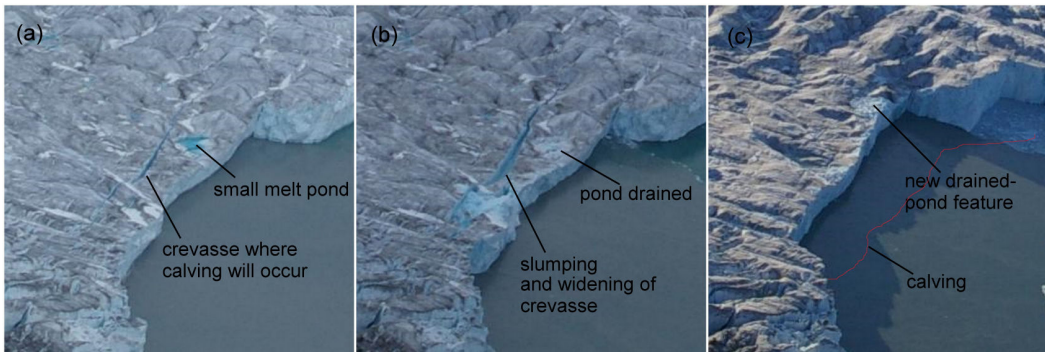


**Figure 3.16. A small potentially meltwater propagation-driven calving event which took place on July 30<sup>th</sup> (a) July 27<sup>th</sup>, 11pm: crevasse, where calving will later takes place, widens. Note melt pond, and location of plume (b) July 29<sup>th</sup>, 7pm: melt pond has drained, and crevasse has widened and begun to slump forwards (c) July 30<sup>th</sup>, 9pm: calving has taken place along the pre-existing crevasse fracture and another melt pond appears to have formed and drained in the intervening time.**

It will now be considered whether any of the water-filled crevasses at the Belcher Glacier terminus could have triggered a calving event, as hypothesized by Benn et al. (2007). In Figure 2.8, the water-filled crevasses identified by the lake-picking algorithm are shown for June 30<sup>th</sup> 2009 at 7am. This is almost the maximum areal extent of water-filled crevasses in 2009, as they began to drain at 7pm that day. A few very small water-filled crevasses which were missed by the algorithm are identified in the foreground. One crevasse pond (marked 'Lake A') is only ~10m from the terminus. However it had drained by July 16<sup>th</sup>, when calving events began and the sea ice broke up. At this stage, the closest lake was ~150m away from the terminus (marked 'Lake B'). Water-filled crevasses were not in the vicinity of ice calved during the major events (July 16<sup>th</sup>-24<sup>th</sup>), though the presence of the water-filled crevasses may have played a role in weakening the ice as it advanced to terminus. The only example of a water-filled crevasse very close to the terminus which potentially triggered a calving event is shown in Figure 3.16. In this case, a crevasse very close to the terminus began to widen on July 27<sup>th</sup>, and

enlarged over several days until calving took place on July 30<sup>th</sup>. A melt pond visible on the surface near the crevasse drained at 7pm on July 29<sup>th</sup>, and was followed by calving between 11am and 1pm on July 30<sup>th</sup>. The melt pond formed on ice that later calved, whilst after the event another small pond appears to have formed for a short time on the surface but must have drained quickly (images are missing due to cloud cover). It is not clear whether there was meltwater in the crevasse, but certainly the presence and drainage of two melt ponds, as well as the continuing flux of the meltwater plume beneath the ice may have weakened the nearby ice, 'priming' it for iceberg calving.

### **3.3.3 Meltwater / Sediment Plume**

The meltwater plume area was mapped in order to assess whether large meltwater discharges caused calving events by temporarily increasing the buoyancy of the glacier terminus and/or increasing the basal melt rate. The evolution of the area of the meltwater/sediment plume during the summers of 2007, 2008 and 2009 is presented in Figure 3.17c, Figure 3.18c and Figure 3.2c respectively. Firstly it should be noted that the 2007 and 2009 datasets are not complete as the camera was removed before the plume had finished discharging for the season, which may have affected the calculation of the integral of the plume area over the melt season. It also explains why the longest duration of plume discharge appeared to occur in 2008. However the most significant control on the seasonal integral of plume area was the camera position in each year. The 2009 integral of plume area was 9.3km<sup>2</sup>, compared with 49.1km<sup>2</sup> in 2007 and 49.9km<sup>2</sup> in 2008. If we compare the length of plume extending east from the prominent medial moraine, only 200m was visible from the 2009 camera position but 2km was seen in 2008 (Figure 2.9). This meant that while small plumes were delimited accurately in 2009, the extents of large plumes were severely underestimated. This is confirmed with cross correlation: there was a strong positive relationship between plume area and modeled runoff (Duncan, 2011) in 2008 (99% significance with no lag,  $r=0.52$ ), whilst in 2009 this relationship was slightly weaker (95% significance

with no lag,  $r=0.39$ ). The results clearly demonstrate the need for multiple cameras to observe different terminus phenomena such as calving or plume activity. The 2009 camera position was better for mapping the calving front, but the 2008 angle showed more of the meltwater/sediment plume. It is therefore unfortunate that the camera installed in the 2008 position did not work during the 2009 season.

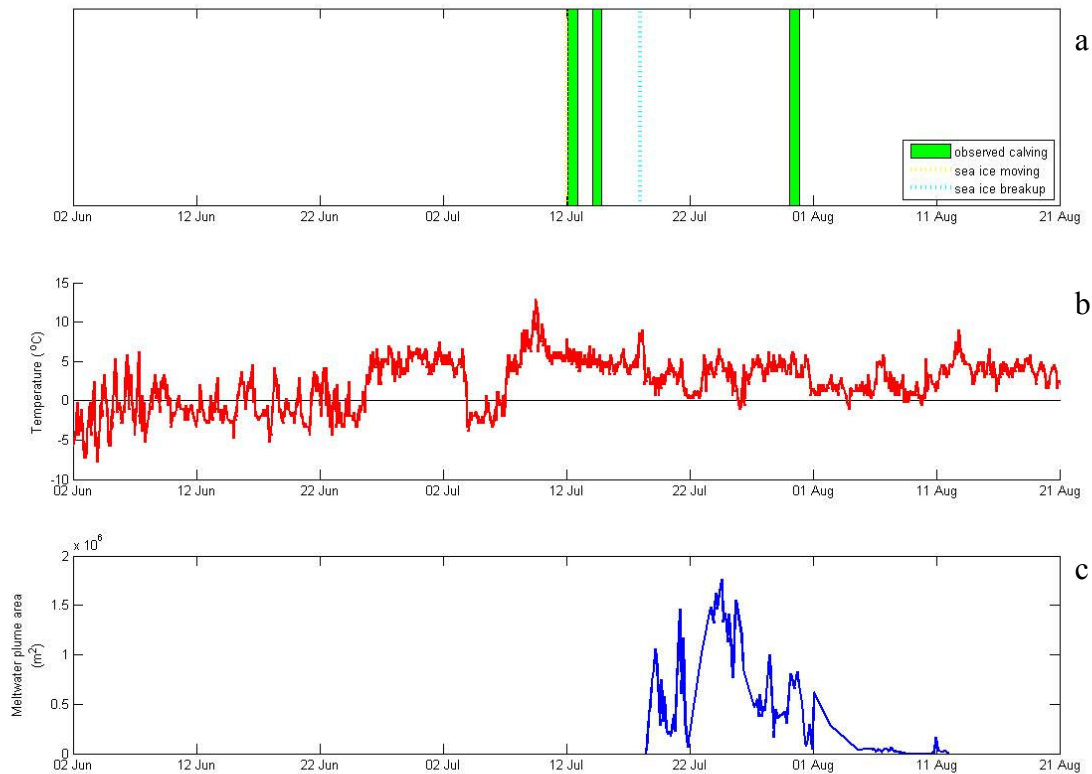


**Figure 3.17. Summary of calving activity, sediment plume calving activity and environmental conditions for summer 2007. a) Bar chart displaying observed calving events as well as the timing of sea ice initial independent movement and final break up. b) Air temperature at Hobo 25, a GPS station close to LBAWS (which was installed in 2008). c) Sediment plume area (modeled runoff was not available as the weather station was not installed).**

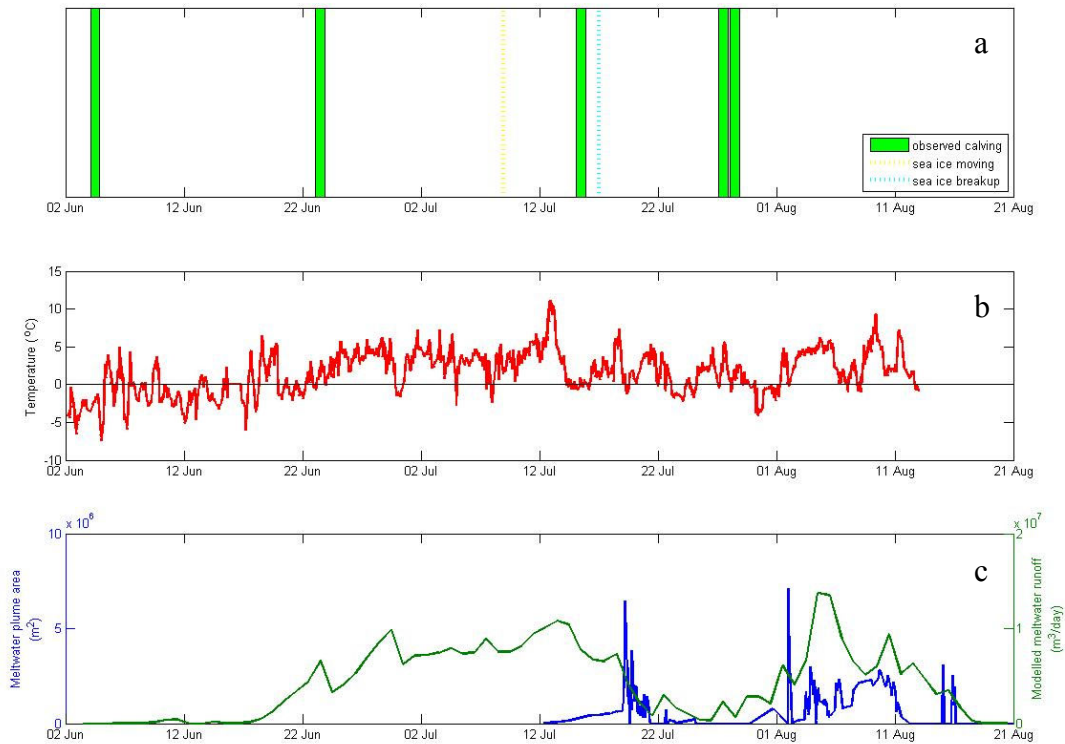


**Figure 3.18. Summary of calving activity, sediment plume calving activity and environmental conditions for summer 2008. a) Bar chart displaying observed calving events as well as the timing of sea ice initial independent movement and final break up. b) Air temperature at LBAWS. c) Sediment plume area and modeled runoff volume.**

MODIS imagery was used to estimate how much of the plume was missing from the 2007-2009 time lapse images, due to the camera positions. A threshold reflectance value was used to automatically identify the plume in the imagery. Comparison of plume extents derived using different threshold reflectance values with those derived from true colour images (bands 1-4-3) in which the plume is visible to the eye suggests a threshold reflectance value of 0.012 is appropriate for the Belcher Glacier system. No reflectance values exceeded 0.12 (the threshold value used by Chu et al., 2009 in their study at Kangerlussuaq). This may reflect the differences in latitude between the sites. The 250m resolution of MODIS data is too low to differentiate the turbid plume from the brackish plume, so it cannot be used to validate the interpretations of the time lapse imagery. However the

MODIS images do suggest a plume continued to emerge in 2009 after the time lapse camera was removed on August 14<sup>th</sup> (Figure 3.19). No quantitative interpretation can be made without ground validation (with the time lapse camera, SSC measurements or stream outflow data) but the results clearly show that sediment (and presumably meltwater) continued to exit the Belcher Glacier terminus. Melt runoff was predicted to cease on August 15<sup>th</sup> (Duncan, 2011) but stored water may have been continuing to drain after melt ceased.

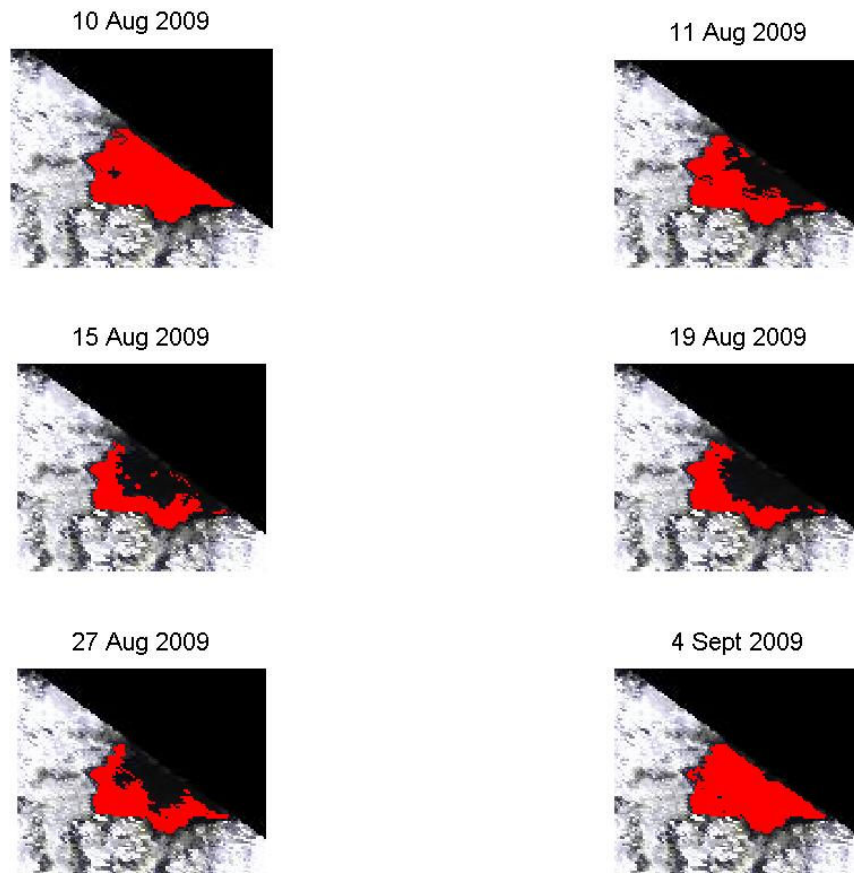


**Figure 3.19. Surface reflectance values from cloud-free MYD09 and MOD09 250m resolution band 1 MODIS images between August 10<sup>th</sup> and September 4<sup>th</sup> 2009. The results are plotted on the same base image (August 11<sup>th</sup> 2009) which is in colour using bands 1-1-2. Only reflectance values >0.012 are shown highlighted in red. The results from August 10<sup>th</sup> to 19<sup>th</sup> match qualitatively to the greenish-grey plume visible in true colour (bands 1-4-3) jpg images (available at 500m resolution) but this greenish-grey is not present on August 27<sup>th</sup> and September 4<sup>th</sup> - although it is not possible to prove that sediment is not present.**

In previous studies of marine meltwater/sediment plumes, such as Chu et al. (2009), the plume was not identified until the sea ice had broken up. This is mainly because the presence of sea ice in the fjord confounds the spectral signal of MODIS imagery and prevents plume detection (Chu et al., 2009). Yet in the Belcher Glacier time lapse imagery it was possible to identify a small plume ( $<0.13\text{km}^2$ ) which emerged at the ice front up to 6 days before sea ice breakup. This plume was only visible once the sea ice surface was covered with water and some sections near the ice cliff had begun to move independently, ahead of full breakout of the sea ice cover in the fjord. The first independent shifting of the sea ice prior to breakup is marked in Figure 3.17 and Figure 3.18a. In 2007 and 2009 it occurred 3-13 days after the air temperature rose and stayed above  $0^\circ\text{C}$  but in 2008 the temperature never remained above  $0^\circ\text{C}$  for more than a few days at a time. Figure 3.18 and Figure 3.2c also present daily runoff for 2008 and 2009, as modeled by Duncan (2011) using a spatially distributed energy balance melt model based on Hock and Holmgren (2005). This melt model was forced using air temperature, relative humidity, wind speed and direction, radiation and precipitation data monitored at three weather stations (included LBAWS) that were installed for this purpose. The appearance of the plume lagged the modeled onset of runoff by an average of 27 days. The only record of snowpack changes available is from 2008, when rapid snow melt and glacier ice exposure occurred between June 26<sup>th</sup> and July 1<sup>st</sup> on areas of the glacier below 1000m (Duncan, 2011). There was likely to have been some melt between June 1<sup>st</sup> and June 26<sup>th</sup> but frequent snow flurries occurred during this period and runoff may have been minimal (Duncan, 2011). The lag between modeled runoff onset (June 17<sup>th</sup>) and plume appearance (July 11<sup>th</sup>) in 2008 was 26 days. The sea ice often breaks up first in the vicinity of the meltwater plume, prior to full breakup, but it is not clear whether the plume emerges beneath the sea ice before this and slowly weakens the sea ice above it through basal melt. A plume would be expected following water-filled crevasse drainage initiation on June 30<sup>th</sup> as it corresponded with a velocity increase which suggested sliding facilitated by basal meltwater.

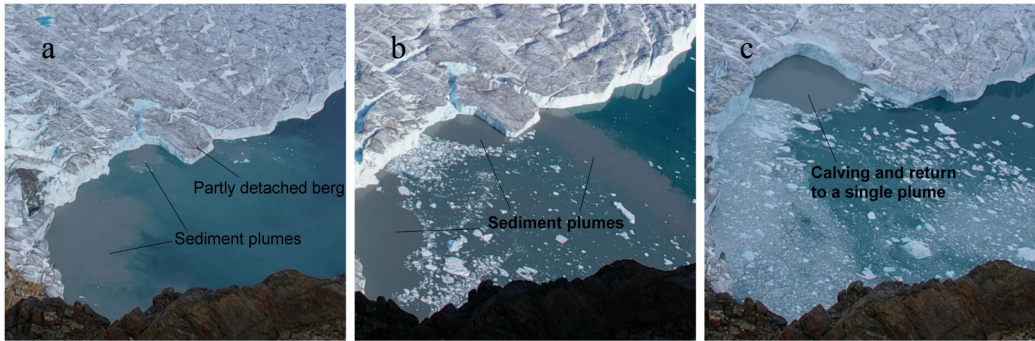


**Figure 3.20. Sequence of changes in the meltwater/sediment plume leading up to a calving event on July 17<sup>th</sup> 2009 (a) Following sea ice break-up, an iceberg was left partly detached, and 2 sediment plumes were emerging on July 16<sup>th</sup> at 11am (b) The plumes then began to emerge in 3 separate places, the newest one on the other side of the soon-to-be-iceberg, shown here on July 17<sup>th</sup> at 9am (c) Calving took place between 11am and 1pm on July 17<sup>th</sup>. This photo was taken at 1pm. The meltwater has reverted to a single plume and the iceberg has been calved off.**

In 2009, the timing of iceberg calving events seems to have been influenced by the location of the meltwater plume, which sometimes also shifted its position and appeared to instigate a calving event. For example the calving events on July 17<sup>th</sup> and 22<sup>nd</sup> were caused by re-routing of meltwater around ice that was about to calve off. On July 16<sup>th</sup>, the plume began emerging on the northern side of an iceberg that was already partly detached (Figure 3.20). There was an increasingly large discharge on both sides of the iceberg until its eventual calving between 9 and 11am on July 17<sup>th</sup>. Meanwhile, from July 20<sup>th</sup> and 22<sup>nd</sup> 2009 the plume began to emerge further north than it had done during the rest of 2007-2009 (Figure 3.21). Prior to this, between July 19<sup>th</sup> at 1am and July 20<sup>th</sup> at 5am, a small 1656m<sup>2</sup> area of ice calved off from near the sediment plume. This may have facilitated re-routing of the meltwater plume in some manner. The ‘bulge’ (see Figure 3.21), which was soon to calve off, also advanced by 734m<sup>2</sup> during this time period, and the plume began to emerge in two locations- one much further north than usual. These displacements were not picked up in Figure 3.2a because the advance offset the small calving event. Following the calving of the ‘bulge’ which occurred by July 22<sup>nd</sup> at 3am, the plume reverted to its ‘normal’ location near the southern margin. It is important to note that the location of the new northern plume was

precisely where a major calving event took place several days later. The implications of these events are two fold. First, iceberg calving can be facilitated by changes in subglacial discharge and is most likely to occur near where the plume exits the glacier. This is either due to an increase in subglacial discharge which raised local flotation, or as a product of basal melt in which mixing of the plume water with seawater lowers the pressure melting point (Motyka et al., 2003). Second, the plume can be rapidly re-routed beneath the terminus, either by changing basal water pressures or by creation of basal channels or fractures in which the water travels.

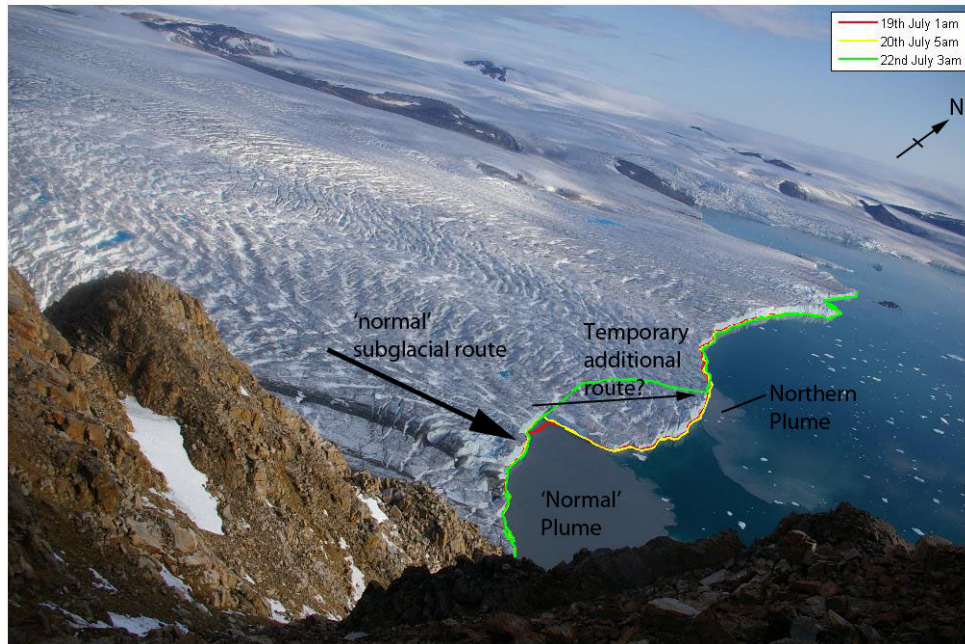


**Figure 3.21.** The sediment plume began to emerge from a new northern location between July 20<sup>th</sup> and 22<sup>nd</sup> 2009, shown here in an image from 7am on July 20<sup>th</sup>. The digitized ice margin positions from July 19<sup>th</sup>, 20<sup>th</sup> and 22<sup>nd</sup> are shown. Note also the small calving event between July 19<sup>th</sup> (red) and 20<sup>th</sup> (yellow), which coincided with the advance of the ice that is about to be calved on July 22<sup>nd</sup>. The assumed ‘normal’ subglacial route of the meltwater, and its temporary additional rerouting beneath the ice that is about to be calved is also shown.

However not all calving events in the time lapse imagery were associated with the presence of subglacial discharge. For example two events in August 2009 occurred at the northern end of the margin where the plume was not observed.

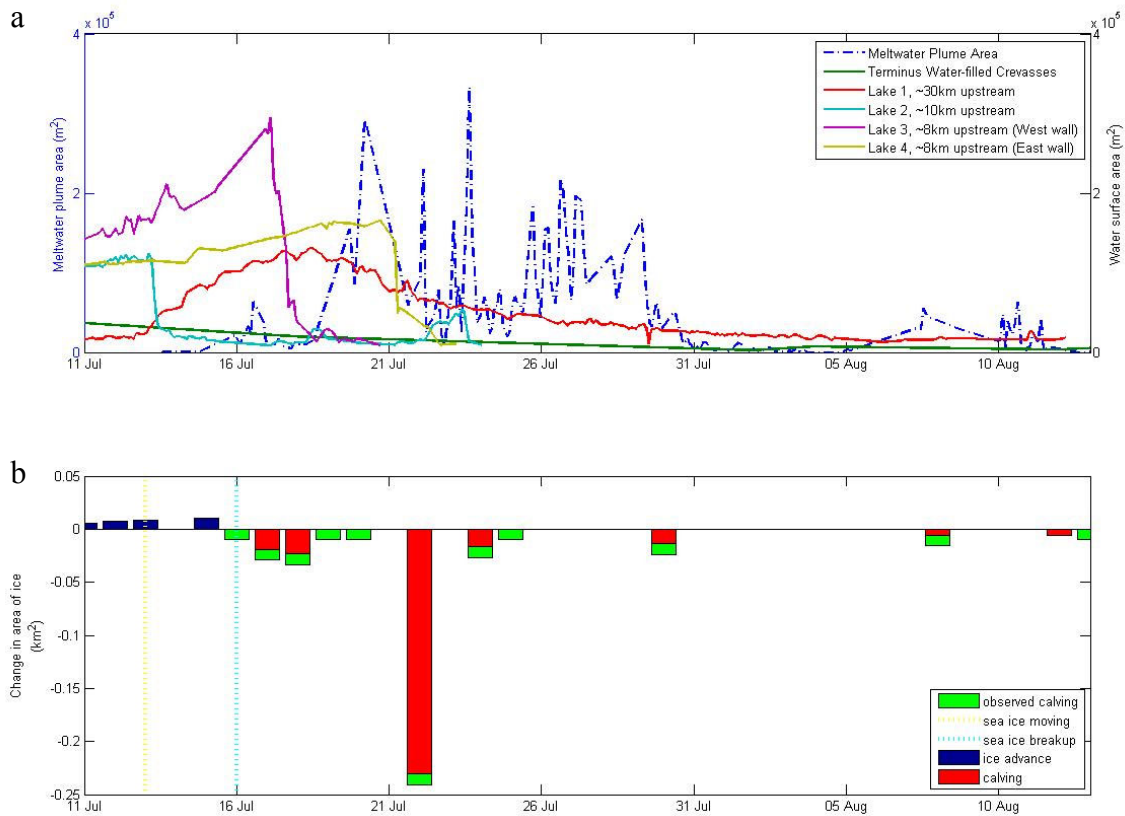


**Figure 3.22. Meltwater plume discharge, lake drainage and calving events between July 11<sup>th</sup> and August 13<sup>th</sup> 2009. The lake drainage dataset is ownership of B. Danielson and is reproduced from Danielson and Sharp (in review) (a) Meltwater plume discharge area, and supraglacial and water-filled crevasse lake areas (legend denotes distance upstream of terminus) (b) Bar chart of calving front area change, presenting only significant advance or retreat of the margin, and times when calving was visually observed. The timing of sea ice initial independent movement and final break up are also shown.**

There was only one calving event after sea ice break up in the 2007 time lapse imagery, and it occurred slightly north of the meltwater plume. Likewise in 2008 the event on July 15<sup>th</sup> occurred just north of the plume, and the large event on July 27<sup>th</sup>/28<sup>th</sup> took place at the northern end of the margin when the plume was not even active. This indicates that calving took place under very different conditions in 2007/8 than in 2009. This may be because the average margin position in 2009 was more advanced than 2007/8, which led to weaknesses in different parts of the ice front (see section 4.2). The meltwater plume does appear to have had some

role in facilitating calving events during the peak of the 2009 melt season, and in the right circumstances it may enhance the calving rate, but its presence alone does not necessitate a calving event. There is also no clear evidence that the meltwater plume responds with a size increase to supraglacial drainage events, as shown in Figure 3.22, but this might be seen better with data of higher temporal resolution.

### **3.3.4 Mélange / Sea ice buttressing**

The changes in the state of the sea ice visible in the 2007-2009 time lapse imagery are used to examine whether the sea ice may have a buttressing effect on the glacier terminus that reduces the incidence of calving events in winter. In 2007 (refer to Figure 3.17) the sea ice and mélange near the plume exit began to move on July 12<sup>th</sup>. This coincided with a calving event near the southern margin that pushed the ice mélange forwards and widened leads in the sea ice behind the mélange. There was a calving event at the northern margin on July 14<sup>th</sup>, which was followed by sea ice breakup by 2am on July 18<sup>th</sup>. However in 2007 the plume was not visible until the sea ice had completely broken up. Upon break-up, water near the southern margin which was affected by the plume was completely free of sea ice but ice chunks remained in the northern part of the time lapse view for an extra day until they were also blown away, and the terminus then remained free of sea ice for the rest of the summer.

In the 2008 time lapse imagery (refer to Figure 3.18), the sea ice began to move independently near the meltwater plume exit on July 11<sup>th</sup> and became increasingly disintegrated until all of the sea ice visible in the 2008 camera view was drifting freely by July 17<sup>th</sup>. The Tarasov camera shows that ice in the northern bay remained coalesced until July 18<sup>th</sup> when leads began to open up (Figure 3.23). Free-floating sea ice plates appeared on the 19<sup>th</sup> and were finally lost from the bay at 4.30am on July 20<sup>th</sup>. This was when sea ice also disappeared from in front of the Belcher Glacier terminus. Sea ice remnants were blown back into the bays at

9pm on July 20<sup>th</sup> and remained floating around for most of the season. Ice in the northern bay and beyond the view of the cameras appears to have been kept the sea ice near the Belcher terminus in place, even though this ice had already disintegrated. Wind played a major role in the eventual disintegration of the sea ice. On the 11<sup>th</sup>, when sea ice near the terminus began to move, the wind was 5-6m/s from the SW. However on the 18<sup>th</sup>, when sea ice in the northern bay began to disintegrate, the wind switched abruptly to the NW at 7am, with increasingly strong winds up to 11.25m/s at 10am when leads were observed to have opened up. There were also strong winds (<11.7m/s) from the west at 4am on the 20<sup>th</sup> when the sea ice was blown out, followed by much lighter winds from the east (<3.5m/s) between 8-9pm when the sea ice returned to the terminus.



**Figure 3.23. Leads opening in the sea ice in the northern bay. Photo taken July 18<sup>th</sup> 2008, 4.30pm, from the *Tarasov Camera*.**

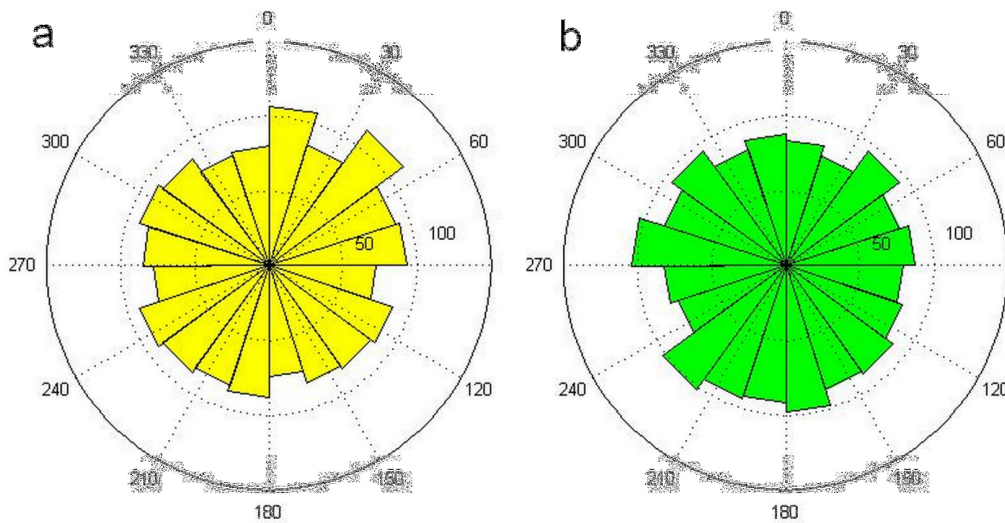


**Figure 3.24. Rose diagrams of wind direction, comparing 1<sup>st</sup> June-12<sup>th</sup> August 2008 (a) to 2009 (b) at LBAWS.**

In 2009, the sea ice first began to move independently on July 13<sup>th</sup>, and break-up had occurred by July 16<sup>th</sup> in coincidence with the first observed calving event of the summer (refer to Figure 3.2). As in 2008, break-up was initially centered on the meltwater plume location, suggesting that the emergence of the plume contributes to local break-up. The audio data suggest that there was particularly active surface runoff in the 24-hour period preceding sea ice breakup. This included substantial amounts of meltwater flowing on the glacier surface or in crevasses, along with rain and frequent local avalanching of debris. Rainfall is likely to have flooded the surface of the sea ice with water, making it increasingly weak. At break-up, which took place anytime between 9am on July 15<sup>th</sup> and 11am on July 16<sup>th</sup>, the wind direction was very variable, coming predominantly from the west but switching regularly to the NE. The wind speed did not exceed 2m/s during this time period. Once the sea ice had broken up, it immediately moved offshore and did not get drawn back to the terminus region. This is in direct contrast to 2008, and a comparison of the prominent wind directions from summer 2008 and 2009 (Figure 3.24) shows that in 2008 there were more winds from the N and NE, whilst in 2009 more were from the W and SW. It is possible that the

higher frequency of westerly winds in 2009 kept sea ice fragments away from the terminus, whilst in 2008 the northerly winds blew sea ice pieces back into the terminus bay.

Evidence presented from the 2007-2009 time lapse imagery and AWS data suggests that in 2008 the wind blew out the sea ice, but not in 2007 and 2009; whilst in 2009 there was a calving event associated with break-up which did not happen in 2007 or 2008. These results indicate that wind conditions can sometimes be the trigger in sea ice breakup, but this breakup is not necessarily accompanied by a calving event. There is no evidence to suggest that major calving is caused by sea ice breakup in response to loss of buttressing support, as suggested by Herdes et al. (in review).

Having determined that summer calving is not driven by the loss of sea ice, I now consider firstly whether calving takes place in the winter, secondly if there is evidence to suggest that the sea ice buttresses the glacier in mid-winter and finally if the changing area of *mélange* in front of the glacier affects the buttressing strength. A *mélange* of icebergs collects on the surface of the sea ice or is trapped within it during the period between freeze-up of the sea ice in the fall (usually in late October) and reinstallation of the time lapse cameras in May. This *mélange* is not on the same scale as that described by Amundson et al. (2010) at Jakobshavn Isbrae but is still of substantially different character to the sea ice beyond the *mélange* (Figure 3.25). At the Belcher Glacier, the *mélange* is mainly chunks of glacier ice which have rolled onto the sea ice during the winter, along with a few larger icebergs that have been incorporated during freeze-up, and some icebergs near the margin which appear to be detached but are held against the terminus by the sea ice (i.e. buttressed). Each year, the *mélange* forms on different areas of the sea ice at the terminus (Figure 3.26), whilst the terminus position changes significantly between August and May. Most of the margin change is attributed to fall calving (given the significant changes between August 14<sup>th</sup> and September 19<sup>th</sup> 2009 in Figure 3.4) but the presence of the *mélange* also indicates calving



Figure 3.25. The *mélange* of icebergs intermingled with sea ice, viewed from the 2009 time lapse camera (a), where the *mélange* is outlined in red, and several perspectives from near the island (b-d), the location of which is marked in (a). (b) and (d) highlight the sharp distinction between sea ice and *mélange*, and (c) shows the buttressing effect of the sea ice, which is preventing several icebergs and smaller disintegrated chunks from falling off the terminus. The red arrows indicate where features in each scene coincide.

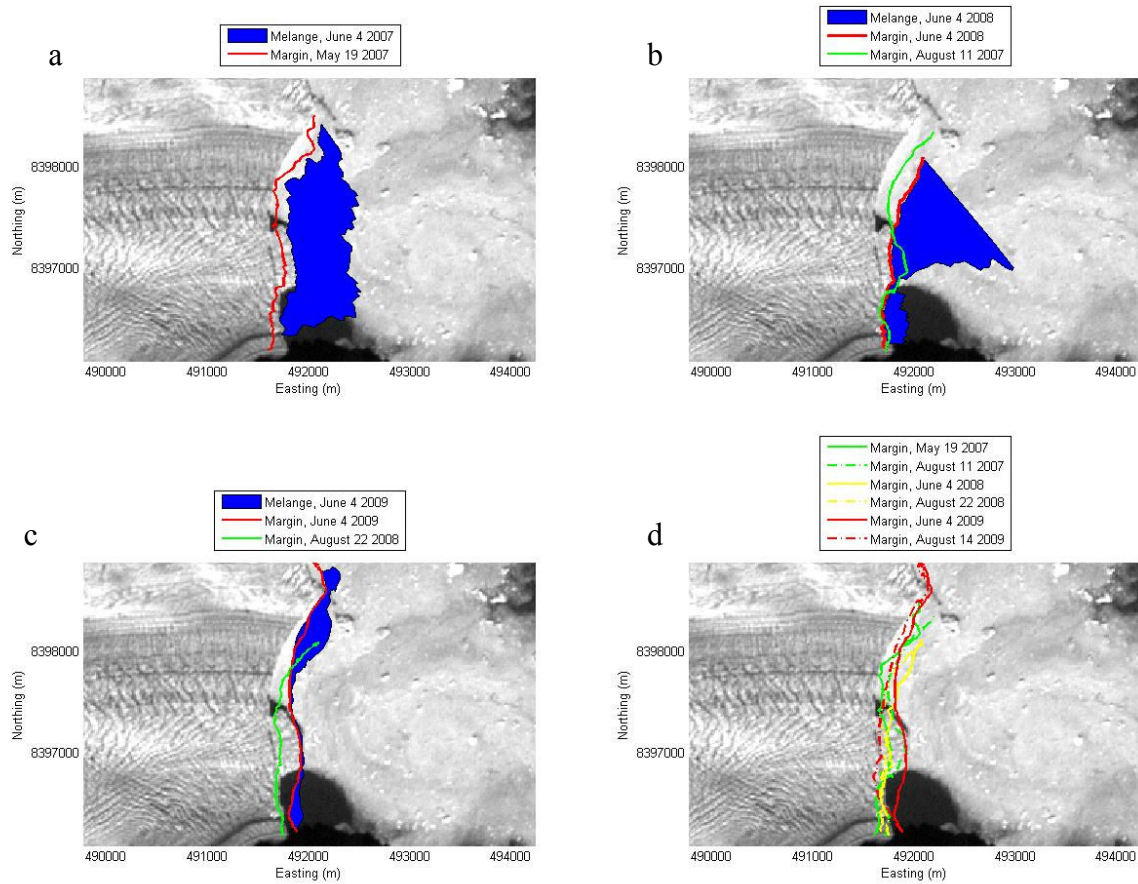


**Figure 3.26. Changes in margin position between fall and spring, with reference to the area of iceberg mélangé on the sea ice by mid-spring for 2007-2009. (a) Initial margin position and mélangé, 2007 (b) Last available fall margin position from 2007 set against spring 2008 margin position and mélangé area (c) Last available fall margin position from 2008 set against spring 2009 margin position and mélangé area (d) First spring position and last fall position for each year, 2007-2009.**

occurred when the sea ice was in place. The area of mélangé in front of the terminus, determined using the same technique for estimating the meltwater plume area, was  $10.03\text{km}^2$  in 2007,  $8.03\text{km}^2$  in 2008, and  $2.58\text{km}^2$  in 2009. Each camera angle was different, so these values do not reflect the full mélangé area and cannot be reliably compared. Nevertheless there appears to have been more winter calving in 2006-2007 and 2007-2008 than in 2008-2009. Figure 3.26d shows that the most significant summer calving took place in 2009: perhaps suggesting more ice was lost in the summer as a result of less ice loss by calving during the preceding winter.

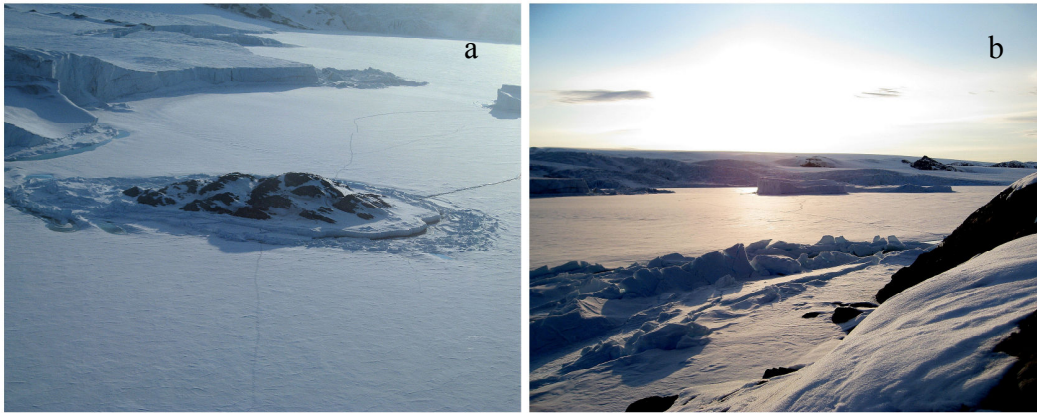


Figure 3.27. State of the sea ice around the island just offshore of the Belcher terminus on May 31<sup>st</sup> 2009. (a) Slabs of sea ice built up around the island (b) view from the island of the deformed sea ice around its margin.

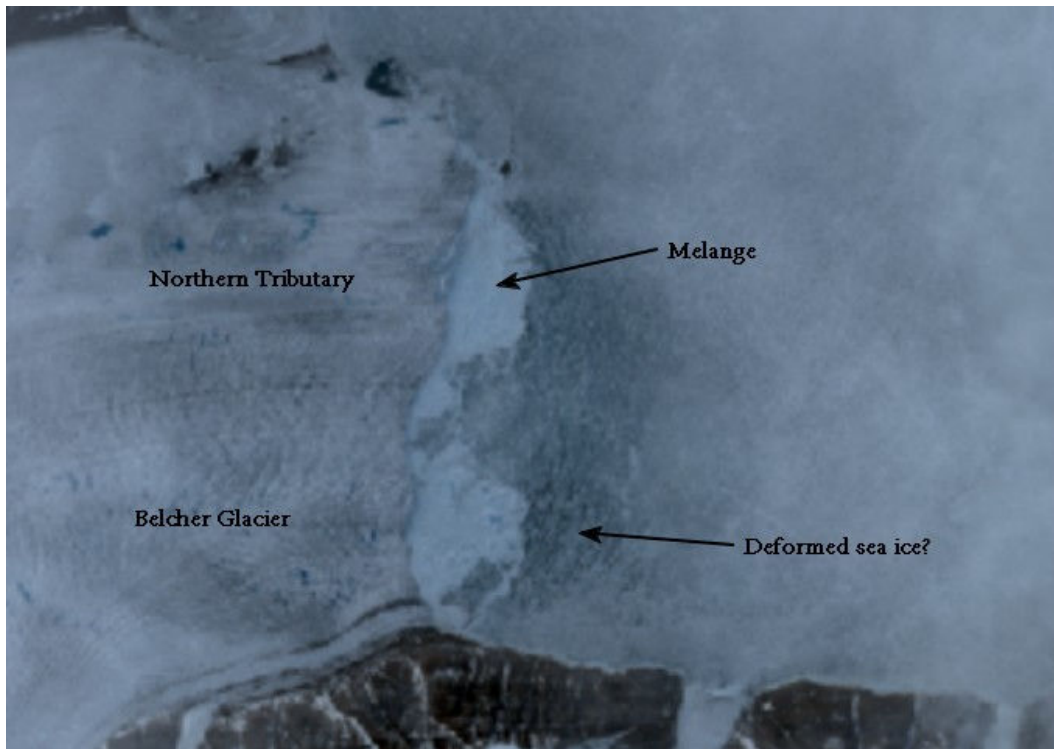


Figure 3.28. Cropped jpeg Digital Globe image from June 24<sup>th</sup> 2011, showing deformation of the sea ice in front of the Belcher Glacier terminus (visible amongst low-lying clouds). The areas of mélange are also very clearly visible.

The relative area of ice mélange in front of the terminus in any given year may influence the degree of buttressing that the mélange/sea ice plate can provide to the glacier ice cliff. Figure 3.25c implies that the mélange, supported by the sea ice plate behind it, applies some resistive stress to the margin which prevents large icebergs being calved during the winter. However it is not clear whether the sea ice remains a rigid plate throughout the winter, or whether calving events or tidal fluctuations weaken its resistive strength. Tide and wave action in the winter would be dampened by the sea ice (Reeh et al., 2001) but as the NOW polynya is sometimes just north of Devon Island, the sea ice plate may only exist within the local bay supported by lateral drag from the embayment and this may mean a winter tidal range still exists. Spring tides could possibly weaken the sea ice. The deformation of the sea ice around the island, shown in Figure 3.27, illustrates that friction exists between the glacier and sea ice but there is not enough evidence to know whether the glacier flow and calving activity is being restricted by the sea ice. Digital Globe imagery from 24<sup>th</sup> June 2011 (Figure 3.28) suggests that the sea ice is being deformed by the forward motion of the glacier. The image is partly obscured by cloud which limits interpretation of the spatial extent of this deformation. However there is no evidence of this deformation in the 2007-2009 imagery. Comparison with the 2009 terminus position mapping (section 3.2.1) and GPS velocity record (Danielson and Sharp, in review) suggests that the rapid acceleration of the terminus region between July 13<sup>th</sup> and 15<sup>th</sup> 2009 coincides with the first independent movements of the sea ice near the plume exit- indicating reduced resistive pressure from the sea ice. However the glacier flow rate was actually decreasing at full sea ice breakup on July 16<sup>th</sup>. Furthermore, the change in the terminus margin position over the winter (Figure 3.26) shows that the sea ice does not completely limit the advance and calving of the glacier terminus; although it may still have some buttressing impact.

### 3.3.5 Tidal Analysis

This section will consider whether the size of the meltwater plume and timing of calving events are influenced by the semi-diurnal, diurnal and long-period frequencies of the tides. The mean tidal range (defined as the difference between the largest and smallest tides in a day) offshore from the Belcher Glacier is  $\pm 1.5\text{m}$ . The minimum daily tidal range during the 2009 summer study period was 1.09m, whilst the maximum was 3.06m. Harmonic analysis can be used to interpret the components of the tide and the relationships between tides, plume extent and iceberg calving. The tidal signal produced by the Webtide model was deconstructed using the Matlab `t_tide` prediction model developed by Pawlowicz et al. (2002). Following O’Neel et al. (2001), the reduction of variance (ROV) was calculated by adding a new constituent for each model run, revealing its relative strength. The five key tidal constituents are listed in terms of decreasing importance in Table 3.5. Each frequency is presented as the number of reoccurrences in one day, alongside its relative phase and amplitude. The Greenwich phase is used, which refers to the phase of an equilibrium response at  $0^\circ$  longitude, nodal-corrected to the specified latitude (Pawlowicz et al., 2002). The M2 constituent dominates the tide (74.5% ROV), followed by the other principal semi-diurnal constituent, S2 (12.2% ROV) and the diurnal constituent K1 (9.9% ROV). This suggests the Belcher tide is a mixed tide of mainly semi-diurnal character.

**Table 3.5. The five largest constituents of the tide in Belcher Fjord, in order of decreasing importance, as modeled in Webtide (Pawlowicz et al., 2002). These results are averages of 2007-2009 tides during the respective field seasons.**

CONSTITUENT	PERIOD (DAYS)	AMPLITUDE	PHASE ( $^\circ$ )	AVERAGE ROV (%)
M2	0.52	$0.84 \pm 0$	$229.2 \pm 0$	73.3
S2	0.5	$0.32 \pm 0$	$118.5 \pm 0.01$	12.0
K1	1.0	$0.28 \pm 0$	$168.3 \pm 0.01$	9.9
N2	0.53	$0.17 \pm 0$	$237.8 \pm 0.02$	2.4
O2	1.08	$0.13 \pm 0$	$277.8 \pm 0.02$	2.2
			Total	99.8

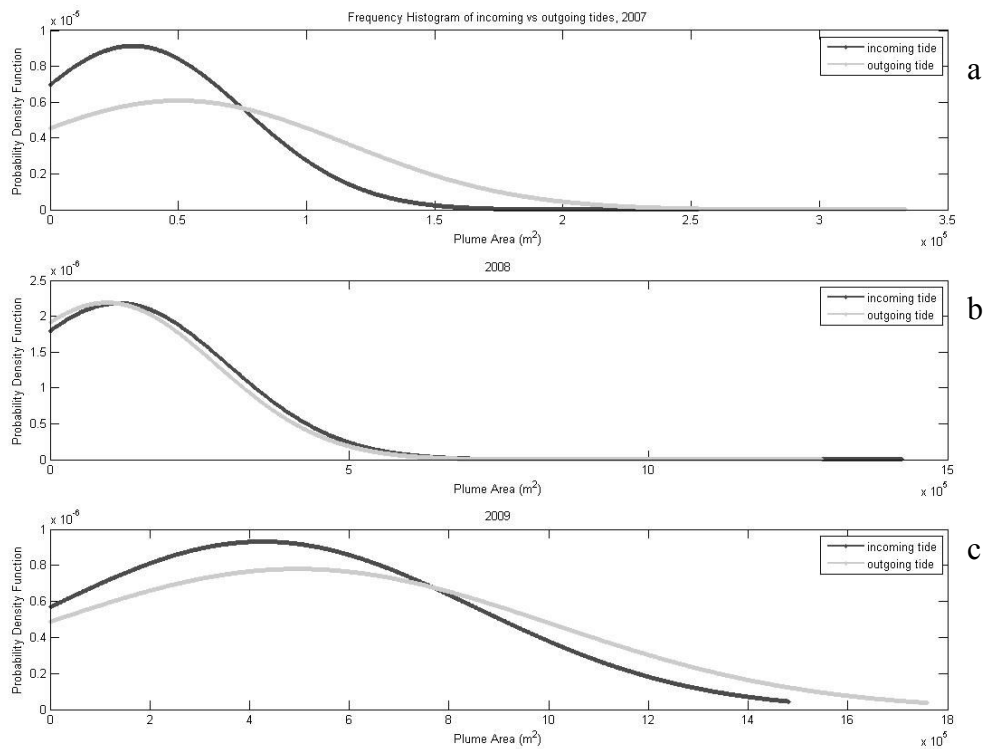


**Figure 3.29. Frequency histograms of plume area for 2007-2009 during incoming and outgoing tides (represented as a binary value).**

The five main diurnal and semi-diurnal components of the tide near the Belcher terminus were compared to the meltwater plume area and calving rate datasets to determine whether the timing and magnitude of events were influenced by the tides. There were no diurnal or semi-diurnal constituents in the 2008 or 2009 plume area datasets. A more basic analysis using a probability density function (following Chu et al., 2009) was also used to classify the data into incoming or outgoing tidal classes (Figure 3.29). In 2008 there was no significant difference in plume area between incoming and outgoing tides, but in 2007, and to a lesser extent in 2009, there was a higher frequency of smaller plumes during an incoming tide. The conflicting results between 2007 and 2008, when the camera positions were the same, suggests a bias towards incoming or outgoing tides in the collection of the plume data. These relationships should be tested further with

both a probability density function and harmonic analysis, with a more complete dataset. The 2008 and 2009 calving datasets each have a significant K1 (diurnal) constituent, with ROV of 5% and 2.6% respectively. However the phases of the signals (which indicate its relative time of arrival at the specified latitude) are far removed from the tidal phase: indicating the small diurnal variation in the calving rate is not a response to the arrival of the tides. Instead, this diurnal component may be a response to ablation, temperature or a diurnal ice velocity component. However the calving dataset is extremely short and sparse, with data gaps due to cloud cover. The small diurnal component of calving should be examined over a longer dataset where more calving events actually take place.

### **3.3.6 Ocean Temperatures**

The temperature of the ocean surface and its depth are analyzed here to assess if there has been recent changes, and if so, what effect they may be having on the stability of the Belcher terminus. The primary source of this information was CTD casts taken offshore from the terminus in 2006 and 2008 (see section 2.3.6). The CTD casts made on the 19<sup>th</sup> September 2006 were taken at several locations in the Belcher Fjord but only two were directly in front of the Belcher terminus (H31 and 80A, Figure 2.2). Other CTD casts sampled on the approach to the Belcher terminus, not shown in Figure 2.2, were made by the CCGS Amundson at (499715°E, 8402362°W) (81A), (505275°E, 8403021°W) (82A) and (511980°E, 8397905°W) (83A). The temperature and salinity profiles from all of these casts are shown in Figure 3.30. The samples were taken in water ranging from 180m to 620m depth yet their temperature and salinity profiles are broadly similar, indicating a strong connection to the open ocean. It should be noted that the CTDs from the Heron launch vessel only reached a maximum depth of 150m so did not reach the bottom of the Belcher Fjord. At shallower depths near the Belcher terminus there are two distinct layers separated by a pycnocline: relatively warm fresher water layer (0.3°C, 31.3g/kg) overlying colder more saline water (-0.8°C, 33.2g/kg). A pycnocline marks a sharp change in water density with depth, caused

by a rapid decrease in temperature and increase in salinity. Stratification is common in Arctic fjords during and at the end of the melt season (Dowdeswell and Cromack, 1991). This stratification is often more a response to variations in salinity than in temperature (Melling, 2002). In September 2006, the pycnocline sat at 50-100m depth. The deeper CTD casts, taken near the coastal shelf, exhibit a third lower layer which is warmer than the layer above it (0°C) and very saline (34.3g/kg). The pycnocline may reflect the presence of sediment-rich fresh water released from the meltwater plume or sea ice melt, but it is difficult to confirm this as the CTD cast take on July 22<sup>nd</sup> was done north of the plume location and on July 30<sup>th</sup> the plume was not active. Therefore the exact thickness of the meltwater plume (which could be used to calculate its volume) cannot be deduced from these measurements.

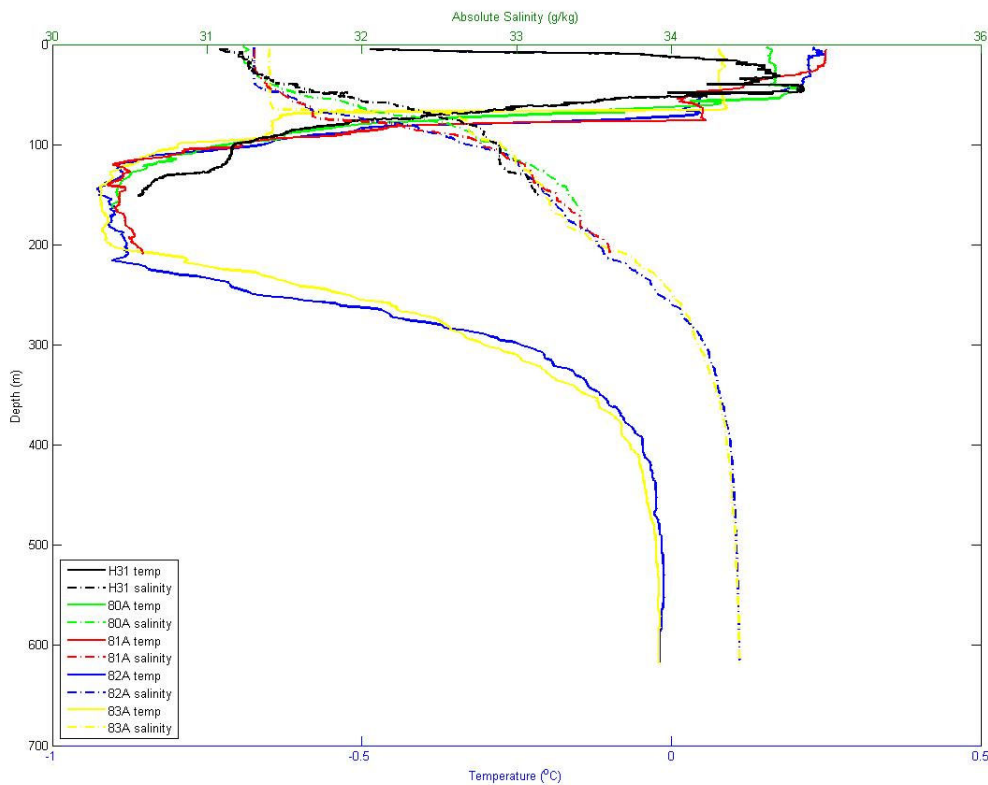


**Figure 3.30. CTD profiles of temperature and salinity collected on 19<sup>th</sup> September 2006 near the Belcher Glacier terminus by the CCGS Amundson (denoted by A- casts) and Heron launch vessel (denoted by H- casts).**

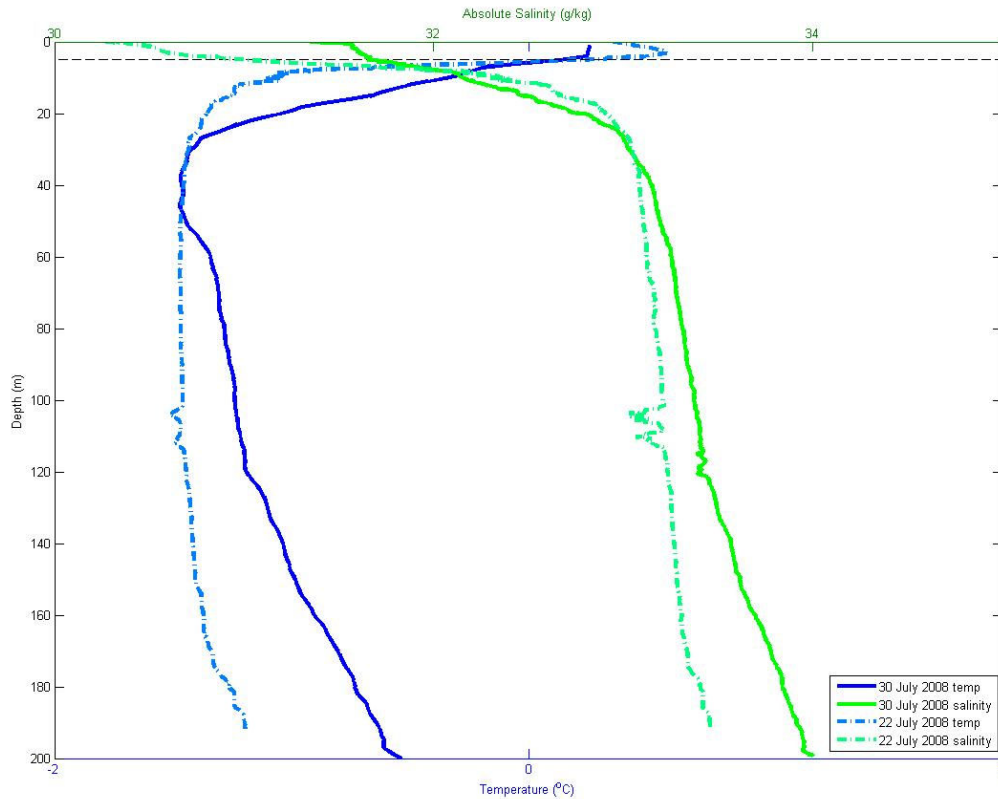


**Figure 3.31. CTD profiles of temperature and salinity collected on 22<sup>nd</sup> and 30<sup>th</sup> July 2008 from the Belcher Glacier terminus by L. Tarasov. The average results are presented here for clarity as 4 very similar CTD casts were within 50m of each other from the glacier terminus.**

In response to the observation that warm Atlantic-sourced water is travelling at depth up the west coast of Greenland towards the Canadian Arctic (Rabe et al., 2010), historical ocean temperature records were examined to determine if there have been any changes off the coast of Devon Island. A series of measurements made between 1978 and 1997 in Jones Sound (between Devon and Ellesmere Island) is available in the World Ocean Database 2005 (Boyer et al., 2005) (Figure 3.32). There were no significant changes in temperature (Figure 3.32) or salinity profiles (not shown) between 1978, 1997 (when warm subsurface waters encroached on Jakobshavn Isbrae, Holland et al., 2008) and 2006/2008 (Figure 3.30 and Figure 3.31). No surface freshening (as was observed near Baffin Island (Zweng and Munchow, 2006)), or warming of the subsurface waters (Rabe et al., 2010) was identified. Therefore it appears that warm Atlantic waters are not

currently penetrating the waters of the CAA around Devon Island, but are being channeled south along Baffin Island, as proposed by Zweng and Munchow (2006).

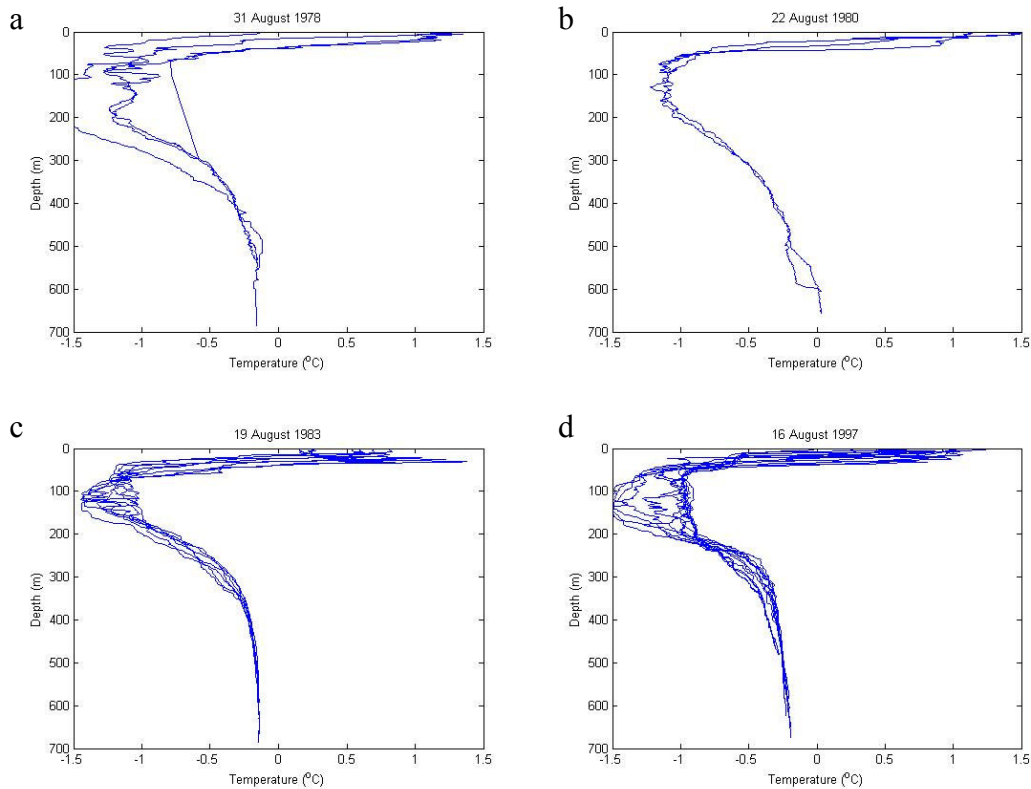


**Figure 3.32. CTD profiles of temperature and depth offshore the Belcher Glacier (in Jones Sound, between Devon Island and Ellesmere Island) between August 1978 and August 1997. Data from the World Ocean Database 2005 (Boyer et al., 2005)**

Sea surface temperature anomaly (SSTA) records from the Reynolds SST dataset (Reynolds et al., 2002) also suggest there have been no significant changes in recent SSTs near the Belcher Glacier. Murray et al. (2010) identified a temporary positive SST anomaly off the coast of SE Greenland between 2003 and 2005, which corresponded with the penetration of warm Atlantic water into the fjords of the coastal glaciers but there are no protracted SST anomalies off the NE coast of Devon Island (Figure 3.33). Between 2007 and 2010, for which these data are available, there was anomalously cold summer SSTs, with smaller anomalously

warm winter SSTs, the most significant of which was in 2009-2010. The general trend between 2000 and 2010 is towards increasingly anomalous cold SSTs during the summer which may reflect increasing sea ice melt in the broader Canadian Arctic region. The limited CTD data available suggest there have not been ocean temperature changes at depth, which is consistent with the stability of the Belcher Glacier terminus position.

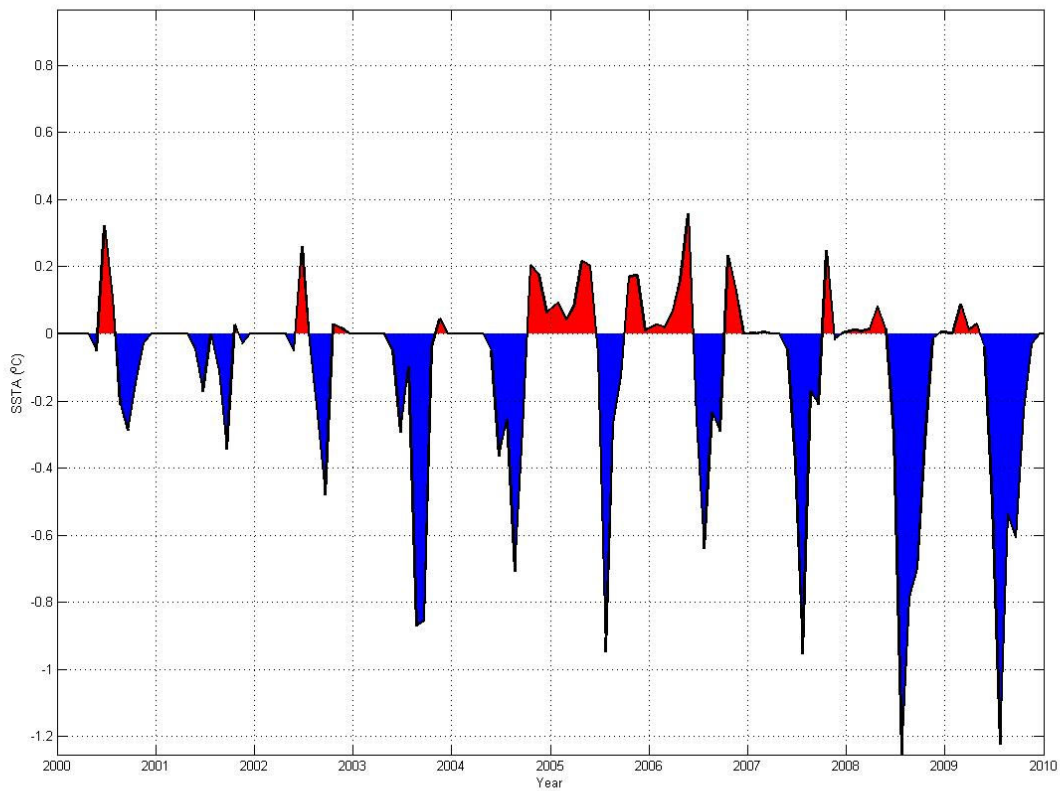


**Figure 3.33. Monthly SSTA values from the 1km grid cell closest to the Belcher Glacier terminus (75.5°N, -81.5°W). Note that the SSTA is relative to a 1971-2000 baseline.**

### 3.3.7 Geometry

The Belcher Glacier's proximity to flotation, which can affect the style and rate of iceberg calving, as well as the stability of the terminus region, was calculated from the height-above-buoyancy criterion,  $H_b$ , described in equation (4). Seawater density,  $\rho_w$ , was calculated from salinity and temperature to be an average of 1027 kg m<sup>-3</sup> whilst ice density was taken to be 917kg m<sup>-3</sup> for bubbly ice at approximately -4°C (Cuffey and Paterson, 2010; Echelmeyer et al., 1991).

Seawater density can vary substantially throughout the season depending on the quantity of meltwater being extruded (O'Neel, 2001); these data were collected in July and September when more freshwater was probably being mixed in. The average ice thickness across the CReSIS transect taken ~500m from the terminus (Figure 2.2 and Figure 2.3b) is 217m but the effective ice thickness is less, once surface voids introduced by crevasses are accounted for (Echelmeyer et al., 2001).

L. Tarasov (unpublished data) measured the depths of 47 crevasses in the terminus region in July 2008; most of them were dry but five contained water (0.3-9m water depth). The maximum crevasse depth measured was 31m, and the average depth was 16m. Following Echelmeyer et al (1991) and O'Neel et al (2003) by assuming a model where flat-topped seracs ~50m wide are separated by ~16m deep triangular chasms, 20m wide at the surface, the void space in the upper 16m of ice is 14%. This would make the average effective cliff height 48m rather than 50.45m, and the total average effective ice thickness at ~500m from the terminus margin would be 214m. The height-above-buoyancy expression is normally evaluated as a cross-sectional average because local hydrostatic equilibrium does not necessarily apply when the ice is in a valley setting (O'Neel et al., 2003). Based on an effective ice thickness of 214m and water depth of 220m from bathymetry data ~700m away from the terminus position ('Offshore Bathymetry B', Figure 2.2 and Figure 2.3b), the height above buoyancy is -32m. This suggests the glacier is likely to be floating; although neither water depth nor ice thickness was measured directly at the terminus margin. If a point measurement of ice thickness at the terminus margin is used (from the longitudinal profile in Figure 2.3a), which was 308m at the centreline, the height-

above-buoyancy is +50m, indicating it is grounded. However as Table 3.6 shows, the ice thickness at the same position on the centerline 500m upstream (at the CReSIS transect) was 322m. This is 105m greater than the average ice thickness of 217m estimated for the CReSIS transect and suggests the centreline measurements of ice thickness are above average thickness, which would be expected as the centreline is the deepest part of the glacier. Nevertheless, these comparisons show that the ice thickness decreases from 500m away to directly at the terminus margin, which suggests the average ice thickness is less at the margin and that the ice is floating above the bed by more than 32m. However the ice thickness data suggests the glacier may be grounded at ~500m from the margin which would mean the Belcher Glacier only has a short floating tongue.

**Table 3.6. Point measurements of ice cliff height and ice thickness at the centerline of the Belcher Glacier and its confluence with the northern tributary, as recorded at the terminus or 500-700m away, where the CReSIS ice thickness transect was made in 2005 (see Figure 2.3). In the column headings, ‘T’ stands for terminus.**

	ICE CLIFF HEIGHT, 500-700M FROM T (M)	ICE THICKNESS, 500-700M FROM T (M)	ICE CLIFF HEIGHT AT T (M)	ICE THICKNESS AT T (M)	EFFECTIVE ICE CLIFF HEIGHT AT T (M)	ICE THICKNESS AT T BASED ON EFFECTIVE FREEBOARD (M)
Centreline position	55	322	31	308	28.7	287
Confluence position	48	291	30	233	27.7	277

To further test whether the glacier is floating, the effective pressure at the glacier bed and the height of the freeboard were examined. If the glacier is floating,  $\rho_{eff}$  (equation 2) should be negative because the basal freshwater/seawater pressure is enough to exceed the local ice overburden. The effective pressure at the bed of the Belcher Glacier, calculated at the 2005 CReSIS transect ~500m from the margin, is estimated to be  $-3.7 \times 10^6$  Pa. This also indicates the glacier is floating. Finally, an estimation of ice thickness and flotation can be made by assuming that floating

ice is nine times thicker under water, based on the height of the glacier freeboard (the height of the ice cliff above sea level). At the transect ~500m from the terminus, this average freeboard height was 50.45m.a.s.l. But the measurements of ice cliff height in Table 3.6 suggest that at the terminus this freeboard is likely to be ~30m.a.s.l. If the effective ice cliff height is ~27m, this would require the floating ice thickness to be ~270m. As the average water depth is 220m at the terminus, this puts the glacier somewhat close to flotation, aligning it with the height-above-buoyancy and subglacial effective pressure measurements which also indicate the Belcher terminus is floating.

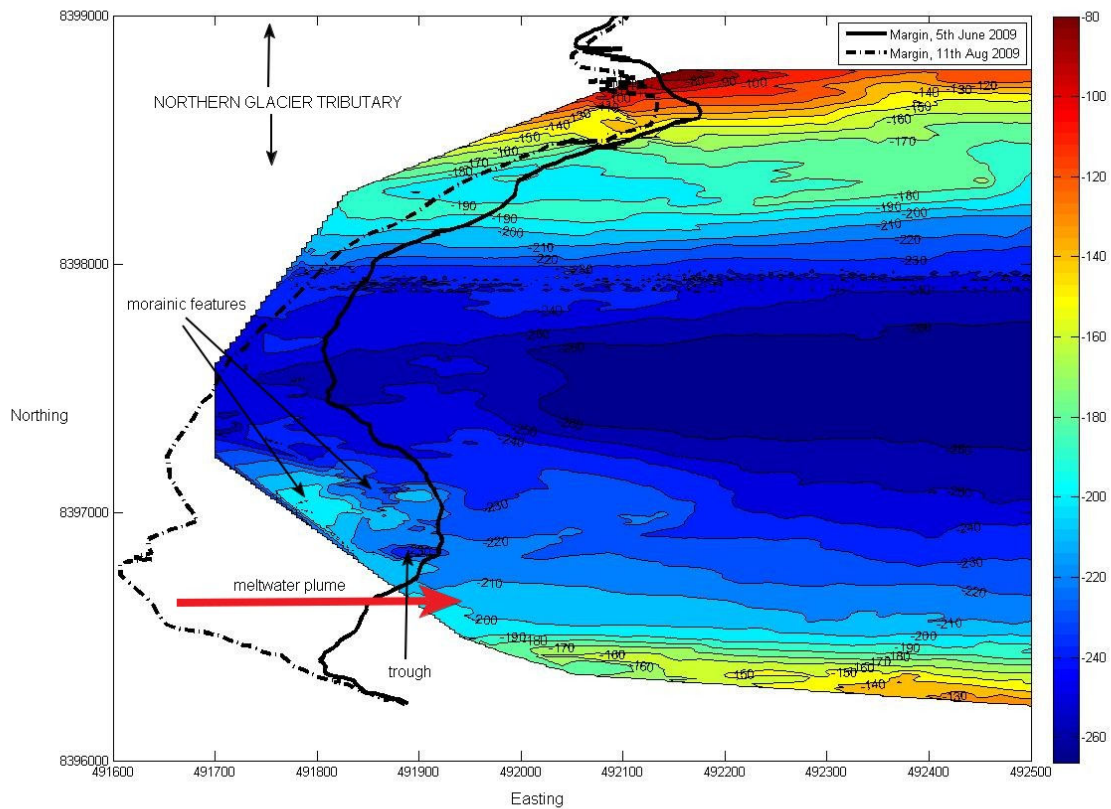


**Figure 3.34. Bathymetry offshore from the Belcher Glacier terminus. Data collected by the CCGS Amundsen in September 2006 (Bell and Hughes-Clark, 2006). Note the positions of the glacier margin in June and August 2009, as well as the location of a trough and moraines. The normal position of emergence of the meltwater plume is also shown.**

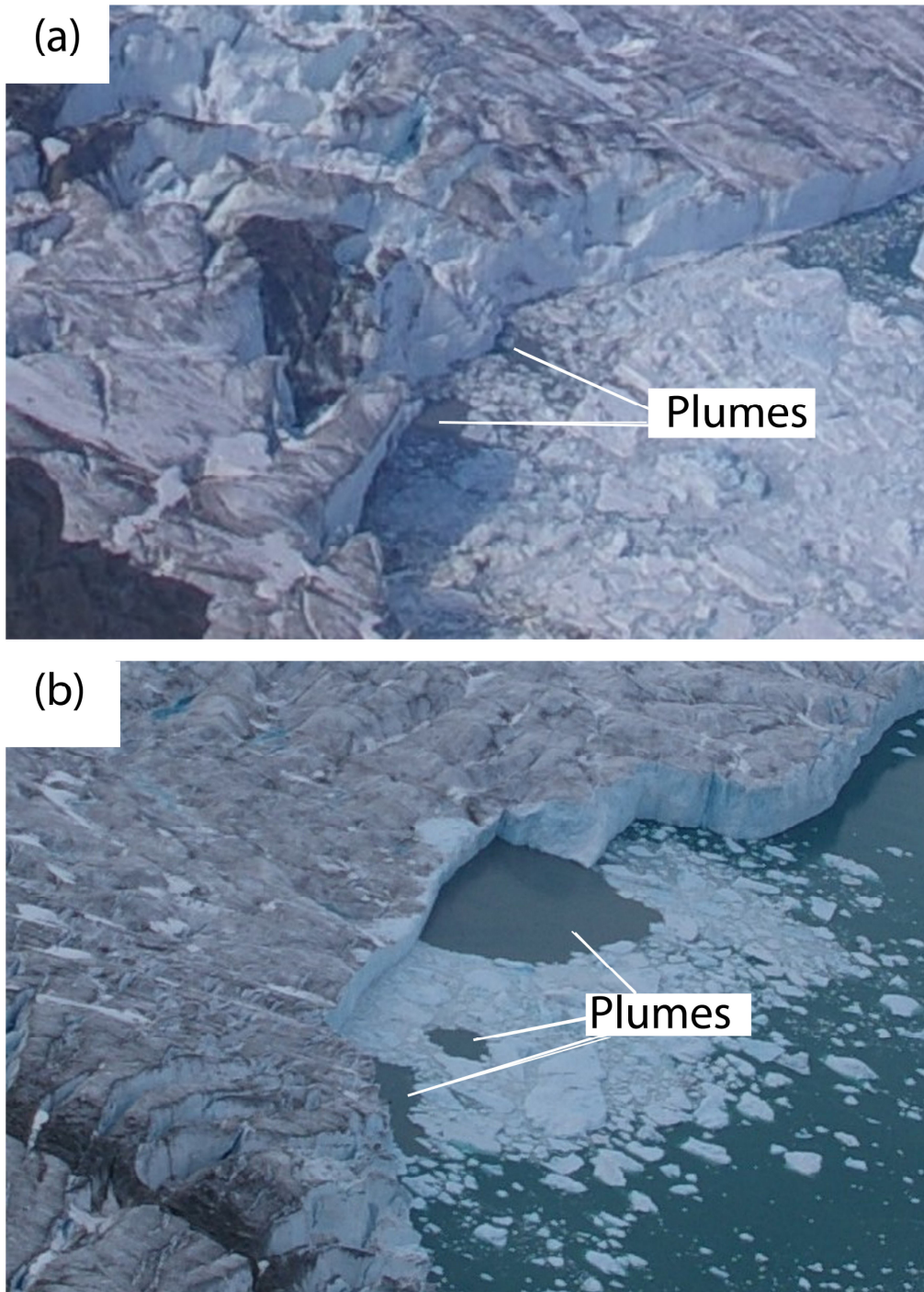


Figure 3.35. Example of small water jets which emerged near the start and end of the season when the plume was small. Image (a) was July 14<sup>th</sup> 2009 at 3pm and (b) was July 31<sup>st</sup> 2009 at 7pm (note the jet which is offset from the ice cliff).

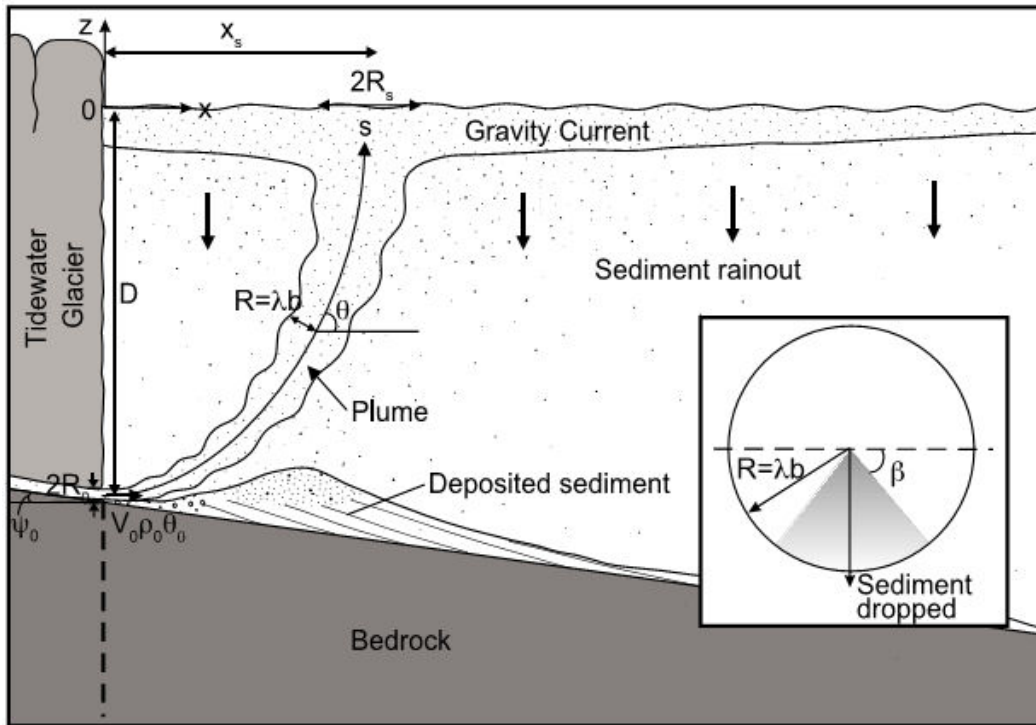


Figure 3.36. A meltwater plume emerges horizontally from a subglacial channel and the momentum of the water causes it to flow away from the glacier front, creating a curved trajectory. The larger and steeper the grounding fan, the closer to the ice front the plume will appear at the surface. Once at the surface the meltwater spreads radially as a surface gravity current. The inset shows a vertical cross section of the plume in which sediment is dropped at angles greater than  $\beta$  (figure from Mugford and Dowdeswell, 2011).

Finally, the geometry of the glacier bed and offshore bathymetry may affect the glacier's stability. The bathymetry is shown in Figure 3.34. The topography profile is fairly uniformly smooth, only with some undulating topography directly in front of the glacier ice cliff. As the troughs and ridges become smoothed towards the east (away from the glacier), this suggests these features are products of sediment deposition from the meltwater plume and iceberg sediment drop-out. The CCGS Amundsen was unable to travel too close to the ice margin, so we are unable to see whether there is a grounding line moraine or fan which could be stabilizing the glacier front. There is a ~40m deep elongate trough (in Figure 2.3b, 'Offshore Bathymetry A') which may be a product of clastic sediment filling in the offshore grabens (Dyke, 1999). The other interesting feature is the trough

apparent in the bed surface data which was calculated by subtracting the ATM surface data from the CReSIS ice thickness transect collected ~500m from the terminus margin (Figure 2.2 and Figure 2.3b). The ice is only ~50m thick here and there appears to be a subglacial channel c.25m deep at approximately 0.25km north of the valley wall. It is not clear whether this bedrock feature extends to the terminus margin but it may do, as the elevation of the ‘Offshore Bathymetry A’ transect is similar although it does not extend fully across the fjord width. If this is the case, it may be the subglacial channel for the meltwater plume and explains why the plume always appears to exit in approximately the same location. Otherwise, the valley shape is relatively symmetrical and sloping at a uniform rate, which does not offer the possibility of local flotation, although it would be most likely at the deepest part of the trough. Further mapping would be useful to determine if there is a grounding line fan which may be stabilizing the glacier. The presence of grounding line sediment is suggested in the ‘confluence’ transect in Figure 2.3a, where the bed slope rises 60m within 1km of the margin. At the start and end of the melt season, when the meltwater/sediment plume is very small, several circular jets can be seen at the water surface, close to the ice front (Figure 3.35). Their proximity to the ice front suggests a grounding line fan is present, built up by sediment released from the meltwater plume which may be stabilizing the terminus margin position and limiting the calving rate (see Figure 3.36).

### **3.4**            *Summary*

The main results from the 2009 field season on the Belcher Glacier, supplemented by data collected between 2006 and 2008 are as follows:

1. Georeferencing of the time lapse imagery is most accurate when all camera rotation angles are included in the photogrammetry model. A method such as Krimmel and Rasmussen (1986) works adequately for

mapping glacier margins but one such as Croitoru and Ethrog (2001) is better.

2. The total volume of ice lost by iceberg calving and basal melt (unknown proportions) between June 4<sup>th</sup> and August 14<sup>th</sup> 2009 was 0.088km<sup>3</sup>. The largest volume of ice lost was on July 22<sup>nd</sup> 2009, in two large tabular sections affecting more than 50% of the ice front. Only 31% of the calving flux was due to ice displacement but this is because 84% of the annual calving volume loss took place between June and September. This means that calving occurred during the winter, from October to May (~14%).
3. Three calving events were identified by the audio recorder, which lasted 1.5-11 minutes. The audio signals reflected sliding of avalanching debris down the glacier front plus 'thuds' indicating when icebergs hit the water. This suggests either that the calving events took place in several phases or that the icebergs disintegrated upon hitting the water.
4. The geophones did not detect any calving events as they appear to be sensitive only to local fracturing. This may be because the surface of the terminus is highly dissected by large crevasses.
5. The geophones did detect clusters of ice fracture events on June 30<sup>th</sup> and July 1<sup>st</sup> 2009 when the water-filled crevasses at the terminus began to drain, indicating that hydro-fracture processes may have been connecting the surface meltwater to the englacial and subglacial drainage system. The initiation of drainage was followed shortly after by a terminus velocity increase and advance of the ice margin.
6. GPS data suggest that calving events are neither a trigger of, nor a response to, a velocity increase in the terminus region. Optical flow results were not reliable and this method of velocity mapping requires further testing on a faster-moving glacier.
7. Only one calving event captured by the 2009 time lapse imagery may have been influenced by the drainage of the water-filled crevasses and melt ponds, and further investigation is needed to determine whether water-

driven crevasse propagation is an influential driver of calving events on the Belcher Glacier.

8. The time lapse camera angle can strongly affect the accuracy and results of mapping glacier ice margins and meltwater sediment plumes. In this study, the 2009 camera position was most accurate for mapping the terminus position but severely underestimated the area of large meltwater plumes.
9. 81% of calving events between June 4<sup>th</sup> and August 14<sup>th</sup> 2009 took place near the normal meltwater plume exit or at locations to which the plume had switched. However, there were no calving events near the meltwater plume in the 2007 or 2008 time lapse observation periods. This suggests that undermining of the terminus by melt water efflux may sometimes facilitate calving, but that it is not a necessary condition for calving to occur.
10. Changes in plume area showed a strong positive correlation with runoff modeled by Duncan (2011), but the plume did not appear to increase in area in response to supraglacial lake drainage events.
11. High winds from the west played a role in sea ice break-up in some years but did not affect the timing of calving events.
12. Mapping of the ice mélange in front of the glacier shows that calving definitely takes place in winter, and that in years when there is less winter calving there tends to be more summer calving.
13. Sea ice does not prevent calving taking place but it may provide sufficient buttressing support of the terminus in winter to prevent large calving events from occurring. Removal of the sea ice in summer does not always lead to either a calving event and or a terminus velocity increase.
14. Calving does not appear to be tidally-influenced and the size of the meltwater plume is not altered by the tides.
15. The general trend in SSTs offshore from the Belcher Glacier between 2000 and 2010 is towards anomalously cold summer SSTs which may reflect increased sea ice melt in the Arctic. There do not seem to have been

any ocean temperature changes at depth, and this may contribute to the continued stability of the Belcher terminus.

16. The terminus of the Belcher Glacier appears to be floating, according to height-above-buoyancy and subglacial effective pressure calculations.
17. The meltwater plume emerges in the same region near the southern margin each year because it is fed by a stream that seems to be located in a bedrock channel c.25m deep.

## Chapter 4. DISCUSSION

### 4.1 *Introduction*

In this chapter I will address the research questions first posed in section 1.4:

3. Does the Belcher Glacier exhibit a calving style and rate which suggests it has a grounded or floating terminus in summer?
4. Are calving events on the Belcher Glacier triggered by:
  - a. A speed-up of the near-terminus region which may be caused by a meltwater pulse or drainage of the terminus water-filled crevasses, which enhance its proximity to flotation?
  - b. Propagation of the terminus water-filled crevasses to the glacier freeboard?
  - c. Removal of buttressing resistance provided by the mélange and sea ice?
  - d. Tidal fluctuations, which reduce the height above buoyancy or lower the buttressing pressure of the seawater, whilst also influencing the meltwater plume discharge?
  - e. A change in ocean temperatures, either at depth or at different times of the year, which could affect the sea ice concentration and/or basal melt rates?

### 4.2 *Belcher Glacier: Grounded or Floating?*

The style and rate of iceberg calving, as well as the height above flotation and the thickness of the glacier freeboard can all be used as evidence for determining whether a glacier terminus is grounded or floating. Two large tabular bergs were discharged from the Belcher Glacier on July 22<sup>nd</sup> 2009. In a large calving event on July 27<sup>th</sup> 2008 the glacier lost an elongate mass of ice from more than 50% of the ice front. Walter et al. (2010) found that floating glaciers such as the Columbia

Glacier in Alaska often lose most of their mass in large, infrequent calving events which produce tabular blocks from up to 50% of the ice front at once. Calving on the Belcher Glacier can be described as infrequent, with only 3-5 major events during a summer period (2007-2009), and a total of 11 events recorded between June and August 2009 that accounted for 44% of the annual ice loss by calving. This compares to 41 calving events observed in four days on the grounded glacier Kronebreen, Svalbard during August 2008 (Chapuis et al., 2010). On many floating glaciers, tabular blocks are defined by rifting perpendicular to glacier flow (Walter et al., 2010), as was the case for both the calving events from Belcher Glacier in 2008 and 2009. However it is usually assumed that calving occurs along rifts that were established upstream from the glacier terminus in zones of horizontal shearing or bending caused by flow around obstacles or sharp changes in the direction of glacier motion (Reeh et al., 2001). The large bergs calved on July 22<sup>nd</sup> 2009 were not predefined by existing rifts, but another berg calved on July 24<sup>th</sup>, and a second iceberg calved in 2008 (Figure 3.8) were. The combination of large, infrequent calving events that can affect 50% of the front and some events which were defined by preexisting rifts indicates that the Belcher Glacier terminus is floating. However there may not always be sufficient damage to the ice upstream of the terminus for large rifts to be established along which calving later takes place.

Some calving events were much larger than others, notably on July 22<sup>nd</sup> 2009, and these significant contrasts in iceberg size may reflect the degree of flotation and the position of the calving front. The Belcher Glacier maintains a very stable ice front position, fluctuating only 100-150m between years (Figure 3.26). In particular, the margin position varies from a relatively straight profile centered on 491800E and an advanced position at 491900E with a bulge at 8397000N. This 'bulge' is evident on imagery from August 11<sup>th</sup> 2007 and June 4<sup>th</sup> 2009, as well as in the year 2000 Landsat 7 ETM+ image (Figure 3.26). The large tabular icebergs calved from the glacier on July 22<sup>nd</sup> 2009 were lost from this 'bulge', whilst other calving events that summer produced bergs that were much smaller and less

tabular. It is hypothesized that the Belcher Glacier is lightly grounded within 500m of the margin, as reflected by the ice thickness changes in Table 3.6 which affected the height-above-buoyancy. However every couple of years the fastest flowing ice at the glacier centreline, the deepest part of the fjord, develops a protruding floating ‘bulge’. Its flotation may be enhanced by basal melt, although without further investigation of this process it remains purely hypothetical. Some basal melt is likely to have contributed to the floating protrusion, otherwise the weight of the ice and its rigid structure would prevent local hydrostatic equilibrium from occurring. The protruding ice is also shaped by the position of the meltwater plume, which enhances the calving rate in the region around it by increasing the basal (and terminal ice cliff) melt rates due to mixing of the seawater and plume discharge (Motyka et al., 2003), as was seen in 2009 when a seasonal embayment formed at the plume exit. However the meltwater plume only seems to facilitate calving events when the terminus is in a slightly advanced position, as it was in June-July 2009. Since Jakobshavn Isbrae is grounded in summer but develops a floating tongue and advances up to 5km in winter (Amundson et al., 2010), it is clear that a glacier can transition between grounded and floating modes relatively quickly and regularly. Basal melt is an important process at the floating tongue of Jakobshavn Isbrae, causing thinning due to submarine melting of  $228 \pm 49 \text{ m yr}^{-1}$  between 1984 and 1985, a rate which may have increased recently due to warmer ocean temperatures (Motyka et al., 2011). Even on grounded glaciers submarine melt can be an important process, periodically undercutting the terminus and triggering calving. For example on LeConte Glacier, Alaska, the basal melt rate was  $12 \text{ m d}^{-1}$  across the submerged ice face, which accounted for 57% of the total summer ice volume loss (Motyka et al., 2003). This evidence from other glaciers suggests basal melt is likely to play a key role in establishing flotation dynamics at the Belcher Glacier terminus but in order to establish basal melt rates further data is required, as discussed in section 4.4.

A grounding line moraine or fan may be beneath the Belcher Glacier margin, contributing to its stability and the complicated calving dynamics. Morainal features are evident in the fjord bathymetry near the glacier's southern margin (Figure 3.34) and could be the edge of a larger grounding fan at the terminus. Such a grounding line feature is most likely to occur near the exit point of the meltwater plume, which may supply significant quantities of sediment to the fjord. For example a grounding line fan was able to build up in front of Kongsvegen, Svalbard in 22 years with a sediment accumulation rate of  $8.91 \times 10^5 \text{ m}^3 \text{ a}^{-1}$  (Trusel et al., 2010). Powell (1990) suggested that if a glacier terminus remains in a quasi-stable position it will develop a grounding line fan, although the rate of deposition depends upon the rock type and the amount of sediment available. At Kongsvegen, the rock type was sedimentary which would likely yield a higher sedimentation rate than at the Belcher Glacier, where the catchment is composed of Precambrian gneiss (Dyke, 1999). Whether there is a grounding line fan or not, which is likely to be most pronounced near the sediment plume, the 'bulge' appears to be self-supporting until it is sufficiently damaged by a combination of basal melt, expansion of water-filled crevasses and ice flexure (particularly as its lateral support is being cut away by the meltwater plume). Then, major calving of tabular icebergs takes place.

Based on the evidence presented in this thesis, it is concluded that the Belcher Glacier is lightly grounded at its terminus margin but has the tendency to develop a protruding bulge which eventually floats and calves off due to undercutting by basal melt and lateral weakening from the meltwater plume. Further measurements of ice thickness and water depth precisely at the terminus margin would be useful to determine unequivocally whether the margin is grounded or floating, as well as possibly being able to identify whether a grounding line fan exists. It should also be noted that the stability of the main glacier trunk is intimately connected to the stability of its northern tributary to which it is attached and shares a 4km-wide fjord. There is a significant c.250m overdeepening at the confluence between the Belcher Glacier and the northern tributary (Figure 2.3)

which may further destabilize both glaciers if one or both were to retreat by ~2km. It is not fully clear how large overdeepenings affect the stability of a glacier, but certain glaciers such as Helheim Glacier, SE Greenland may retreat rapidly as they are on a reverse bed slope (Nick et al., 2009). Yet the presence of a reverse bed slope, particularly in a local overdeepening does not necessarily make the glacier unstable if there is a lot of lateral drag provided by valley walls to support the glacier (Vieli and Nick, 2011). Therefore future studies should consider the stability and mass balance of the northern tributary (tributary 6) as well as of the main Belcher Glacier trunk.

### **4.3            *Potential Calving Triggers***

Having determined that the Belcher terminus margin is lightly grounded with a short floating protrusion along its centerline, I will now discuss whether the range of mechanisms investigated in this study did actually appear to prompt calving events.

#### **4.3.1 Meltwater-driven Terminus Velocity Changes**

It is possible that summer iceberg calving from grounded or floating portions of the Belcher Glacier ice front is a response to velocity accelerations. Many of the speed-ups at the terminus appear to be caused by lake and water-filled crevasse drainage events further upglacier (Danielson and Sharp, in review). Nevertheless there was no immediate calving response to a meltwater-driven velocity flux increase, and similarly the terminus ice did not respond with a velocity increase to the redistribution of stress following a calving event. Vieli and Nick (2011) expect that any calving event will lead to a redistribution of ice stresses, and therefore a velocity increase, because the lost ice is no longer resisting the glacier behind it. Yet even after the largest events on the Belcher Glacier, such as on July 22<sup>nd</sup> 2009, no velocity response was recorded by the terminus GPS, which was located less than 300m from the margin. This suggests that summer iceberg calving from

the Belcher Glacier is neither the 'slave to' nor the 'driver of' terminus velocity, as was proposed by Benn et al. (2007). Instead, the relationship between calving and velocity is primarily controlled by the local geometry. In particular, lateral drag on the ice can dampen the effects of calving on velocity (Hulbe et al., 2008).

#### **4.3.2 Propagation of water-filled crevasses**

Benn et al. (2007) proposed that the calving rate could be predicted from crevasse depths, surface velocity and strain rates: this would determine how long it took water-filled crevasses to propagate to the glacier freeboard and cause calving. If this were the case on the Belcher Glacier, a lot of water-filled crevasses would be expected close to the terminus margin where they could instigate calving. However, in 2009 only one calving event may have been a response to water-driven crevasse propagation, and it involved drainage of a melt pond rather than a water-filled crevasse. Therefore, propagation of water-filled crevasses is unlikely to trigger calving events on the Belcher Glacier because there are very few water-filled crevasses within 100m of the terminus. Yet these water-filled crevasses may play an important role in damaging the ice and propagating fractures towards the freeboard. Water-filled crevasse propagation may be a more significant process on ice shelves and fully floating ice tongues with almost horizontal surface slopes where water might collect more extensively. It could also be a process which threatens glaciers that are less stable than the Belcher Glacier and closer to catastrophic retreat. This effect was seen on the Larsen B Ice Shelf in Antarctica, where extensive surface ponding occurred for several years prior to ice shelf breakup and calving which were eventually caused by water-filled crevasse propagation (Scambos et al., 2004). These observations indicate that it is important to monitor the area of water-filled crevasses on the terminus of the Belcher Glacier because if their area grows substantially over time and encroaches closer to the terminus they are more likely to damage and weaken the ice, which eventually leads to iceberg calving.

### 4.3.3 Mélange / Sea ice buttressing

Evidence from the 2007-2009 time lapse imagery does not indicate that the breakup of the sea ice and mélange control the timing of major summer calving events. Most of the buttressing resistance is likely to be lost by late June when extensive melt ponds have formed on the sea ice surface, weakening the ice. This is particularly likely once the sea ice behind the mélange breaks up, which tends to occur first before full break up near the glacier terminus takes place. Amundson et al. (2010) also found that the buttressing effect of the mélange/sea ice at Jakobshavn Isbrae was lost in spring once the sea ice retreated to within several kilometers of the glacier terminus. In general it seems that the buttressing effect of sea ice and mélange is very site-specific and its influence depends upon the bed and ice front geometry. Clearly, a 10km-long mélange such as occurs at Jakobshavn Isbrae has a much larger resistive strength than the 100-300m width of mélange at the Belcher Glacier terminus. The thickness of the sea ice will also affect the buttressing strength but an estimate of sea ice thicknesses around Devon Island is not available. If the sea ice is constrained within a narrow fjord, it could be expected to have a greater resistive impact on glacier flow than free-floating sea ice. For example Herdes et al. (in review) observed that the Fitzroy Glacier, another glacier draining the NE of Devon Ice Cap, tended to lose its sea ice later than the Belcher Glacier and the Fitzroy is in a narrow fjord (~1km wide). This would suggest that the sea ice had a greater buttressing effect on the terminus of the Fitzroy Glacier compared to the Belcher Glacier, given that they are in the same geographical area. Nevertheless, the buttressing support of the sea ice in mid-winter at the Belcher Glacier cannot be disproven without rigorous analysis of the strength of the sea ice. In future projects, this could be done through force balance analysis, by comparing the driving force of the forward motion of the terminus ice cliff with the back force exerted by the sea ice plate on the terminus (see Cuffey and Paterson, 2010, p307-309). Until then, it is concluded that the sea ice/mélange may buttress the terminus during winter, reducing the number of calving events and the amount of ice advance, but this resistance is gradually lost as summer approaches. By the time of the eventual break-up of the

melt-weakened sea ice in July the sea ice does not appear to have any remaining buttressing strength and its removal did not appear to result in either acceleration of ice flow in the terminus region or a concentration of calving events from the Belcher Glacier. This conclusion contrasts that of Herdes (2009) and Herdes et al. (in review) who found that major calving events from the Belcher Glacier in Radar-Sat 1 imagery from 1997-2008 coincided with the annual break-up of the sea ice. It seems that the release of the *mélange* trapped in the sea ice (icebergs which had broken off during the winter) was mistaken for a large calving event each year at the time of sea ice breakup. The icebergs would have rotated and disintegrated further during the breakup sequence and were produced by a bright backscatter (due to high surface roughness common in freshly shattered ice) which was mistaken to be a new, extremely large, calving event.

#### **4.3.4 Tidal flexure**

Another question is whether any of the summer calving events on the Belcher Glacier were triggered by tidal flexure (due to spring or neap tides, or a large tidal range within a day). The calving events observed did not seem to occur preferentially at particularly low or high tides. Nevertheless there were only 11 calving events observed in the detailed 2009 records, and fewer in 2007 and 2008, so the database on which to base such a conclusion is sparse. The lack of response to tidal fluctuations could suggest that the glacier is well grounded and not affected by the changes in subglacial water pressure that can be caused by the tides (Amundson et al., 2010). Herdes et al. (in review) also did not find a clear relationship between tide levels and calving events on the Belcher Glacier between 1997 and 2008. This suggests that the calving rate on the Belcher Glacier does not respond to the  $\pm 1.5$  m tidal fluctuations that it is exposed to during open water conditions. The glacier may still respond with vertical motion due to the rise and fall of the tides, but this would have to be investigated with a network of GPS stations located close to the terminus.

### **4.3.5 Ocean temperatures**

A wealth of results from Greenland (e.g. Murray et al., 2010) suggest that the stability of glaciers is influenced by ocean temperatures, particularly because changing sea ice concentrations and basal melt rates can affect the calving rate. The SST results from the region offshore from the Belcher Glacier indicate that there was increasingly anomalously cold surface water in the region between 2000 and 2010, in direct contrast to the warm surface and subsurface waters penetrating many parts of Greenland. A limited dataset of CTD measurements from 1978 to 2008 suggests that there has been no major change in ocean temperature at depth. This indicates that warm Atlantic-sourced subsurface water is not reaching the Canadian High Arctic, but is being channeled south along Baffin Island (Zweng and Munchow, 2006; Rabe et al., 2010). If the cool summer SSTs reflect cooler water at depth (as suggested by Murray et al., 2010), they may be acting to reduce the basal melt rate at Belcher Glacier, which could then also limit the calving rate, although a long enough time series is not available to examine this. Nevertheless, the cool surface waters near the Belcher Glacier are likely to be reinforcing the current stability of the glacier terminus. Given the dramatic response of the Greenland glaciers to changing ocean temperatures (e.g. Holland et al., 2008), it is nevertheless apparent that changing ocean currents and temperatures in the Canadian Arctic region need better monitoring.

## **4.4 *Limitations***

The results presented above have highlighted several limitations of this study and identified a number of ways in which it could be improved upon in the future. Ice thickness and basal topography in the vicinity of the glacier terminus should be measured independently of each other so that an accurate calculation of terminus buoyancy can be made. In order to capture the full sequence of a calving event and better understand the style of terminus disintegration, time lapse imagery must be collected at an interval as close as possible to 10 seconds during periods of active summer calving (Amundson et al., 2010). Over the rest of the summer,

images should be collected at sub-hourly intervals. It would be best to install a series of cameras if a range of phenomena are to be investigated (e.g. calving rate, meltwater plume extent, terminus movement with optical flow) in order to achieve the optimum camera angle and position for each aspect, as well as for redundancy. Time lapse imagery from the fall and winter, taken at peak light conditions each day, would provide further information about calving during this period as well as about the timing of sea ice coagulation. A network of passive seismometers installed close to the terminus would support investigations of the calving style and rate, as establishing the frequency and source of fracturing events could help determine whether or not the Belcher Glacier is completely grounded at the bed (Walter et al., 2010). Ideally seismic observations should be continued during the fall and winter to examine whether the fracturing processes continue throughout the year. Geophones should also be installed with lower gain sensitivity in case a lot of small, frequent fractures were being missed, and geophones should also be placed in a dense network because on this glacier only local fractures were detected.

Several other improvements could be made to this study of potential calving triggers. Ice thickness should be measured at two flux gates upstream of the terminus in two consecutive summers in order for the contribution of basal melt to be calculated, following Motyka et al. (2011). More numerous CTD casts in the offshore terminus region are required to provide the data needed to calculate basal melt rates. These casts should penetrate the full thickness of the plume outflow to determine its temperature and SSC profiles. If CTD casts were made through the meltwater plume they could also be used to determine the plume thickness and calculate the volume of water expelled from the subglacial system, following Motyka et al. (2003) and Trusel et al. (2010). The volume of seasonal meltwater discharge could then be compared with the modeled runoff (from Duncan, 2011) to examine whether late season hysteresis of the sediment plume takes place, as suggested by Chu et al. (2009), or whether a quantity of meltwater is stored within the glacier overwinter, as happens on some land-terminating glaciers (e.g. Hodson

et al., 2005). This could be further examined with a model such as *SedPlume* (Mugford and Dowdeswell, 2011), if it were used to investigate meltwater plume volume rather than long term sedimentation rates.

#### **4.5            *Implications***

The implications of the results presented in this thesis are that individual calving events are not triggered by a single identifiable phenomenon. Calving events on the Belcher Glacier were not caused by sudden velocity changes, break-up of the sea ice/mélange, tidal fluctuations or propagation of meltwater-filled crevasses. The location of calving was sometimes affected by the presence of the meltwater plume and this may be a reflection of higher basal melt rates in the vicinity of the plume outflow which undermine the glacier terminus (Motyka et al., 2003). The timing of a calving event triggered by the meltwater plume also seems to be strongly influenced by the position of the terminus, which reflects the ice and bed geometry. The geometry of the glacier is one of the primary controls on the proximity to flotation, which affects terminus stability. Therefore these results suggest that the ice and bed geometry, as well as the basal melt rate and the general flux of ice being delivered to the terminus are significant controls on the calving rate and stability of the Belcher Glacier. By extension, it is hypothesized that a change in ocean temperature, which alters the basal melt rate, is expected to strongly influence the stability of the glacier terminus (Motyka et al., 2011).

As there does not seem to be a single identifiable cause for iceberg calving, this also points towards the stochastic and non-linear nature of the process. This means that whilst calving is a deterministic process (ice will inevitably fall from the terminus margin eventually) it is impossible in practical terms to predict the frequency or magnitude of an event, despite near-constant monitoring with GPS and seismometers (Bassis, 2011). The iceberg calving rate may reflect self-organized criticality, where complex dynamic systems adapt (often through failure) until they reach a stable state (Kavanaugh, 2009), although it is impossible

to know whether a small ice fracture (or an external forcing such as loss of sea ice buttressing) will do nothing or trigger a cascade of large calving events.

Earthquake fault systems are a well known example of self-organized criticality, and Kavanaugh (2009) also showed that subglacial water pressure events on Trapridge Glacier, Yukon, Canada, reflected this non-linear organization. A model such as Bassis (2011) which relies on statistical physics to understand the probability of iceberg calving may provide a different insight into the iceberg calving process which requires further investigation.

Furthermore, the results suggest that the size, timing and style of a calving event are partly controlled by processes acting on the ice upglacier of the terminus. After all, the basal melt rate only affects the grounded ice face or the floating portion of a terminus and the stability of the margin is mainly influenced by the ice and bed geometry at its current pinning point. The amount of damage afflicted on the ice that is transported towards the grounding zone is probably one of the most significant controls on iceberg calving. Meltwater ponding on the surface and in crevasses is likely to play a major role in weakening the ice and inflicting the damage. Pralong et al. (2003) and Pralong and Funk (2005) used continuum damage mechanics to model the evolution and propagation of damaged ice regions to the margin, and found the ice to be particularly sensitive to changing local geometry. The damage is received at a range of scales which begins as microcracks within ice crystals, but Pralong and Funk (2005) focused on the mesoscale formation of local ice cracks that may later culminate in larger crevasses or failure (calving). Fracture formation due to water pressure changes was an important aspect of their model. They tested the criterion on a lake-calving glacier and a hanging glacier in Switzerland. Precise knowledge of the glacier geometry and the damage parameters was necessary to model the calving of an ice block accurately. Development of a macroscale version of this criterion which is less computationally expensive would be valuable so that it can be applied to whole glaciers and ice caps. The iceberg calving framework proposed by Amundson and Truffer (2010) could potentially provide this macroscale model as

it is general enough to apply to any calving margin and is computationally inexpensive. However it consists of two parameterizations based on unknown physical laws and requires further criteria (such as the relationship between geometry, flow and crevasse spacing, and a better parameterization for ice shelf calving) to be developed before it can be incorporated into glacier and ice sheet models.

## **4.6**            *Summary*

In this chapter we examined the potential triggers of iceberg calving from the Belcher Glacier and concluded that the glacier is probably lightly grounded at its terminus but every few years seems to develop a slightly advanced protruding bulge along its centreline which begins to float due to undercutting by basal melt, erosion of its lateral stability by the meltwater plume. Once enough damage is inflicted upon the ice, the protrusion calves off as a series of tabular icebergs. It was also noted that as the Belcher Glacier shares a fjord with its northern tributary, the stability of the two glaciers are likely to be inextricably linked.

It was suggested that individual calving events are not typically caused by a single trigger mechanism and instead may reflect a stochastic, essentially unpredictable process. Calving from the margin is most likely to be a product of the basal melt rate, the current ice and bed geometry, and the overall flux of ice through the terminus gate. Yet it is also a reflection of the amount of damage inflicted on the ice upstream of the margin, so it was suggested that a macroscale version of the Pralong and Funk (2005) ice damage model might be better able to explain seasonal variations in the calving rate from Belcher Glacier than a model based on response to specific fracture-triggering events. A framework such as that proposed by Amundson and Truffer (2010) may also be able to achieve this. Several limitations of the study of calving on the Belcher Glacier were reviewed and improvements for future research were suggested.

## Chapter 5. CONCLUSIONS

The motivation for this thesis was to identify the major controls on the rate and style of iceberg calving from a tidewater glacier, the Belcher Glacier, in the Canadian High Arctic. The first challenge was to detect iceberg calving events during the summer of 2009. Time lapse imagery was an excellent method of doing this, although a shorter time interval between photographs appears necessary to observe calving in action and see how the ice front disintegrates. The results show that the ice margin can be accurately delimited, and the change in area can be calculated if the image is georeferenced. For this, an algorithm which used all of the camera rotation angles provided the most reliable result. The total volume of ice lost by iceberg calving and basal melt between June 4<sup>th</sup> and August 14<sup>th</sup> 2009 was 0.088km<sup>3</sup>. This accounted for 44% of the total annual ice flux through the glacier terminus. Approximately 16% of annual calving took place in the winter, between October and May. The audio recorder successfully detected calving events, although the orientation of the microphone was paramount in this. The three calving events identified lasted 1.5-11 minutes and suggested that either the calving took place in several phases, or that the iceberg disintegrated upon hitting the water (as each event was associated with a lot of avalanching of debris and several large 'thuds'). The two-component geophones did not detect calving events because they were only sensitive to very local fracturing events. They would need to be installed closer to the terminus to be effective in detecting calving. The geophones did record hydro-fracturing near the water-filled crevasses caused by the establishment of connections between the surface, englacial and subglacial drainage systems. The geophones also detected a large earthquake that occurred in Baffin Bay.

Once calving events had been identified, the second phase of the project was to determine whether the timing of these events was controlled by internal glacier dynamics or external factors acting at the ice-ocean interface. It was concluded

that on the Belcher Glacier, dynamics plays a significant role in ‘priming’ the terminus ice for failure due to the interactions of the ice flow with the ice and bed geometry. This is particularly the case if/where the terminus is buoyant because this exposes the ice to different stresses and increases the surface area susceptible to basal melt. Meltwater ponding on the ice surface and in crevasses may also play a significant role in damaging and weakening the ice. However once the ice reaches the margin it is exposed to a different set of interactions with seawater which can also influence calving.

It appears that the Belcher Glacier is probably lightly grounded at its terminus but every few years it advances slightly and develops a protruding bulge in the vicinity of its centreline. This protrusion begins to float, possibly due to differences in the basal topography, and active undercutting by basal melt. The ice is further weakened if its lateral support is eroded by the meltwater plume, in the vicinity of which the local calving rate is enhanced. 81% of the calving events between June and August 2009 took place near the normal exit point of the meltwater plume, or in other locations to which the plume was rerouted immediately prior to the calving event. Eventually, once a threshold of damage is exceeded, the protrusion calved off as a series of tabular icebergs (the form of which strongly suggests this ice was floating prior to calving). From 2007-2009, the timing of calving did not seem to have been controlled by increases in ice velocity near the terminus, the break-up of the sea ice, tidal flexure of the terminus, or local propagation of meltwater-filled crevasses. Instead the results suggest that basal melt rates, and by extension ocean temperatures, may be significant controls on calving but this hypothesis needs to be investigated further. It is also concluded that calving is not driven by a single phenomenon, but instead is a stochastic process which reflects the progressive accumulation of damage to the ice from several different sources during its travel towards the terminus. A model such as those proposed by Pralong and Funk (2005) or Amundson and Truffer (2010) should be used to further investigate the calving process.

## Bibliography

1. Adrian, R.J., 2004. Twenty Years of Particle Image Velocimetry. 12<sup>th</sup> International Symposium on Application of Laser Techniques in Fluid Mechanics.
2. Ahn, Y. and Box, J.E., 2010. Glacier velocities from time-lapse photos: technique development and first results from the Extreme Ice Survey (EIS) in Greenland. *Journal of Glaciology*, 56 (198):723-734.
3. Alley, R.B. et al., 2008. A Simple Law for Ice-Shelf Calving. *Science*, 322: 1344.
4. Amundson, J.M. and Truffer, M., 2010. A unifying framework for iceberg-calving models. *Journal of Glaciology*, 56(199): 822-830.
5. Amundson, J.M. et al., 2008. Glacier, fjord, and seismic response to recent large calving events, Jakobshavn Isbrae, Greenland. *Geophysical Research Letters*, 35(L22501): doi:10.1029/2008GL035281.
6. Amundson, J.M. et al., 2010. Ice melange dynamics and implications for terminus stability, Jakobshavn Isbrae, Greenland. *Journal of Geophysical Research F: Earth Surface*, 115(1).
7. Andersen, M.L. et al., 2010. Spatial and temporal melt variability at Helheim Glacier, East Greenland, and its effect on ice dynamics. *Journal of Geophysical Research F: Earth Surface*, 115(4).
8. Atcheson, B., Heidrich, W., Ihrke, I., 2009. An evaluation of optical flow algorithms for background orientated schlieren imaging. *Exp. Fluids*, 46: 467-476.
9. Bassis, J.N., 2011. The statistical physics of iceberg calving and the emergence of universal calving laws. *Journal of Glaciology*, 57 (201): 3-16.
10. Baker, S., Scharstein, D., Lewis, J.P., Roth, S., Black, M.J., Szeliski, R., 2007. A Database and Evaluation Methodology for Optical Flow. *Proc. Eleventh IEEE International Conference on Computer Vision*.

11. Bell, T. and Hughes-Clark, J., 2006, unpublished data. Memorial University of Newfoundland and University of New Brunswick, Canada.
12. Benn, D., Gulley, J., Luckman, A., Adamek, A. and Glowacki, P.S., 2009. Englacial drainage systems formed by hydrologically driven crevasse propagation. *Journal of Glaciology*, 55(191): 513-523.
13. Benn, D.I., and Evans, D.J.A., 2010. *Glaciers and Glaciation*, 2<sup>nd</sup> ed. Hodder.
14. Benn, D.I., Hulton, N.R.J. and Mottram, R.H., 2007a. 'Calving laws', 'sliding laws' and the stability of tidewater glaciers. *Annals of Glaciology*, 46: 123-130.
15. Benn, D.I., Warren, C.R. and Mottram, R.H., 2007b. Calving processes and the dynamics of calving glaciers. *Earth-Science Reviews*, 82(3-4): 143-179.
16. Boon, S. and Sharp, M., 2003. The role of hydrologically-driven ice fracture in drainage system evolution on an Arctic glacier. *Geophysical Research Letters*, 30(18): CRY 1-1 - 1-4.
17. Boon, S., Burgess, D.O., Koerner, R.M. and Sharp, M.J., 2010. Forty-seven years of research on the Devon Island ice cap, Arctic Canada. *Arctic*, 63(1): 13-29.
18. Bourgault, D., 2008. Shore-based photogrammetry of river ice. *Canadian Journal of Civil Engineering*, 35(1): 80-86.
19. Boyer, T.P., Antonov, J.I., Garcia, H.E., Johnson, D.R., Locarnini, R.A., Mishonov, A.V., Pitcher, M.T., Baranova, O.K., Smolyar, I.V., 2006. *World Ocean Database 2005*. S. Levitus, Ed., NOAA Atlas NESDIS 60, U.S. Government Printing Office, Washington, D.C., 190 pp.
20. Brown, C.S., Meier, M.F. and Post, A., 1982. Calving speed of Alaska tidewater glaciers with applications to the Columbia Glacier, Alaska.
21. Brox, T., 2005. *From Pixels to Regions: Partial Differential Equations in Image Analysis*. Ph.D. thesis, Department of Mathematics and Computer Science, Saarland University, Saarbrücken, Germany.

22. Brox, T., Bruhn, A., Papenberg, N. and Weickert, J., 2004. High accuracy optical flow estimation based on a theory for warping, *Lecture Notes in Computer Science (including subseries Lecture Notes in Artificial Intelligence and Lecture Notes in Bioinformatics)*, pp. 25-36.
23. Burgess, D. and Sharp, M.J., 2008. Recent changes in thickness of the Devon Island ice cap, Canada. *Journal of Geophysical Research B: Solid Earth*, 113(7).
24. Burgess, D.O. and Sharp, M.J., 2004. Recent changes in areal extent of the Devon Ice Cap, Nunavut, Canada. *Arctic, Antarctic, and Alpine Research*, 36(2): 261-271.
25. Burgess, D.O., Sharp, M.J., Mair, D.W.F., Dowdeswell, J.A. and Benham, T.J., 2005. Flow dynamics and iceberg calving rates of Devon Ice Cap, Nunavut, Canada. *Journal of Glaciology*, 51(173): 219-230.
26. Chapuis, A., Rolstad, C., Norland, R., 2010. Interpretation of amplitude data from ground-based radar in combination with terrestrial photogrammetry and visual observations for calving monitoring of Kronebreen, Svalbard. *Annals of Glaciology*, 51 (55): 34-40.
27. Chen, W., and Barron, J.L., 2010. High Accuracy Optical Flow Method Based on a Theory for Warping: 3D Extension. *ICAR (1)*: 250-262.
28. Chu, V.W. et al., 2009. Sediment plume response to surface melting and supraglacial lake drainages on the Greenland ice sheet. *Journal of Glaciology*, 55(194): 1072-1082.
29. Conley, E., and Cloud, G., 1986. Practical applications of double-exposure noncoherent-light speckle photography. *Applied Optics*, 25 (14), 2246-2248.
30. Copland, L., Mueller, D.R. and Weir, L., 2007. Rapid loss of the Ayles Ice Shelf, Ellesmere Island, Canada. *Geophysical Research Letters*, 34(21).
31. Copland, L., Sharp, M.J. and Nienow, P.W., 2003. Links between short-term velocity variations and the subglacial hydrology of a predominantly cold polythermal glacier. *Journal of Glaciology*, 49(166): 337-348.

32. Corripio, J.G., 2004. Snow surface albedo estimation using terrestrial photography. *International Journal of Remote Sensing*, 25(24): 5705-5729.
33. Cowan, E.A. and Powell, R.D., 1990. Suspended sediment transport and deposition of cyclically interlaminated sediment in a temperate glacial fjord, Alaska, USA. *Glacimarine environments: processes and sediments*: 75-89.
34. Croitoru, A. and Ethrog, U., 2001. Photo Orientation under unstable conditions: A robust trial and error approach using range ratios. *Photogrammetric Record*, 17(97): 63-87.
35. Cuffey, K.M., and Paterson, W.S.B., 2010. *The Physics of Glaciers*, 4<sup>th</sup> ed. Elsevier.
36. Danielson, B. and Sharp, M., in review. Associating Ice Flow Variations with Supra-Glacial Lake Drainage Events on a Tidewater Glacier. *Annals of Glaciology*, special issue: 'Interactions of Ice Sheets and Glaciers with the Ocean'.
37. Das, S.B. et al., 2008. Fracture propagation to the base of the Greenland ice sheet during supraglacial lake drainage. *Science*, 320(5877): 778-781.
38. De Juan, J., Elosegui, P., Nettles, M., Larsen, T., Davis, J., Hamilton, G., Stearns, L., Andersen, M., Ekstrom, G., Ahlstrom, A., Stenseng, L., Khan, S.A., Forsberg, R., 2010. Sudden increase in tidal response linked to calving and acceleration at a large Greenland outlet glacier. *Geophysical Research Letters*, 37, L12501.
39. Dowdeswell, J., Benham, T., Gorman, M., Burgess, D.O. and Sharp, M.J., 2004. Form and flow of the Devon Island Ice Cap, Canadian Arctic. *Journal of Geophysical Research*, 109(F02002).
40. Dowdeswell, J.A. and Cromack, M., 1991. Behaviour of a glacier-derived suspended sediment plume in a small Arctic inlet. *Journal of Geology*, 99(1): 111-123.
41. Dowdeswell, J.A., 2006. The Greenland ice sheet and global sea-level rise. *Science*, 311(5763): 963-964.

42. Duncan, A., 2011. Spatial and Temporal Variations of the Surface Energy Balance and Ablation on the Belcher Glacier, Devon Island, Nunavut, Canada. Masters thesis, Department of Earth and Atmospheric Sciences, University of Alberta, Canada.
43. Dunphy, M., Dupont, F., Hannah, C.G., Greenberg, D., 2005. Validation of a modelling system for tides in the Canadian Arctic Archipelago. Can. Tech. Rep. Hydrogr. Ocean Sci. 243.
44. Dyke, A.S., 1999. Last Glacial Maximum and deglaciation of Devon Island, Arctic Canada: Support for an Innuitian ice sheet. *Quaternary Science Reviews*, 18(3): 393-420.
45. Echelmeyer, K., Clarke, T.S. and Harrison, W.D., 1991. Surficial glaciology of Jakobshavn Isbrae, West Greenland: part I. Surface morphology. *Journal of Glaciology*, 37(127): 368-382.
46. Ekstrom, G., Nettles, M. and Abers, G.A., 2003. Glacial Earthquakes. *Science*, 302(5645): 622-624.
47. Gardner, A.S., Moholdt, G., Wouters, B., Wolken, G.J., Burgess, D., Sharp, M.J., Cogley, J.G., Braun, C., Labine, C., 2011. Sharply increased mass loss from glaciers and ice caps in the Canadian Arctic Archipelago. *Nature*, doi:10.1038/nature10089.
48. Giesen, R.H., van den Broeke, M.R., Oerlemans, J. and Andreassen, L.M., 2008. Surface energy balance in the ablation zone of Midtdalsbreen, a glacier in southern Norway: Interannual variability and the effect of clouds. *Journal of Geophysical Research D: Atmospheres*, 113 (21).
49. Gogineni, S., Jezek, K., Paden, J., Allen, C., Kanagarathnam, P., Akins, T., 2005. Radars for Imaging and Sounding of Polar Ice Sheets. Workshop on Radar Investigations.
50. Greisman, P., Grant, S., Blaskovich, A., van Hardenburg, B., 1986. Tidal Propagation Measurements in Baffin Bay, Lancaster Sound, and Nares Strait. Canadian Contractor Report of Hydrography and Ocean Sciences, 25.

51. Gudmundsson, G.H., 2007. Tides and the flow of Rutford Ice Stream, West Antarctica. *Journal of Geophysical Research F: Earth Surface*, 112(4).
52. Halverson, M.J. and Pawlowicz, R., 2008. Estuarine forcing of a river plume by river flow and tides. *Journal of Geophysical Research C: Oceans*, 113(9).
53. Hannah, C.G., Dupont, F., Collins, A.K., Dunphy, M. and Greenberg, D., 2008. Revisions to a Modelling System for Tides in the Canadian Arctic Archipelago, Ocean Sciences Division, Maritimes Region, Fisheries and Oceans Canada.
54. Haug, T., Kaab, A., Skvarca, P., 2010. Monitoring ice shelf velocities from repeat MODIS and Landsat data – a method study on the Larsen C ice shelf, Antarctic Peninsula, and 10 other ice shelves around Antarctica. *The Cryosphere*, 4: 161-178.
55. Herdes, E., 2009. The Relationships between Iceberg Calving and Sea Ice Conditions on Devon Ice Cap, Nunavut. Undergraduate thesis, Department of Geography, University of Ottawa, Canada.
56. Herdes, E., Copland, L., Danielson, B., Sharp, M., in review. Relationships between iceberg calving and sea ice conditions on NE Devon Ice Cap, Nunavut. *Annals of Glaciology*, special issue: 'Interactions of Ice Sheets and Glaciers with the Ocean'.
57. Hock, R. and Holmgren, B. 2005. A distributed surface energy balance model for complex topography and its application to Storglaciaren, Sweden. *Journal of Glaciology*, 51(172): 25–36.
58. Hodson, A., Kohler, J., Brinkhaus, M., Wynn, P., 2005. Multi-year water and surface energy budget of a high-latitude polythermal glaciers: evidence for overwinter water storage in a dynamic subglacial reservoir. *Annals of Glaciology*, 42, 42-46.
59. Holland, D.M., Thomas, R.H., De Young, B., Ribergaard, M.H. and Lyberth, B., 2008. Acceleration of Jakobshavn Isbrae triggered by warm subsurface ocean waters. *Nature Geoscience*, 1(10): 659-664.

60. Horn, B.K.P. and Schunck, B.G., 1981. Determining optical flow. *Computer vision*: 185-203.
61. Howat, I.M., Box, J.E., Ahn, Y., Herrington, A. and McFadden, E.M., 2010. Seasonal variability in the dynamics of marine-terminating outlet glaciers in Greenland. *Journal of Glaciology*, 56(198): 601-613.
62. Howat, I.M., Joughin, I. and Scambos, T.A., 2007. Rapid changes in ice discharge from Greenland outlet glaciers. *Science*, 315(5818): 1559-1561.
63. Howat, I.M., Joughin, I., Tulaczyk, S. and Gogineni, S., 2005. Rapid retreat and acceleration of Helheim Glacier, east Greenland. *Geophysical Research Letters*, 32(22): 1-4.
64. Hulbe, C., MacAyeal, D.R., Denton, G.H., Kleman, J. and Lowell, T.V., 2004. Catastrophic ice shelf breakup as the source of Heinrich event icebergs. *Palaeoceanography*, 19(PA1004): doi:10.1029.
65. Hulbe, C.L., Scambos, T.A., Youngberg, T. and Lamb, A.K., 2008. Patterns of glacier response to disintegration of the Larsen B ice shelf, Antarctic Peninsula. *Global and Planetary Change*, 63(1): 1-8.
66. Iken, A., Rothlisberger, H., Flotron, A. and Haeberli, W., 1983. The uplift of Unteraargletscher at the beginning of the melt season - a consequence of water storage at the bed? *Journal of Glaciology*, 29(101): 28-47.
67. Johannessen, O.M., Koravlev, A., Miles, V., Miles, M.W., Solberg, K.E., 2010. Interaction between the Warm Subsurface Atlantic Water in the Sermilik Fjord and Helheim Glacier in Southeast Greenland. *Survey Geophysics*. DOI 10.1007/s10712-011-9130-6.
68. Joughin, I. et al., 2008a. Seasonal speedup along the western flank of the Greenland ice sheet. *Science*, 320(5877): 781-783.
69. Joughin, I. et al., 2008b. Ice-front variation and tidewater behaviour on Helheim and Kangerdlugssuaq Glaciers, Greenland. *Journal of Geophysical Research F: Earth Surface*, 113(1).
70. Joughin, I., Abdalati, W. and Fahnestock, M., 2004. Large fluctuations in speed on Greenland's Jakobshavn Isbræ glacier. *Nature*, 432(7017): 608-610.

71. Kavanaugh, J.L. and Clarke, G.K.C., 2001. Abrupt glacier motion and reorganization of basal shear stress following the establishment of a connected drainage system. *Journal of Glaciology*, 47(158): 472-480.
72. Koerner, R. M., 1977. Devon Island ice cap: Core stratigraphy and paleoclimate. *Science*, 196 (4285): 15-18.
73. Koerner, R.M., 2005. Mass balance of glaciers in the Queen Elizabeth Islands, Nunavut, Canada. *Annals of Glaciology*, 42: 417-423.
74. Krabill, W., Gogineni, P., Demuth, M.N., 2006. Glacier elevation and ice thickness data derived from Airborne LiDAR and Ice Penetrating RaDAR surveys over the reference monitoring glaciers and ice caps of the Canadian Arctic Islands, 2005, 2006, Geol. Surv. of Canada, Ottawa, Ontario, Canada.
75. Krimmel, R.M. and Rasmussen, L.A., 1986. Using sequential photography to estimate ice velocity at the terminus of Columbia Glacier, Alaska. *Annals of Glaciology*, 8: 117-123.
76. Lahet, F., and Stramski, D., 2010. MODIS imagery of turbid plumes in San Diego coastal waters during rainstorm events. *Remote Sensing of Environment*, 114: 332-344.
77. Laidre, K.L., Heide-Jrgensen, M.P., Ermold, W. and Steele, M., 2010. Narwhals document continued warming of southern Baffin Bay. *Journal of Geophysical Research C: Oceans*, 115(10).
78. Lihan, T., Saitoh, S.I., Iida, T., Hirawake, T. and Iida, K., 2008. Satellite-measured temporal and spatial variability of the Tokachi River plume. *Estuarine, Coastal and Shelf Science*, 78(2): 237-249.
79. Macayeal, D.R., Okal, E.A., Aster, R.C. and Bassis, J.N., 2009. Seismic observations of glaciogenic ocean waves (micro-tsunamis) on icebergs and ice shelves. *Journal of Glaciology*, 55(190): 193-206.
80. McGrath, D. et al., 2009. Sediment plumes as a proxy for local ice-sheet runoff in Kangerlussuaq Fjord, West Greenland. *Journal of Glaciology*, 56(199): 813-821.

81. McGrath, D., 2009. Sediment Plumes in Sondre Stromfjord, Greenland as a proxy for runoff from the Greenland Ice Sheet. Masters thesis, Department of Geography, University of Colorado, U.S.A.
82. Meier, M.F. and Post, A., 1987. Fast Tidewater Glaciers. *Journal of Geophysical Research*, 92(B9): 9051-58.
83. Meier, M.F. et al., 2007. Glaciers dominate eustatic sea-level rise in the 21st century. *Science*, 317(5841): 1064-1067.
84. Melling, H., 2002. Sea ice of the northern Canadian Arctic Archipelago. *Journal of Geophysical Research C: Oceans*, 107(11): 2-1.
85. Miller, R.L. and McKee, B.A., 2004. Using MODIS Terra 250 m imagery to map concentrations of total suspended matter in coastal waters. *Remote Sensing of Environment*, 93(1-2): 259-266.
86. Moon, T. and Joughin, I., 2008. Changes in ice front position on Greenland's outlet glaciers from 1992 to 2007. *Journal of Geophysical Research F: Earth Surface*, 113(2).
87. Motyka, R.J. et al., 2011. Submarine melting of the 1985 Jakobshavn Isbrae floating tongue and the triggering of the current retreat. *Journal of Geophysical Research F: Earth Surface*, 116(1).
88. Motyka, R.J., Fahnestock, M. and Truffer, M., 2010. Volume change of Jakobshavn Isbrae, West Greenland: 1985-1997-2007. *Journal of Glaciology*, 56(198): 635-646.
89. Motyka, R.J., Hunter, L., Echelmeyer, K.A. and Connor, C., 2003. Submarine melting at the terminus of a temperate tidewater glacier, LeConte Glacier, Alaska, U.S.A. *Annals of Glaciology*, 36: 57-65.
90. Mugford, R.I. and Dowdeswell, J.A., 2011. Modeling glacial meltwater plume dynamics and sedimentation in high-latitude fjords. *Journal of Geophysical Research F: Earth Surface*, 116(1).
91. Murray, T. et al., 2010. Ocean regulation hypothesis for glacier dynamics in southeast Greenland and implications for ice sheet mass changes. *Journal of Geophysical Research F: Earth Surface*, 115(3).

92. Murray, T., Smith, A.M., King, M.A. and Weedon, G.P., 2007. Ice flow modulated by tides at up to annual periods at Rutford Ice Stream, West Antarctica. *Geophysical Research Letters*, 34(18): L18503.
93. Neave, K.G. and Savage, J.C., 1970. Icequakes on the Athabasca Glacier. *Journal of Geophysical Research*, 75(1351-62).
94. Nettles, M. et al., 2008. Step-wise changes in glacier flow speed coincide with calving and glacial earthquakes at Helheim Glacier, Greenland. *Geophysical Research Letters*, 35(24).
95. Nettles, M., and Ekstrom, G., 2010. Glacial Earthquakes in Greenland and Antarctica. *Annual Review of Earth and Planetary Sciences*, 38 (467-491).
96. Nick, F.M., Vieli, A., Howat, I.M. and Joughin, I., 2009. Large-scale changes in Greenland outlet glacier dynamics triggered at the terminus. *Nature Geosci*, 2(2): 110-114.
97. O'Neel, S. and Pfeffer, W.T., 2007. Source mechanics for monochromatic icequakes produced during iceberg calving at Columbia Glacier, AK. *Geophysical Research Letters*, 34(L22502).
98. O'Neel, S., Echelmeyer, K.A. and Motyka, R.J., 2001. Short-term flow dynamics of a retreating tidewater glacier: LeConte Glacier, Alaska, U.S.A. *Journal of Glaciology*, 47(159): 567-578.
99. O'Neel, S., Echelmeyer, K.A. and Motyka, R.J., 2003. Short-term variations in calving of a tidewater glacier: LeConte Glacier, Alaska, U.S.A. *Journal of Glaciology*, 49(167): 587-598.
100. O'Neel, S., Marshall, H.P., McNamara, D.E. and Pfeffer, W.T., 2007. Seismic detection and analysis of icequakes at Columbia Glacier, Alaska. *Journal of Geophysical Research F: Earth Surface*, 112(3).
101. Pawlowicz, R., Beardsley, B. and Lentz, S., 2002. Classical tidal harmonic analysis including error estimates in MATLAB using TDE. *Computers and Geosciences*, 28(8): 929-937.
102. Pelto, M.S., and Warren, C.R., 1991. Relationship between tidewater glacier calving velocity and water depth at the calving front. *Annals of Glaciology*, 15: 115–118.

103. Pfeffer, W.T., 2007. A simple mechanism for irreversible tidewater glacier retreat. *Journal of Geophysical Research F: Earth Surface*, 112(3).
104. Pralong, A. and Funk, M., 2005. Dynamic damage model of crevasse opening and application to glacier calving. *Journal of Geophysical Research B: Solid Earth*, 110(1): 1-12.
105. Pralong, A., Funk, M. and LÄ¼thi, M.P., 2003. A description of crevasse formation using continuum damage mechanics. *Annals of Glaciology*, 37: 77-82.
106. Qamar, A., 1988. Calving icebergs: A source of low-frequency seismic signals from Columbia Glacier, Alaska. *Journal of Geophysical Research*, 93(6615-23).
107. Rabe, B., Münchow, A., Johnson, H.L., Melling, H., 2010. Nares Strait hydrography and salinity field from a 3 year moored array, *J. Geophys. Res.*, 115, C07010, doi:10.1029/2009JC005966.
108. Radić, V. and Hock, R. 2010. Regional and global volumes of glaciers derived from statistical upscaling of glacier inventory data. *Journal of Geophysical Research*, 115, F01010.
109. Radic,V. and Hock, R., 2011. Regionally differentiated contribution of mountain glaciers and ice caps to future sea-level rise. *Nature Geoscience*. 4: 91–94.
110. Reeh, N., Thomsen, H.H., Higgins, A.K. and Weidick, A., 2001. Sea ice and the stability of north and northeast Greenland floating glaciers. *Annals of Glaciology*, 33: 474-480.
111. Reynolds, R.W., Rayner, N.A., Smith, T.M., Stokes, D.C., Wang, W., 2002. An improved in situ and satellite SST analysis for climate, *J.Clim.*, 15 (13): 1609-1625.
112. Rignot, E. and Steffen, K., 2008. Channelized bottom melting and stability of floating ice shelves. *Geophysical Research Letters*, 35(2).
113. Sand, P. and Teller, S., 2006. Particle video: Long-range motion estimation using point trajectories, *Proceedings of the IEEE Computer*

- Society Conference on Computer Vision and Pattern Recognition, pp. 2195-2202.
114. Sand, P., 2006. Long-Range Video Motion Estimation using Point Trajectories. Ph.D. thesis, Department of Electrical Engineering and Computer Science, Massachusetts Institute of Technology, U.S.A.
  115. Scambos, T.A., Bohlander, J.A., Shuman, C.A. and Skvarca, P., 2004. Glacier acceleration and thinning after ice shelf collapse in the Larsen B embayment, Antarctica. *Geophysical Research Letters*, 31(18): L18402 1-4.
  116. Scambos, T.A., Dutkiewicz, M.J., Wilson, J.C. and Bindshadler, R.A., 1992. Application of image cross-correlation to the measurement of glacier velocity using satellite image data. *Remote Sensing of Environment*, 42(3): 177-186.
  117. Scambos, T.A., Hulbe, C., Fahnestock, M. and Bohlander, J., 2000. The link between climate warming and break-up of ice shelves in the Antarctic Peninsula. *Journal of Glaciology*, 46(154): 516-530.
  118. Sharp, M., Burgess, D.O., Cogley, J.G., Ecclestone, M., Labine, C., Wolken, G.J., 2011. Extreme melt on Canada's Arctic ice caps in the 21<sup>st</sup> century. *Geophysical Research Letters*, 38, L11501.
  119. Short, N.H., and Gray, A.L., 2005. Glacier dynamics in the Canadian High Arctic from RADARSAT-1 speckle tracking. *Canadian Journal of Remote Sensing*, 31 (3): 225-239.
  120. Sikonia, W.G., 1982. Finite element glacier dynamics model applied to Columbia Glacier, Alaska. US Geological Survey Professional Paper, 1258 B.
  121. Sohn, H.G., Jezek, K.C. and Van Der Veen, C.J., 1998. Jakobshavn Glacier, West Greenland: 30 years of spaceborne observations. *Geophysical Research Letters*, 25(14): 2699-2702.
  122. Sun, D., Roth, S. and Black, M.J., 2010. Secrets of optical flow estimation and their principles, *Proceedings of the IEEE Computer Society Conference on Computer Vision and Pattern Recognition*, pp. 2432-2439.

123. Sylvestre, T.J., 2009. Spatial Patterns of Snow Accumulation across the Belcher Glacier Basin, Devon Island, Nunavut, Canada. Masters thesis, Department of Geography, University of Ottawa, Canada.
124. Thomas, R.H. et al., 2003. Investigation of surface melting and dynamic thinning on Jakobshavn Isbrae, Greenland. *Journal of Glaciology*, 49(165): 231-239.
125. Trusel, L.D., Powell, R.D., Cumpston, R.M., Brigham-Grette, J., 2010. Modern glaciomarine processes and potential future behaviour of Kronebreen and Kongsvegen polythermal tidewater glaciers, Kongsfjorden, Svalbard. In: Howe, J.A., Austin, W.E., Forwick, M., Paetzel, M. (eds): *Fjord Systems and Archives*. Geological Society, London, Special Publications, 344: 89-102.
126. Tsai, V.C. and Ekstrom, G., 2007. Analysis of glacial earthquakes. *Journal of Geophysical Research F: Earth Surface*, 112(3).
127. Van der Veen, C.J., 2002. Calving glaciers. *Progress in Physical Geography*, 26(1): 96-122.
128. Van Wychen, W., 2010. Spatial and Temporal Variations in Ice Motion, Belcher Glacier, Devon Island, Nunavut, Canada. Masters thesis, Department of Geography, University of Ottawa, Canada.
129. Vieli, A. and Nick, F.M., 2011. Understanding and Modelling Rapid Dynamic Changes of Tidewater Outlet Glaciers: Issues and Implications. *Surveys in Geophysics*: 1-22.
130. Vieli, A., Funk, M. and Blatter, H., 2001. Flow dynamics of tidewater glaciers: A numerical modelling approach. *Journal of Glaciology*, 47(159): 595-606.
131. Walter, F. et al., 2010. Iceberg calving during transition from grounded to floating ice: Columbia Glacier, Alaska. *Geophysical Research Letters*, 37(15).
132. Walter, F., Deichmann, N. and Funk, M., 2008. Basal icequakes during changing subglacial water pressures beneath Gornergletscher, Switzerland. *Journal of Glaciology*, 54(186): 511-521.

133. Williamson, S., Sharp, M., Dowdeswell, J., Benham, T., 2008. Iceberg calving rates from northern Ellesmere Island ice caps, Canadian Arctic, 1999-2003. *Journal of Glaciology*, 54 (186): 391-400.
134. Yang, Q., Parvin, B., Mariano, A., 2000. Singular Features in Sea Surface Temperature Data. *IEEE Transactions on Geoscience and Remote Sensing*, 38(5): 516-520.
135. Zwally, H.J. et al., 2002. Surface melt-induced acceleration of Greenland ice-sheet flow. *Science*, 297(5579): 218-222.
136. Zweng, M.M. and Manabe, A., 2006. Warming and freshening of Baffin Bay, 1916-2003. *Journal of Geophysical Research C: Oceans*, 111(C7).